Year : 2013

The Tumor Suppressive Role of WIFl in Glioblastoma

Vassallo Iréne

UNIL | Université de Lausanne
Faculté de biologie et de médecine

Laboratoire de Biologie et Génétique des Tumeurs Cérébrales
Service de Neurochirurgie, Département des Neurosciences Cliniques
Centre Hospitalier Universitaire Vaudois (CHUV)

The Tumor Suppressive Role of WIF1 in Glioblastoma

Thèse de Doctorat ès Science de la Vie (PhD)

présentée à la
Faculté de Biologie et de Médecine de l'Université de Lausanne

par

IRENE VASSALLO
Diplômée en Biotechnologie médicale et pharmaceutiques
Université de Gênes (Italie 2009)

Jury
Prof. Pouw Schoumans Jacqueline, President
Prof. Monika Hegi, Thesis director
Prof. Tatiana Petrova, PhD program committee representative
PD Dr. Phil Shaw, Expert
Prof. Adrian Merlo, Expert

Lausanne 2013

UNIL | Université de Lausanne
Faculté de biologie
et de médecine

Ecole Doctorale

Doctorat ès sciences de la vie

Imprimatur

Vu le rapport présenté par le jury d'examen, composé de

Président	Madame	Prof. Jacqueline **Schoumans Pouw**
Directeur de thèse	Madame	Prof. Monika E. **Hegi**
Experts	Madame	Prof. Tatiana **Petrova**
	Monsieur	Dr Phil **Shaw**
	Monsieur	Prof. Adrian **Merlo**

le Conseil de Faculté autorise l'impression de la thèse de

Madame Irene Vassallo

"Master degree in biotechnology" de l'Université de Gênes, Italie

intitulée

The Tumor Suppressive Role of WIF1 in Glioblastoma

Lausanne, le 28 février 2014

pour Le Doyen
de la Faculté de Biologie et de Médecine

Prof. Jacqueline Schoumans Pouw

Table of contents

Table of contents 3

Abstract 6

Résumé 8

Glioma Tumors and Glioblastomas 10

1.The Pathobiology of Gliomas 10

2. Management and Survival of Glioblastoma Patients 13

The WNT Pathways 16

1. The Canonical WNT pathway 16

2. The Non-canonical WNT pathways 18

3. WNT Pathways Agonists and Antagonists 20

WNT inhibitory factor 1 – WIF1 21

Implications of the WNT Pathways in Tumor Development and Progression 24

WIF1 association with cancer 25

WNT Pathway in Glioblastoma, The State of the Art 27

WIF1 project: introduction and goals 28

1. Project introduction 28

2. Project goals 34

Results and Discussion 35

Establishment of WIF1 Stably Expressing Glioblastoma Cell Lines 35

Stable expression of WIF1 inhibits the canonical WNT pathways 36

Anchorage-Dependent and Anchorage-Independent Growth of *WIF1* overexpressing glioblastoma cells 38

Analysis of *in vivo* Tumorigenicity of WIF1-overexpressing Clones 40
WIF1 Overexpression Promotes a Senescence-like Phenotype 41
Characterisation of the *WIF1*-Inducible Glioblastoma Cells 43
1. Development of a *WIF1*-Inducible Cell Line 43
2. WIF1 Induction Impairs Cell Growth Both *in vitro* and *in vivo* 46
3. WIF1 Induction Reduces Migration Capability 49
4. WIF1 inducible clones show a larger percentage of senescent cells 50
Luciferase-Based Analysis of Canonical WNT and WNT5α/JNK/AP-1 Non-Canonical WNT Signaling Pathways. 51
Phosphorylation of ERK and p38 are the main changes in WIF1 induced cells 53
Analysis of the Gene Expression Profile of WIF1 Induced Cells 59
MALAT1 is Overexpressed in Glioblastoma Samples 62
MALAT1 Downregulation Reduces Migration Capability *in vitro* 64
MALAT1 Downregulation is *WNT5α*-Dependent 67
Migration *in vivo*: How *WIF1* and *MALAT1* Affect Cell Invasion 68
LURAP1L: a Potential Tumor Suppressor Gene Downstream of WIF1 Signaling Pathway 71
LURAP1l Overexpression Reduces Growth Capability 73
Conclusions and Future Perspectives 76
Material and Methods 81
Glioblastoma Tissues 81
Prediction of Genomic Copy Number Amplifications in Glioblastoma by a Hidden Markov Model 81
DNA Isolation, Methylation-Specific PCR 82

Glioblastoma Cell Lines 82
Plasmids and Small Interference RNAs 83
Cell transfection and generation of stable cell lines 84
Luciferase-based assays to measure signaling pathways activity 85
Crystal Violet Assay 85
Colony formation Assay 86
Colony formation Assay in Soft Agar 86
Cell migration and invasion assays 86
Nude Mouse Tumorigenicity Assay 87
Flow Cytometry Measurement of Cell Morphology 88
Protein analysis 88
Histochemistry 89
RNA Isolation and Reverse Transcription PCR 90
WIF1-induced LN229 gene expression profile 91
Statistical analysis 91
Glossary 92
References 95

Abstract

Expression based prediction of gene alterations identified WNT inhibitory factor I (*WIF1*) as a new candidate tumor suppressor gene involved in glioblastoma. *WIF1* encodes a secreted WNT antagonist and it is strongly down-regulated in most glioblastoma as compared to normal brain both by genomic deletion and WIF1 promoter hypermethylation. *WIF1* expression in glioblastoma cell lines inhibited cell proliferation *in vitro* and *in vivo* and strongly reduced migration capability. Interestingly, *WIF1* expression induced a senescence-like phenotype characterized by the appearance of enlarged, flattened and multinucleated cells positive for the presence of senescence associated β-galactosidase, a late marker of senescence. It is of note that *WIF1* induced senescence, in glioma cell lines, is independent of either p53 or pRB, two pathways that have been widely associated with this process. The analysis of the signaling pathways downstream of WIF1 brought some interesting results. *WIF1* expression inhibited the canonical pathway but alteration of this pathway alone couldn't explain all the WIF1-induced effects. Some *WIF1*-related changes were attributed to inhibition of the non-canonical pathway, as we could prove by downregulation of *WNT5α*, the main ligand of the non-canonical WNT pathway. For example, a drastic reduction of phosphorylation of both ERK and p38 was detected when either overexpressing *WIF1* or downregulating *WNT5α*. Due to the complexity of the non-canonical pathway is difficult to define the precise mechanism of signal transduction. We have excluded the involvement of the WNT5α-JNK-AP1

pathway and preliminary results suggest the implication of the WNT-calcium signaling, but further evidence is needed.

Moreover, from the analysis of the gene expression profile of *WIF1* expressing cells we could select a very interesting candidate: *MALAT1*, a non-coding RNA widely associated with migratory capability in many different types of tumors. We found *MALAT1* to be overexpressed in glioblastoma specimens compared to normal brain and to be associated with total tumor volume. The downregulation of *MALAT1* by RNAi (RNA interference) drastically impairs migration, thus it is a very interesting potential target in the context of invasive tumors such as glioblastoma.

Résumé

WIF1 a été sélectionné en tant que putatif suppresseur de tumeurs dans le cadre des glioblastomes par une analyse qui a était conduit à partir des données d'expression de gènes provenant d'environ 80 glioblastomes. *WIF1* code pour une protéine destinée à la sécrétion qui antagonise la voie de WNT et son expression est fortement sous-exprimé dans la plupart des glioblastome par rapport à tissu cérébral normal. Cette sous-expression est due à deux mécanismes différents: à la délétion de la partie génomique codant pour *WIF1* et à l'hyper méthylation de son promoteur.

La surexpression de *WIF1* réduit la capacité de prolifération des cellules de glioblastome *in vitro* ainsi que *in vivo* et elle réduit aussi leur capacité migratoire. Il est intéressant de remarquer que l'espression de *WIF1* induit un phénotype sénescent caractérisé par l'apparition de cellules aplaties, multi nucléées et positives pour l'activité de l'enzyme β-galactosidase associée à la sénescence, un marqueur tardif de la sénescence. Il est à noter que le phénotype sénescent qui est induit par WIF1 est indépendant de p53 et pRB, deux voies qui ont été largement associées à ce processus. L'analyse des les voies de signalisation en aval de *WIF1* a apporté des résultats intéressants. L'expression de *WIF1* inhibe la voie canonique de WNT, mais l'altération de cette voie seule ne pouvait pas expliquer tous les effets induits par *WIF1*. Nous avons pu prouver que certains changements sont liés à l'inhibition de la voie non-canonique qui est activée par WNT5α. Par exemple, une réduction drastique de la phosphorylation de ERK et p38 à la fois a été détectée lorsque *WIF1* a été surexprimé ou *WNT5α* sous-

exprimé. En raison de la complexité de la voie non–canonique, il est difficile de définir le mécanisme précis de la transduction du signal. Nous avons exclu l'implication de la voie JNK-WNT5α-AP1 et les résultats préliminaires suggèrent l'implication de la voie de signalisation appelée WNT-calcium.

En plus, l'analyse du profil d'expression génique de cellules sur-exprimant *WIF1* nous a permis d'identifier un candidat très intéressant: *MALAT1*, un ARN non-codants largement associés à la capacité migratoire dans nombreux types de tumeurs. Nous avons trouvé que *MALAT1* est surexprimé dans les échantillons de glioblastome par rapport à tissu cérébral normal et il est associé au volume total de la tumeur. La sous-expression de *MALAT1* altère considérablement la migration des cellules tumorales. Donc, *MALAT1*, est une cible potentielle très intéressante dans le cadre d'une tumeur invasive telle que le glioblastome.

Introduction

Glioma Tumors and Glioblastomas

1.The Pathobiology of Gliomas

Gliomas are the most common primary intracranial malignancy in humans, accounting for more than 70% of all brain tumors. Gliomas are separated into four grades according to the World Health Organization (WHO) criteria, from I to IV following increasing malignancy [1].

Astrocytoma and oligodendroglioma fall into the grade II category where the tumor lesions are characterized by hypercellularity and the median survival is 5 to 8 years. The grade III group includes anaplastic astrocytoma and anaplastic oligodendroglioma. Their histopathological analysis shows hypercellularity accompanied by nuclear atypia and mitotic figures. The survival is around 3 years.

Glioblastoma is defined as grade IV and is the most frequent and malignant type with an incidence of 2-3 new cases per 100'000 population per year. Usually it affects adults between 45 and 70 and patient survival is extremely dismal, ranging between of 12–18 months [2, 3]. The histopathology of this tumour is extremely variable: it is defined as composed of poorly differentiated astrocytic tumour cells with mitotic activity and nuclear atypia. The main features which distinguish glioblastoma from lower grade glioma are the presence of microvascular proliferation and necrosis. Moreover, often, necrotic foci are surrounded by hypercellular zones called pseudopalisades (Figure 1).

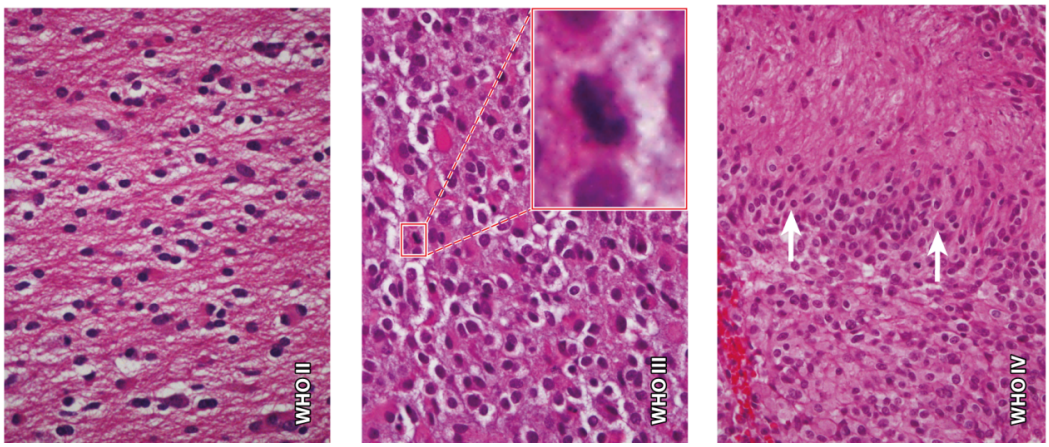

Figure 1- Representative pictures of the different WHO grade (from II to IV). Grade II: hyper-cellularity. Grade III: hyper-cellularity and nuclear atypia. Grade IV: hyper-cellularity, nuclear atypia and pseudopalisading necrosis (white arrows). (Modified from Huse T., et al. [4])

Glioblastoma can be further divided in two groups: primary and secondary. Primary glioblastoma manifests *de novo* without any evidence of a pre-existing lesion, while secondary glioblastoma develops from a lower grade glioma (II or III) [5]. Oligodendroglioma and anaplastic oligodendroglioma never progress in to a grade IV.

Primary and secondary glioblastoma constitute different diseases, the study of their genetic alterations has indeed shown that they evolve through different genetic pathways. Figure 2 describes the main genetic alterations accordingly to tumor type and degree of malignancy of adult glioma [6].

The grade II astrocytomas carry, in more than 50% of the cases, mutations of the tumor suppressor gene *TP53* and loss of heterozygosity on chromosome 17p. Gains on chromosome 7 are also common. Recently, mutations of the isocitrate dehydrogenase 1 (*IDH1*) gene (or on *IHD2*) have been identified in the vast majority of grades II and III gliomas [7]. Moreover, *ATRX* alterations are found frequently in association with *IDH1/2* and *TP53* mutations [8].

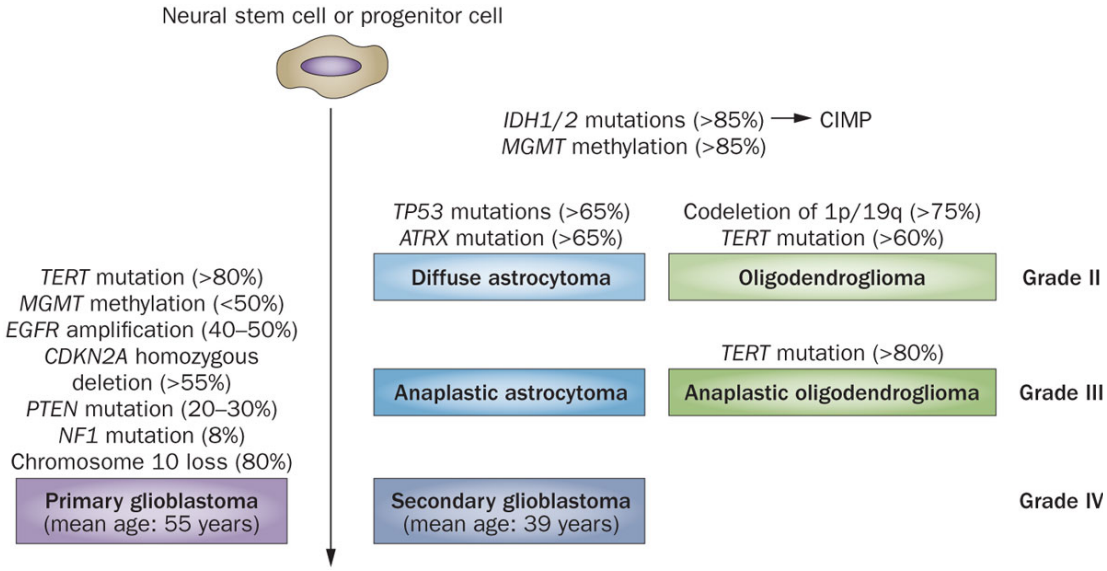

Figure 2 - Pathogenetic and epigenetic evolution of glioma in adults. Percentages indicate proportion of patients with indicated characteristic genetic alteration in each type of glioma. The mean age of primary glioblastoma is 55 years, whereas secondary glioblastoma are frequently observed in younger patients: mean age 39 years. Picture taken from Hegi, M. E. & Stupp, R. (2013)[9]

Grade III glioma shows additional genetic changes on key tumor suppressor genes such as: *CDKN2A, CDKN2B,* and *p14ARF*. Grade II and III oligodendroglioma are genetically different from the grade II and III astocytoma: they usually carry *TERT* mutation and codeletion of 1p/19q [10]. Using these genetic differences it's possible to easily distinguish oligodendroglioma from astocytoma while using histological analysis to correctly classify them, is not trivial.

Primary glioblastoma shows a complex pattern of alterations with inactivation of various tumor suppressor genes and activation of proto-oncogenes. The most important alterations being *EGFR* amplification, *PTEN* mutation, trisomy of chromosome 7, and monosomy of chromosome 10. Recently, *TERT* mutations have been added as characteristic feature of primary glioblastoma: 83% of tested cases carried *TERT* mutations while only 10% in secondary Grade IV [10]. On the

contrary, *IDH1* mutations are nearly never found in primary glioblastomas, yet are commonly detected in secondary glioblastomas, again showing the different origin of these two diseases.

2. Management and Survival of Glioblastoma Patients

The standard care for glioblastoma patients consists of a multidisciplinary approach that encompasses surgical resection, radiotherapy (RT), and concomitant and adjuvant chemotherapy [11].

The first step is surgery, where the main goal is the reduction of the symptoms that are due to tumor-induced compression of surrounding tissue. It has been shown that a more aggressive resection is associated with improved outcome. A tumor resection of > 98% doubles survival over that following biopsy alone [12]. Subsequent to surgical resection, the chemotherapeutic agent Temozolomide (TMZ) is administered daily during radiotherapy, and its use is continued after as a maintenance treatment.

TMZ is an oral alkylating agent that is rapidly absorbed and it doesn't usually provoke strong side effects [13]. The mechanism of action is through DNA methylation: the most important alteration caused by TMZ is the alkylation of the O6-position of guanine. This modification, when not repaired, acts as a trigger for apoptosis and cytotoxicity. The DNA repair enzyme methylguanine methyltransferase (MGMT) is responsible for the reparation of O6-methylguanine but it's often not expressed in glioblastoma patients due to promoter methylation. The lack of *MGMT* expression is indeed the key of the effectiveness of TMZ: it has been shown that only the subjects whose tumors harboured a methylated *MGMT* promoter benefited from TMZ, whereas the

others didn't [14]. Thanks to this study *MGMT* has become the first and still only predictive factor for therapy response and hence survival of glioblastoma patients.

The standard of care has been established during the randomised phase III trial EORTC-26981-22981 where one of the eligibility criteria for patients was a limit in age < 70. This resulted in a lack of knowledge about how to treat the group that includes elderly patients. For patients older than 70 years, less aggressive therapy is usually employed, using RT or TMZ alone. Recently, results from the NORDIC randomised phase III trial, have shown that in elderly patients standard RT is associated with poor outcomes and that TMZ and hypofractionated-RT are better therapy options. This study has also confirmed the predictive role of MGMT methylation [15].

Despite this multidisciplinary approach the survival is still extremely dismal with a median around 15 months. Age at diagnosis plays a very important role, for patients > 60 years old the survival drops to less then 12 months. The cause of death is usually the recurrence of the original tumor. Virtually, all glioblastomas re-grow within 2 cm from the location of the original neoplasm. This is due to the extremely high capability of glioblastoma cells to migrate and to invade the surrounding brain structures, increasing the difficulty of extensive surgical resection and thus leading to recurrences (Figure 3).

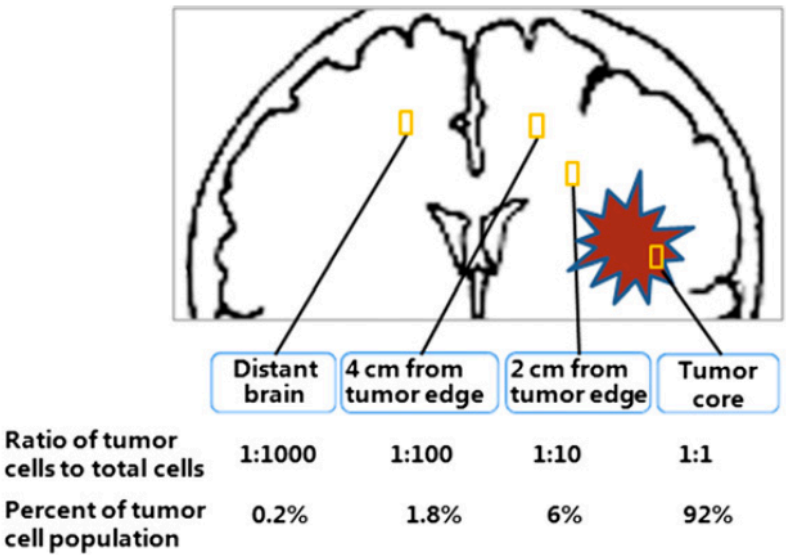

Figure 3 - The model for glioma invasion: glioma cells migrate along the already existing brain structures. As consequence of such extended invasion the resection is not 100% complete and it is followed by tumor relapse. Figure adapted from Wang et al. [16].

The WNT Pathways

1. The Canonical WNT pathway

The WNT signaling is implicated in many fundamental mechanisms that control cell proliferation, cell polarity, cell fate and tissue homeostasis [17]. The importance of this pathway was made clear by the level of evolutionary conservation: WNT ligands are conserved in all metazoan animals [18]. The first branch of the WNT signaling that has been discovered and intensively studied is called the canonical WNT pathway or β-catenin dependent pathway (Figure 4). The name is attributed to the main output of this complex signaling cascade, which regulates the available amount of the β-catenin in the nucleus. Subsequently, β-catenin regulates the transcription of a plethora of target genes.

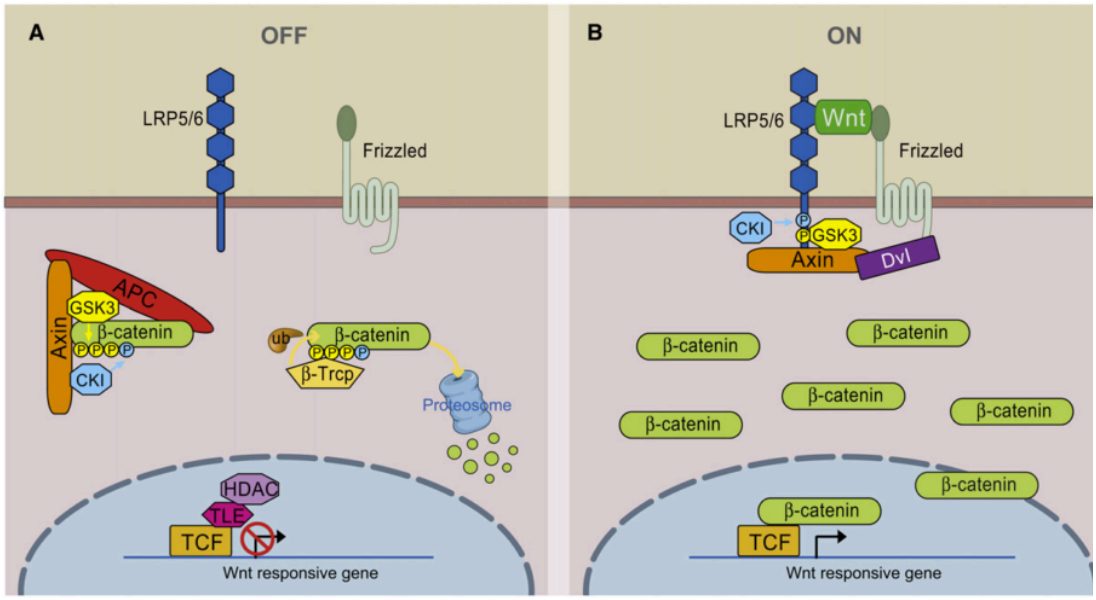

Figure 4 – The two states of the canonical WNT pathway: on the left is a scheme of the OFF state while on the right is pictured the activated state. Figure from Bryan T. MacDonald et al [19]

In mammals, there are 19 different WNT ligands, which are cysteine-rich proteins of approximately 350–400 amino acids [20]. Upon translation WNT ligands enter the endoplasmic reticulum where they undergo multiple post-translational modifications. The most important being glycosylation and acylation, where the latter is essential for their biological activity. After maturation WNT ligands are secreted and they can bind to proteoglycans and lipoprotein particles to form gradients, necessary for the correct signal transduction.

As mentioned before, when WNT ligands are not available the machinery to degrade β-catenin, named the destruction complex, is active.

This complex includes different proteins: Axin, adenomatosis polyposis coli (APC), protein phosphatase 2A (PP2A), glycogen synthase kinase 3 (GSK3) and casein kinase 1α (CK1α). β-catenin degradation is achieved by its phosphorylation at different residues by both kinases CK1α and GSK3. These modifications create a binding site for the E3 ubiquitin ligase β-Trcp that, subsequently, ubiquinates β-catenin. Ubiquitinated β-catenin is then recognised as a substrate for proteasomal degradation [21].

When WNTs are available they bind to the receptors and start the activation of the signaling. There are different receptors involved: the most important are the Frizzled (FZD) receptors, encoded by 10 different genes in the human genome, and low-density lipoprotein receptor related protein 5 or 6 (LRP5/6).

The binding of WNT proteins to the extracellular domain of FZ and LRP5/6 induces the phosphorylation of the cytoplasmic tail of Lrp5/6 by GSK3 generating several docking sites for Axin. The delocalisation of Axin to the cytoplasmatic membrane disrupts the destruction complex thus impairing the

degradation of β-catenin. The increased availability of β-catenin is reflected in an increase of translocation into the nucleus, by a poorly defined mechanism, where it serves as a co-activator for the TCF/LEF transcription factors.

The TCF/LEF family of transcription factors are the main partners for β-catenin. When β-catenin is degraded and not available in the nucleus TCF represses gene expression by interacting with the repressor TLE1. WNT pathway activation induces the accumulation of β-catenin in the nucleus where it interacts with TCF, displacing TLE1 and activating gene transcription by recruiting other co-activators [22].

2. The Non-canonical WNT pathways

The non-canonical WNT pathways are less characterised than the canonical pathway. They are generally defined as WNT or FZD dependent signaling that are β-catenin independent. As is shown in Figure 5, there are many different signaling cascades described. Often the boundaries between the depicted branches are not rigid and the overlap between them shouldn't be underestimated.

The Planar Cell Polarity Pathway (PCP)

One of the non-canonical WNT pathways is the planar cell polarity (PCP) pathway. This pathway was first discovered and defined in *Drosophila*. What is known in vertebrates, is that the binding of WNT5a and WNT11 to Fz receptor is

involved in the regulation of cytoskeleton and cell adhesion. The signaling runs through activation of DVL and, usually, via activation of ROCK and JNK [23].

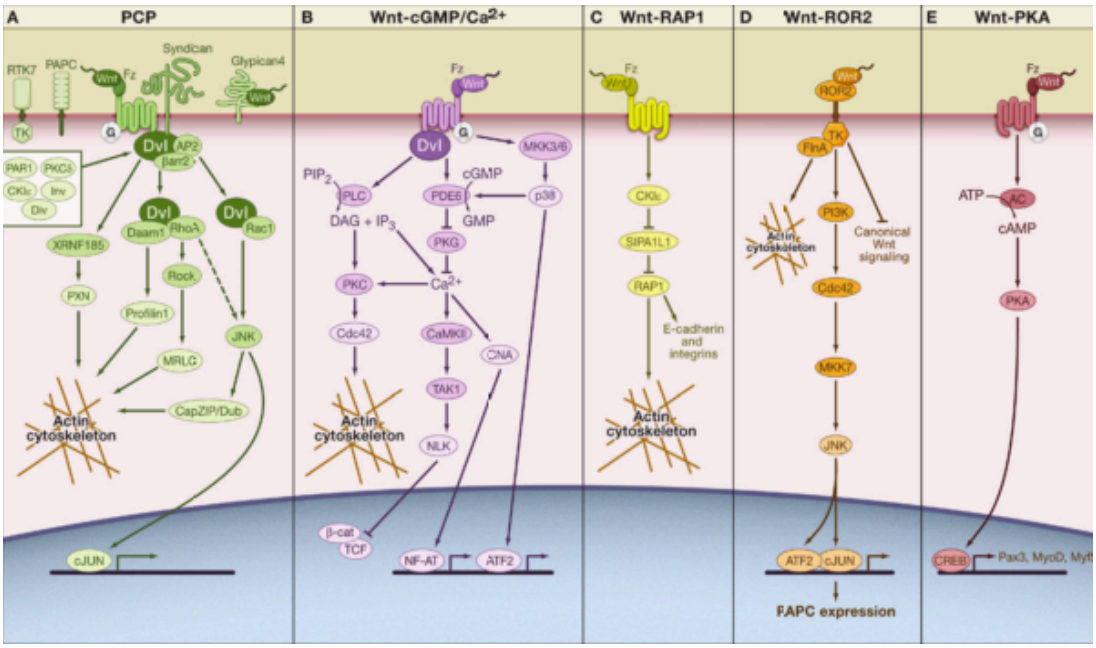

Figure 5. An overview of the different non-canonical WNT signaling pathways. The cartoon is taken from Semenov, M. et al. [24].

The Calcium Pathway

WNT5 and WNT11 have also been implicated in promoting a different non-canonical WNT pathway named the calcium pathway. The binding with the receptor, usually Fz2, regulates the intracellular Ca^{2+} level. This pathway activates protein kinase C (PKC) and CaMKII affecting cell adhesion and inhibiting the canonical WNT pathway. The stimulation of p38 kinase, via MKK3/6, has also been described [25].

Other Non-Canonical Pathways

Several other less defined signaling pathways have been described in vertebrates. Here is a concise list of what is known:

1 - WNT8 is implicated in the WNT-RAP1 axes that controls the actin cytoskeleton and cell adhesion during vertebrate gastrulation.

2 - ROR2 is a receptor that when is bound to WNT5α it activates the JNK pathway, resulting in activation of the transcription factors ATF2 and cJUN. Wnt5a/ROR2 signaling has been shown to downregulate β-catenin signaling.

3 - WNT-PKA signaling is instead implicated in myogenesis. WNT1 and WNT7α cause an increase in cAMP levels, which activates PKA and the transcription factor CREB.

3. WNT Pathways Agonists and Antagonists

The WNT pathway is finely regulated by a plethora of secreted proteins that act as agonists or antagonists (Figure 6).

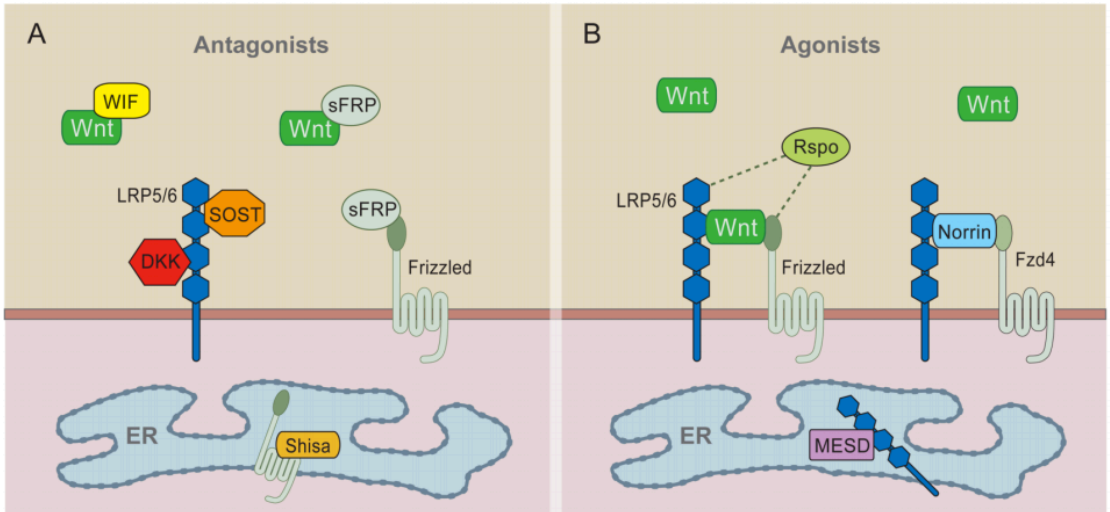

Figure 6 – WNT pathway agonists and antagonists: a schematic view.
A) Antagonists: WIF and sFRP work as decoy by binding to WNT ligands and preventing the interaction with the designated receptors. DKK and SOST/ WISE proteins prevent the formation of the interaction between FZD and LRP6. SHISAs prevent the transport of FZD from the ER to the membrane.
B) Agonists. WNT ligands interact with the receptors and activate the downstream signaling. Norrin works as a WNT ligand, but it binds only to Fz4. Picture taken from MacDonals et al.(2009)[19].

The first group of antagonists includes the secreted Frizzled related proteins (sFRPs), and WNT inhibitory protein 1 (WIF1). They are secreted proteins that bind to WNT ligands and prevent their interaction with the receptors. Since they can bind to the majority of WNT ligands they are able to inhibit both the canonical and the non-canonical pathways [26]. Two other distinct classes of WNT inhibitors are the Dickkopf (DKK) family and the Wise/SOST family. These antagonists can modulate only canonical WNT signaling by destabilisation of FZD-LRP6 receptor [27-29].

The last group includes the Shisa protein. Here the mechanism of inhibition is based on the retention of FZD protein in the endoplasmic reticulum [30].

For what concerns the agonists of the WNT pathway Norrin and R-spondin proteins are the two main players. Although Norrin is not related to WNT family proteins, it functions like a WNT ligand. It binds with high affinity the receptor Fz4 and induces the activation of the WNT canonical signaling [31]. The R-spondin family can instead positively regulate both canonical and non-canonical WNT signaling pathways. Although the R-spondin-dependent regulation of the WNT pathway has been established in several *in vitro* and *in vivo* studies, it's still unknown if they activate the pathway independently or in complex with other WNT ligands [32].

WNT inhibitory factor 1 – WIF1

The human *WIF1* gene is located on the chromosome 12q14.2. It is oriented on the minus strand and comprises 10 exons spanning 71007 bp of genomic DNA. The mRNA produced is 2304 base pair long. The promoter region of *WIF1* has

been cloned and studied by Reguart et al. [33], and its structure is shown in Figure 7. Regulatory elements in the *WIF1* promoter comprise a TATA box and binding sites of the transcription factors: Engrailed, E2F, GLI-Krueppel, NF-κB, and MYC. The CpG island, located upstream of the *WIF1* transcriptional start site, when hypermethylated is responsible for WIF1 expression downregulation.

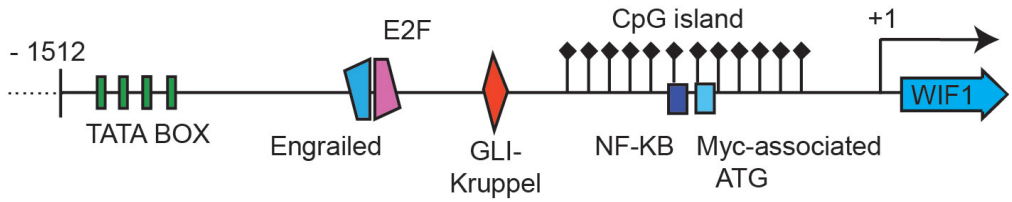

Figure 7. Structure of human *WIF1* promoter

WIF1 is a protein of 379 aminoacids, composed of a signal peptide for extracellular secretion, a WIF domain, five EGF repeats and a hydrophilic C terminus (Figure 8).

Figure 8. WIF1 protein structure

The WIF domain is responsible for the binding with the WNT ligands and to olfactomedin 1, a protein involved in neuronal differentiation [34]. In development WIF1 starts to be produced during somitogenesis and maintains its

expression in adults mainly in the lung, heart, and at the cartilage-mesenchyme interface (data derived from Xenopus, zebrafish and mouse).

WIF1 is a secreted WNT inhibitor that works by sequestering soluble WNT proteins. It prevents the interaction between WNT morphogens and their specific receptors (Figure 9). WIF1 has been shown to bind to agonists of both, the canonical and the non-canonical WNT pathway. In contrast to other inhibitors like DKKs that can inhibit only the β-catenin dependent pathway, WIF1 can block the activation of both the canonical and the non-canonical WNT signaling pathway [35]. It has been shown by Malinauskas et al. that WIF1 has a modular mechanism of inhibition [36]. The WIF domain is responsible for the binding with WNT ligands and the five EGF-like domains seems to be partially involved in the extracellular localization of WIF1. The essential formation of gradients of WNT morphogens during development is mediated by interaction of the EGF-like domains and some glycosaminoglycans, namely heparin and heparan sulfate.

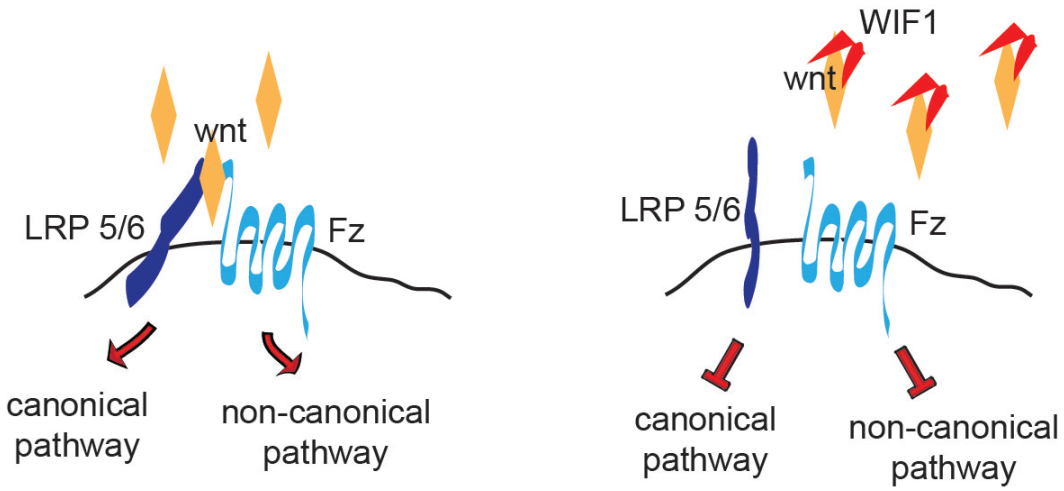

Figure 9. WIF1 inhibition mechanism.

Implications of the WNT Pathways in Tumor Development and Progression

The WNT pathway controls many aspects of cell fate, cell growth and tissue homeostasis, thus it's not surprising that abnormalities in WNT signaling are found in a wide range of cancers [37].

The close association between tumor development and WNT pathways is indeed well described by the anecdote of how the first *WNT* encoding gene was discovered in mice. *WNT1* was identified as an inducer of mammary tumor formation in mice when infected with the murine mammary tumor virus [38].

With recent progress in sequencing technology the list of *WNT*-related alterations is constantly growing. The most famous and common alterations are those that affect the *APC* gene. *APC* defects are both the cause of familial adenomatous polyp

osis, a syndrome that ultimately leads to colorectal cancer, and mutations are found in the vast majority of all sporadic colorectal cancers [39]. Beside mutations, epigenetic modifications in DNA and chromatin status have been shown to play an important role in tumor progression by modulation of expression of *WNT* genes [40]. Indeed, genome-wide analysis of promoter DNA methylation in different cancers showed common repression of WNT pathway inhibitors such as *sFSR1, WIF1* and *DKKs* [41].

Another mechanism that has been described concern chromatin modifications that lead to gene activation. The carboxyl terminus of β-catenin can associate with many chromatin-remodelling enzymes that mediate the establishment of histone marks associated with highly active genes [42].

WIF1 association with cancer

WIF1 expression deregulations have been associated with several type of cancer:

1) **Cervical cancer**. *WIF1* is downregulated by promoter hypermethylation in 87.5% of primary cervical cancer. Peritumoral *WIF1* gene transfer induces apoptosis and inhibits growth and invasion [43]

2) **Primary non-small-cell lung carcinoma** (NSCLC). *WIF1* is frequently downregulated and this downregulation is correlated with *WIF1* promoter hypermethylation [44].

3) **Osteosarcoma**. Hypermethylation of the *WIF1* promoter is found in the majority of osteosarcoma cell lines tested and it correlates with *WIF1* mRNA downregulation [45].

4) **Hepatocellular carcinoma** (HCC). *WIF1* is frequently dowregulated through promoter hypermethylation [46].

5) **Mesothelioma**. *WIF1* promoter methylation was reported from 73.9% of mesothelioma tissues and in 100% of tested mesothelioma cell lines [47]

6) **Renal cell carcinoma** (RCC) *WIF1* is downregulated by promoter methylation and when re-expressed induces apoptosis in RCC cells [48].

7) **Bladder cancer.** Epigenetic inactivation of *WIF1* in bladder cancer deregulates WNT pathway activation. *WIF1* re-expression induces a G1-arrest via p27 and p21 accumulation [49, 50].

8) **Esophageal adenocarcinoma** (EAC). Epigenetic alteration of *WIF1* is an early event in the carcinogenesis of EAC. It's suggested to be involved in the progression from Barrett's esophagus (BE) to EAC thus *WIF1* hypermethylation

is proposed to be used as a diagnostic and predictive marker for increased EAC risk in BE patients. [51].

9) **Gastrointestinal cancers.** *WIF1* expression has been reported to be downregulated in 80.0% of esophageal, 74.2% of gastric, 82.0% of colorectal, and 75% of pancreatic cancer tissues. *WIF1* silencing, mediated by hypermethylation, is proposed to be an early event in colorectal carcinogenesis [52].

10) **Breast Cancer.** 67% of breast adenocarcinoma (Stages II or III) shows aberrant *WIF1* promoter methylation [53].

11) **Salivary gland pleomorphic adenoma.** *WIF1* is rearranged resulting in a *HMGA2/WIF1* fusion transcript. In consequence of this fusion WIF1, that in normal salivary gland tissue is highly expressed, becomes downregulated. On the contrary, HMGA2 that in normal tissue is not expressed is strongly upregulated [54].

WNT Pathway in Glioblastoma, The State of the Art

Many different groups have been studying the role of the WNT signaling pathway in glioblastoma. Although there are publications showing the involvement of WNT in glioblastoma a complete view concerning this topic is still missing.

For what concern the biological role, the activation of the WNT canonical pathway has been associated with maintenance of glioma-initiating cells (GICs). β-catenin signaling is crucially involved in controlling stem cell fate during development and it has been shown that in glioblastoma it has a role in the maintenance of the self-renewing capability of GICs [55].

The alteration of the pathway is achieved on many different levels. In contrast to other cancers, mutations are not really common. The analysis of either *APC* or the *β-catenin* encoding locus has not identified mutations. Only recently a mutation has been clearly associated with WNT pathway activation: FAT1 inhibits the canonical pathway by binding β-catenin and preventing its nuclear localization[56]. Mutations of FAT1 have been identified in glioblastoma [56]. Deregulation of several WNT antagonists has also been reported, including secreted frizzled-related proteins, DKK, and NAKED [41].

The non-canonical WNT pathway has not been extensively investigated and there are only two papers concerning the role of WNT5α in glioblastoma. Both publications found *WNT5α* to be an oncogene, involved in the maintenance of the invasive phenotype of glioblastoma [57, 58].

WIF1 project: introduction and goals

1. Project introduction

The WIF1 project derives from results obtained in the analysis of the genomic copy number aberrations of a cohort of glioblastoma patients.

Frozen tumor samples were collected in the context of a randomised phase III trial aimed to test radiotherapy and concomitant TMZ as treatment for glioblastoma [11]. From this cohort 67 tumors were extensively profiled: gene expression analysis was already established previously as reported in Murat et al. [59] and copy number aberration analysis was performed using the Array Comparative Genomic Hybridization (aCGH) technique. One of the goals of the aCGH project was to discover new genetic alterations to explain pathological molecular mechanisms that contribute to glioblastoma malignancy.

Data derived from High-throughput techniques carries a lot of new information but, however, extracting relevant and reliable information from such data is not trivial. aCGH data are usually really noisy due to a combination of different reasons such as tumor heterogeneity and contamination with normal tissue. Moreover, when the final aim is to find targets suitable for drug design, it should not be forgotten that, besides genomic alterations, there are many other pathological mechanisms that can contribute to altered gene expression. For example, both alterations of chromatin status and gene promoter methylation have been shown to be extremely important in modulating gene expression and thereby tumor development. Here, to minimize the risk of selecting false positive

or biologically irrelevant targets, a multidimensional approach was chosen. Genomic alterations were predicted from the gene expression profiles using a hidden markov model (HMM), developed by Dr. Mauro Delorenzi of the Swiss Institute of Bioinformatics (SIB). This approach allowed the prediction of deregulated loci of interest since changes in expression reflect both genomic alterations and epigenetic changes.

By using these methods a very interesting genomic region was discovered on chromosome 12q14–12q15. Two well-known oncogenes, *CDK4* and *MDM2*, are encoded in this region [60]. They are very often amplified in glioblastoma and the amplification of these two regions was also predicted by our analysis. However, the interesting feature of the selected genomic region is the portion that is in between the two amplified loci where the probability of amplification is extremely low. The overall region is relatively small; as such it wouldn't be expected to find two distinct amplified peaks. This observation could point to a region, located between the two amplified loci, potentially targeted for expression silencing (Figure 10A).

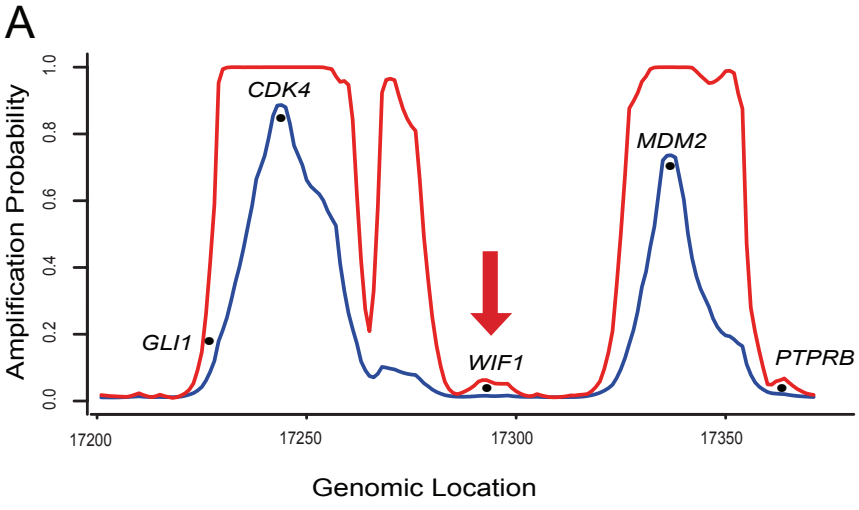

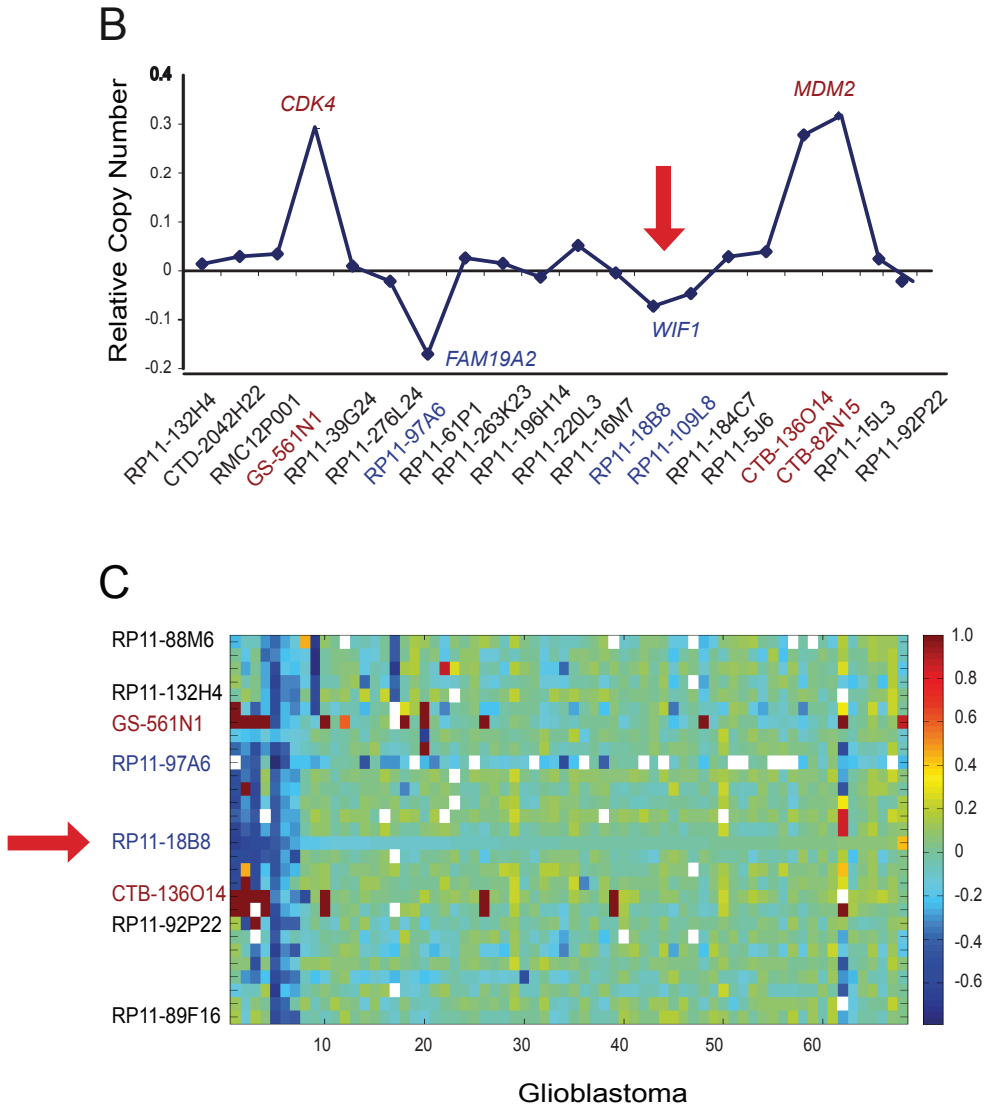

Figure 10. Gene expression–based prediction of copy number aberrations (CNAs) in glioblastoma.
(A) The maximum (red) and mean (blue) amplification probabilities on chromosome 12q14–12q15 were estimated from gene expression data. The interrogated region flanked by CDK4 and MDM2 encompasses a 11 Mb window. (B) The respective mean DNA copy number of this chromosomal region was determined by aCGH. The bacterial artificial chromosome (BACs) corresponding to CDK4 and MDM2 are shown in red. (C) The heat map visualizes the structure of the aCGH data shown in (B) for the genomic region encompassing 12q13 to 12q15 from 68 glioblastomas. The BACs are ordered by their genomic position, while the glioblastomas on the x-axis are ordered by similarity using Sorting Points into Neighborhood software [61]. Blue depicts deletion; red, amplification; and white, missing data. The red arrows show where the locus that encodes for WIF1 is located. Figure taken from Lambiv et al. [62]

The low probability of amplification predicted from the gene expression profile data was indeed confirmed by aCGH. Figure 10B and C show the aCGH results.

The mean DNA copy number of the region 12q14–12q1 is presented in figure 7B, here it is indeed possible to see the confirmation of the deletion of the two loci located between *CDK4* and *MDM2*. Most samples exhibit a deletion between these two loci thus suggesting a merged amplicon of *CDK4* and *MDM2* probably organized extrachromosomally in double minutes [63, 64]. Among the potential candidate target genes, encoded from the deleted loci, *WIF1* was the most interesting. As explained in the introduction, this gene encodes a secreted WNT antagonist [34, 35] and it is thus predestined as a candidate tumor suppressor. The interaction of WIF1 with WNT ligands blocks their binding with the cell surface cognate receptor, thus downregulating activation of the pathway. Hence, loss of *WIF1* expression is expected to aberrantly activate WNT signaling, which is associated with cancer. CpG island hypermethylation of the *WIF1* promoter as a silencing mechanism has been described in several epithelial cancers [49, 52] and more recently also in glioma where it seems to be associated with tumor grade [65].

Moreover, *WIF1* expression in the glioma data set was encouraging: the expression was significantly lower in glioblastoma than in 4 nonneoplastic brain tissues (Figure11A). The low expression of *WIF1* in glioblastoma was also confirmed in all 5 independent glioblastoma data sets analyzed [66-70](Figure 11B)

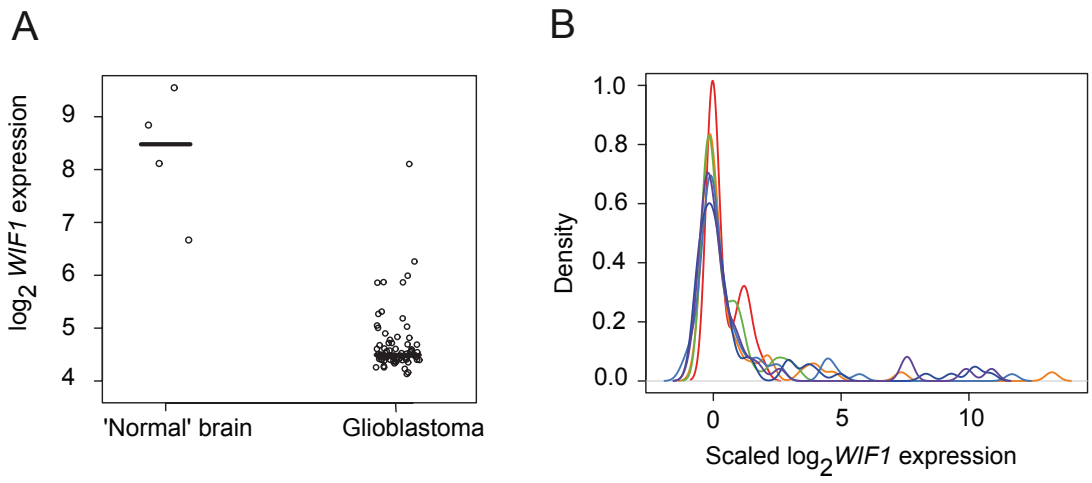

Figure 11. WIF1 expression is significantly low in glioblastoma when compared with normal brain tissue. (A) WIF1 expression (Affymetrix probe set 204712_at) in glioblastoma is significantly lower than in non-neoplastic brain tissues (P value < 0.001), as determined in our gene expression data set. (B) Low WIF1 expression was confirmed in 5 independent glioblastoma data sets (Freije et al. [69], red; Rich et al.[68], violet; Phillips et al.[67], orange; Sun et al.[66], dark blue; Horvath et al.[70], green; our data set, Murat et al.[59], light blue). WIF1 expression values are median centered within each data set independently. Figure taken from Lambiv et al. [62]

The expression data suggested low *WIF1* expression in 76% of glioblastoma and corresponding analysis of the aCGH data showed hemizygous deletions at the *WIF1* locus in only 10% (7/69). A more extended study of *WIF1* downregulation showed that this discrepancy was the result of alternative mechanisms of silencing rather than only genomic deletion. The analysis of the *WIF1* promoter by methylation-specific PCR (MSP) revealed hypermethylation in 2 of 6 glioblastomas with hemizygous deletion. In an extended series of 110 glioblastoma, 26% exhibited a methylated *WIF1* promoter (Figure 12), and most established glioblastoma cell lines (14 of 15) showed hypermethylation of the *WIF1* promoter.

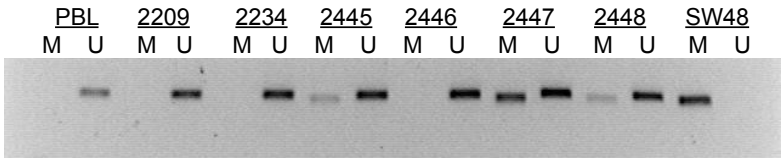

Figure 12 - Promoter methylation of *WIF1* in glioblastoma. DNA isolated from peripheral blood lymphocytes (PBLs) and the colon cancer cell line SW48 served as controls for unmethylated (U) and methylated (M) WIF1 promoter status, respectively. Glioblastomas 2445, 2447, and 2448 contain a methylated WIF1 promoter, whereas the others harbor only an unmethylated gene promoter. Figure taken from Lambiv et al. [62]

To functionally confirm the epigenetic deregulation of *WIF1,* several glioblastoma cell lines were treated with the DNA demethylating agent 5-aza-cytidine (5-AZA) for 96 h. *WIF1* expression was restored upon the demethylation treatment (Figure 13).

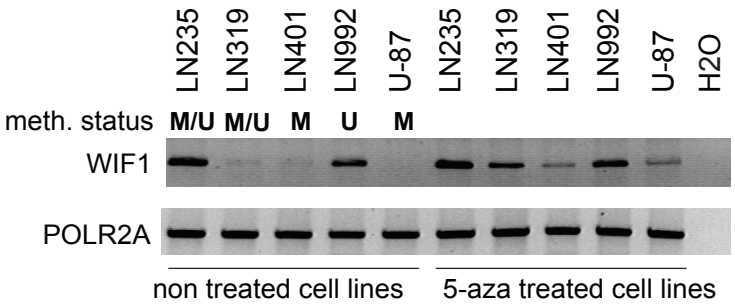

Figure 13. 5-AZA-treatment induces *WIF1* re-expression in methylated glioblastoma cell lines
Glioblastoma cell lines were treated with the DNA demethylating agent 5-aza-cytidine for 4 days. All 3 *WIF1* nonexpressing cell lines with a methylated *WIF1* promoter re-expressed *WIF1* mRNA in response to 5-aza-cytidine treatment (LN319, LN401, U87). Only LN992 was completely unmethylated. The lower panel shows mRNA expression of the *POLR2A* gene used to control for mRNA quality. The methylation status of the cell lines displayed was determined by MSP. Figure taken from Lambiv et al. [62]

These data show the presence of two different mechanisms playing a role in targeting *WIF1* for silencing: epigenetic modifications and genomic alterations. Complementing mechanisms to ensure downregulation are key indications for the presence of tumor suppressor genes: the "two-hit hypothesis" implies that both alleles that code for a particular tumor suppressor must be affected before an effect is manifested [71].

2. Project goals

WIF1 was identified to be a potential tumor suppressor gene in glioblastoma. The exhaustive analysis of *WIF1* functions was needed to have a better understanding of its tumor-suppressive functions. Moreover the characterisation of the molecular mechanism behind the tumor-suppressive phenotype could lead to the identification of new target for therapy.

The main goals of this project were:

1. Characterisation of cellular phenotype upon reintroduction of *WIF1* expression.
2. Evaluation of tumor suppressive functions both *in vitro* (growth and agar assay) and *in vivo* (Xenofraft in nude mice)
3. Analysis of pathway alterations induced by *WIF1* re-expression

Results and Discussion

Establishment of WIF1 Stably Expressing Glioblastoma Cell Lines

The first experiments were performed using two cell lines: LN319 and LN229 [72]. The first cell line, LN319, was transfected with either the empty vector (pcDNA3.1) or with the WIF1 expressing construct (pcDNA3.1_WIF1). After the selection, resistant clones were selected and characterised for *WIF1* expression both on the RNA level (real time PCR) and on the secreted protein level by ELISA (Figure 14A).

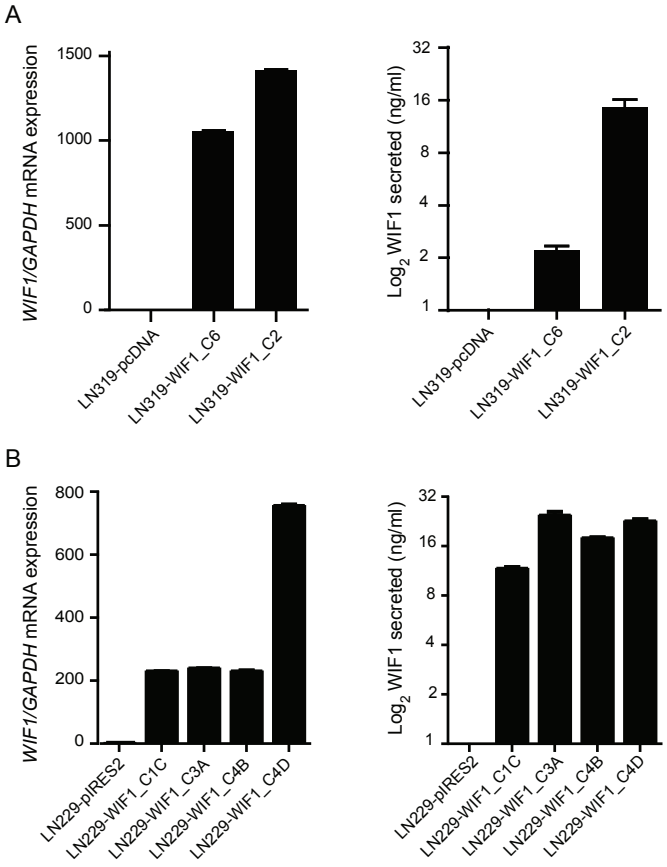

Figure 14 - Characterisation of WIF1 stable expression. The mRNA level was detected by Real Time PCR and the secreted amount of protein via specific ELISA in LN319 clones (A) and LN229 clones (B). Figure taken from Lambiv et al. [62]

The LN229 cells were instead transfected with a different backbone plasmid named pIRES2-EGFP. This plasmid allows the generation of stable cell lines that, in addition to the gene of interest, express a green fluorescence protein (EGFP). The presence of EGFP is indeed a tool to facilitate the process of selection and subsequent immunostaining/tracing of the engineered cells. As for the other cell line, many clones were initially selected and after testing for *WIF1* expression few clones were retained for follow-up studies (Figure 14B)

Stable expression of WIF1 inhibits the canonical WNT pathways

We further investigated the biological effects of WIF1 in the glioblastoma cell lines LN319 and LN229. Clones selected from stably transfected cells were characterized for WNT pathway activity. The activation of the β-catenin dependent pathway was measured by using a luciferase-based reporter assay based on two different plasmids: TOP-Flash and FOP-Flash. Both plasmids contain TCF/LEF-binding sites and a minimal promoter. The difference between the two plasmids is that TOP contains the optimal TCF-binding sites and FOP contains the mutated binding sites. The ratio of the luciferase values derived from TOP and FOP measure the activation of the WNT pathway (TOP) normalised to the background/noise signal (FOP). *WIF1* overexpressing LN319 and LN229 cells showed reduced WNT pathway activity compared with the respective control cells (Figure 15A). The downregulation of the canonical pathway was also confirmed by measuring the expression of AXIN2, a prototypic WNT target gene [73] (Figure 15B). The specificity of the observed effect on the WNT pathway was determined by silencing of WIF1 by siRNAs. WIF1 knock-

down indeed rescued transactivation of the TCF reporter in the ectopically expressing WIF1 LN319 cells, confirming that the detected attenuation of the WNT pathway was indeed WIF1 dependent (Figure 15C-D).

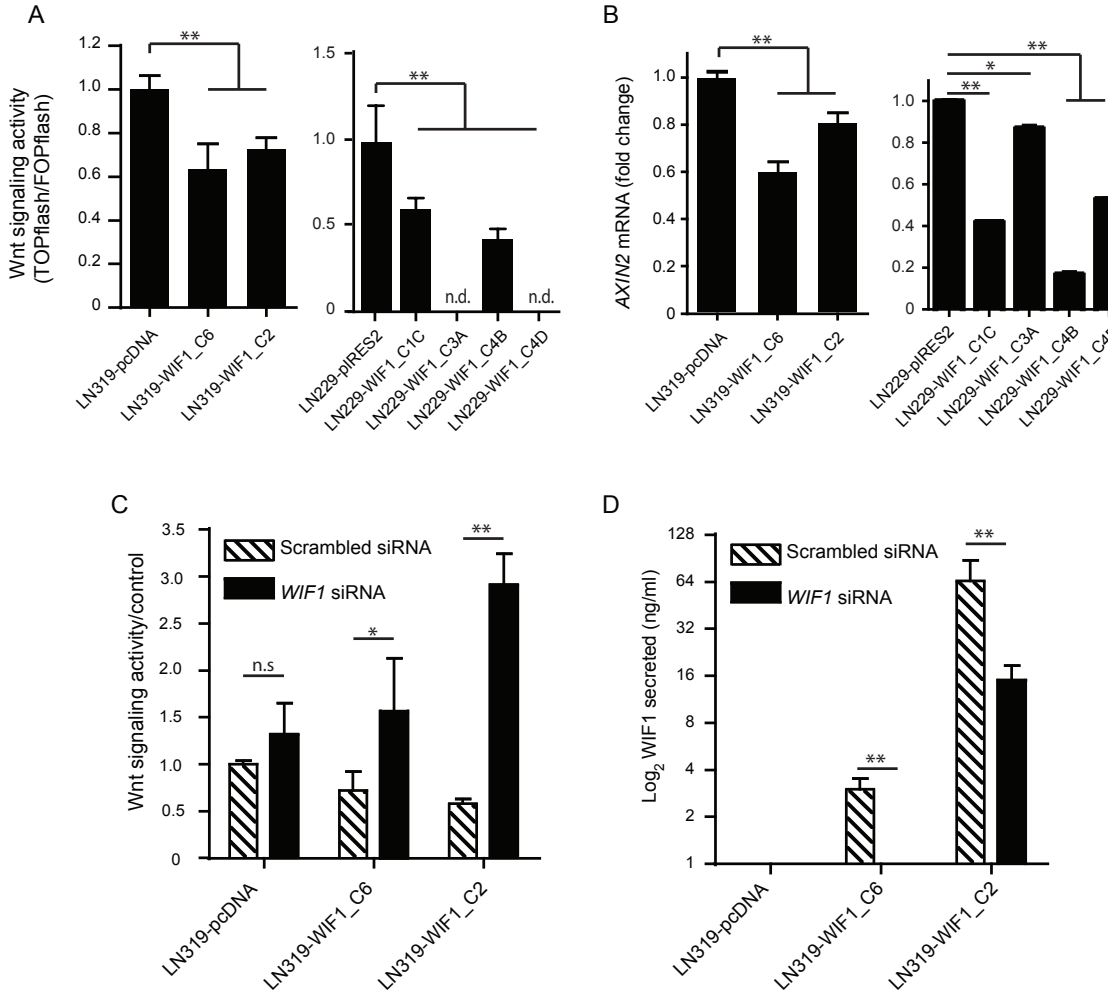

Figure 15. LN319 and LN229 clones stably transfected with WIF1 show reduced WNT pathway signaling. WNT pathway was measured both with the TCF luciferase reporter (A) and by measuring AXIN2 mRNA expression (B). The n.d. abbreviation in the panel A stands for "not detectable": the luciferase signal was below out threshold of detection. The specificity of the *WIF1*-induced effects in the LN319 clones was controlled by transfection of specific siRNAs against *WIF1* or a respective scrambled control. WNT pathway was measured using the TCF reporter (C) and WIF1 secretion using ELISA (D). Figure taken from Lambiv et al. [62]

Anchorage-Dependent and Anchorage-Independent Growth of *WIF1* overexpressing glioblastoma cells

The *WIF1*-expressing cell clones were used to investigate the effect of *WIF1*-mediated downregulation of the WNT pathway on proliferation. Anchorage-dependent proliferation measured over 3 days was significantly decreased in both WIF1-overexpressing LN319 and LN229 (Figure 16).

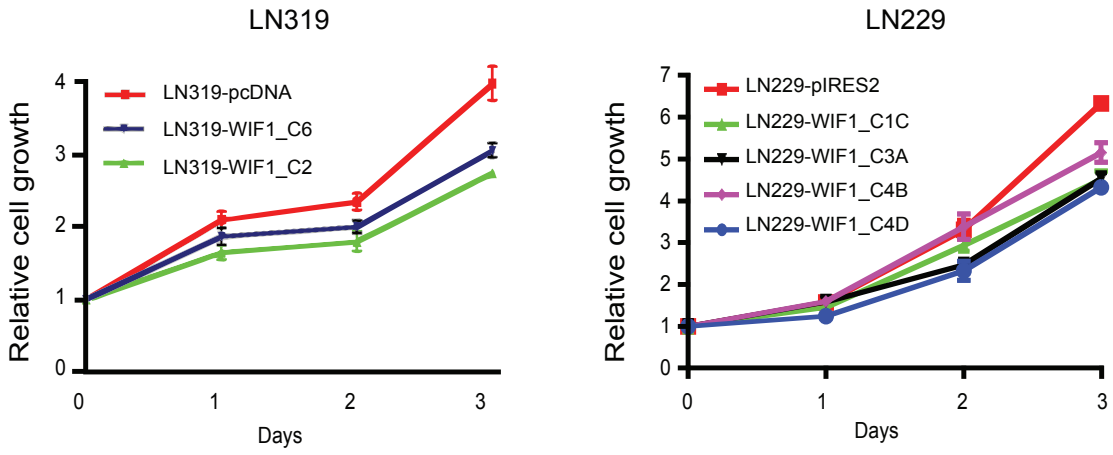

Figure 16 - WIF1 overexpression reduces the growth potential of LN319 and LN229 cells in vitro. Growth of WIF1-transduced LN319 clones and the respective empty vector control (pcDNA3.1) was followed over 3 days in culture (left panel). The same is shown for the LN229 cell lines (right panel).

Even more striking results were obtained investigating the effects on anchorage-independent cell growth. The ability to form colonies in soft agar after 3 weeks of culture was greatly reduced upon *WIF1* overexpression (Figure 14). During the soft agar experiment, we observed that *WIF1*-overexpressing clones were initially able to proliferate, forming very small clusters of cells, but then stopped dividing after a few days, potentially in response to increasing concentrations of secreted WIF1. In accordance, the colony formation potential was reduced in a

WIF1 dose-dependent manner. The high expressing *WIF1* clone LN319-*WIF1*_C2 displayed 90% fewer colonies, while in the intermediate clone LN319-*WIF1*_C6, the colony number was reduced by 63% (Figure 17 A and B). The phenotype in the LN229 was even more remarkable: three out of four *WIF1* overexpressing clones completely lost the ability to form colonies (Figure 17 C and D)

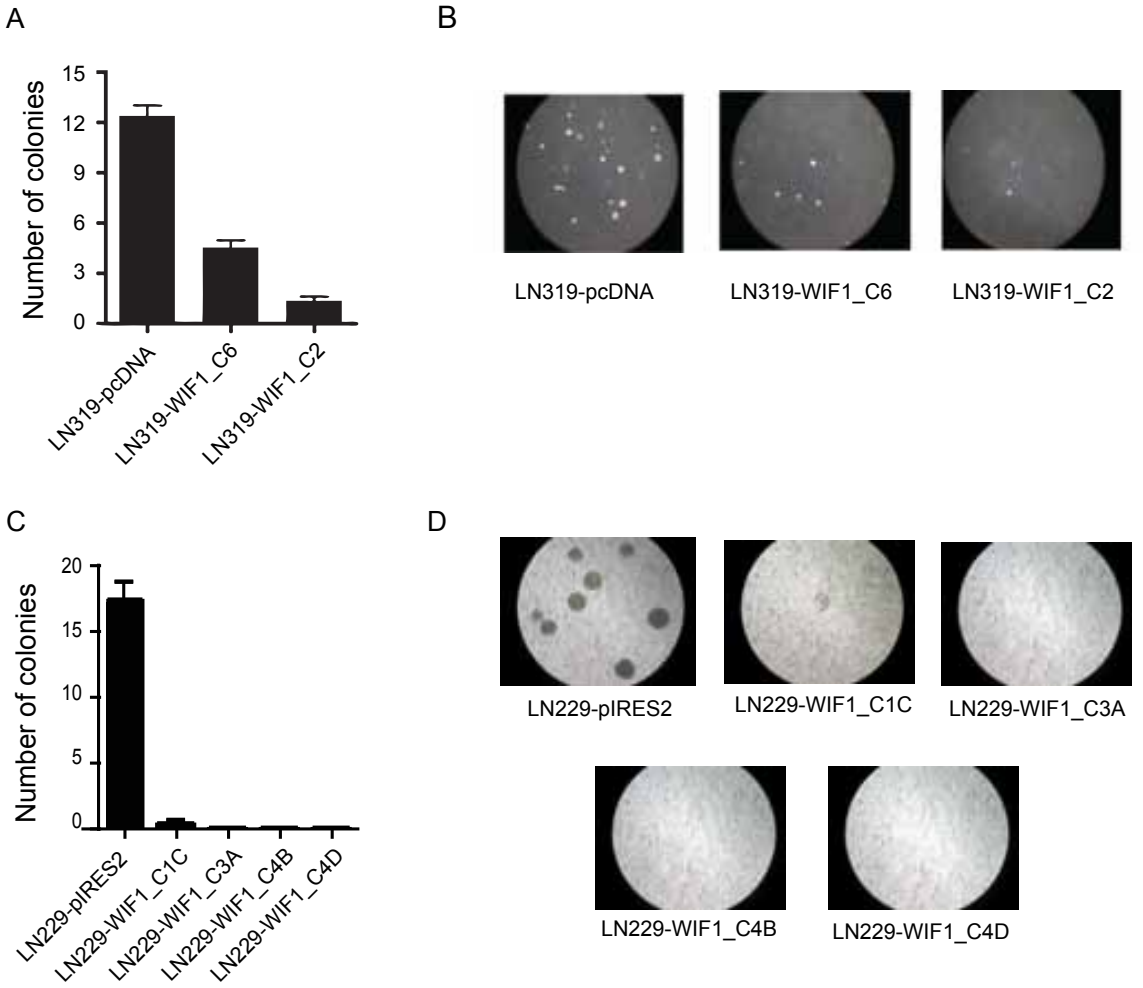

Figure 17. WIF1 reduces colony formation capability. Anchorage-independent growth was evaluated in soft agar; representative images are shown for LN319 (B) and LN229 (D). The average number of colonies counted in 10 randomly chosen fields is reported (A and C).

Analysis of *in vivo* Tumorigenicity of WIF1-overexpressing Clones

Ectopic expression of *WIF1* in LN319 cells completely suppressed the inherent tumorigenicity of this glioblastoma cell line. While mice injected with control cells started to develop tumors 25 days after injection, no tumors were detectable in the mice injected with WIF1-expressing cell clones over the observation period of 100 days (Fig. 18). Altogether, these experiments suggest an important role of the WNT pathway in the development of glioblastoma and a tumor suppressing function for *WIF1*.

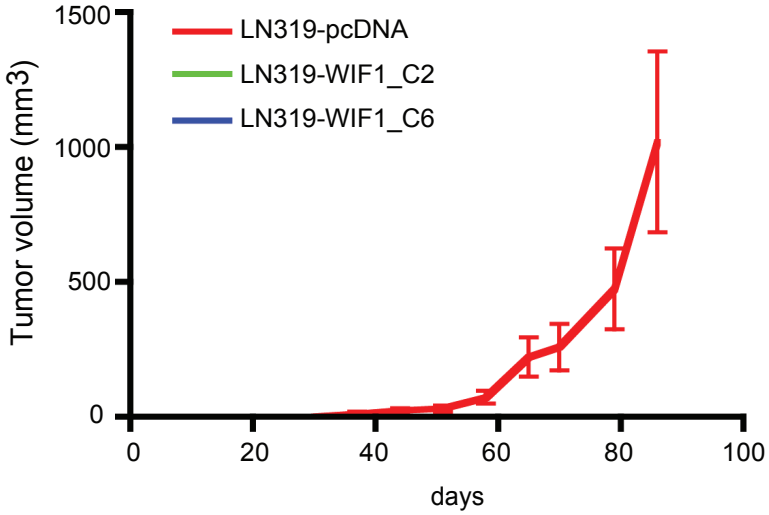

Figure 18. Tumor growth kinetics of nude mouse xenografts, after subcutaneous injection of WIF1-overexpressing clones and the corresponding empty vector control cells are displayed. The WIF1-overexpressing clones did not form any measurable tumors. The average tumor volume per group (5mice) is reported. Figure taken from Lambiv et al. [62]

WIF1 Overexpression Promotes a Senescence-like Phenotype

Observation of *WIF1*-overexpressing cells (LN319 and LN229) until confluence revealed a striking change in morphology. While control cells started to grow on top of each other without apparent contact inhibition, the *WIF1*-expressing cells displayed a phenotype reminiscent of senescent cells with increased cell size. Next we evaluated recognized markers for senescence, including enhanced granularity of the cytoplasm, appearance of multinucleated cells, and presence of senescence-associated β-galactosidase activity. [74, 75]. Quantification of morphological changes was performed using fluorescence-activated cell sorting analysis.

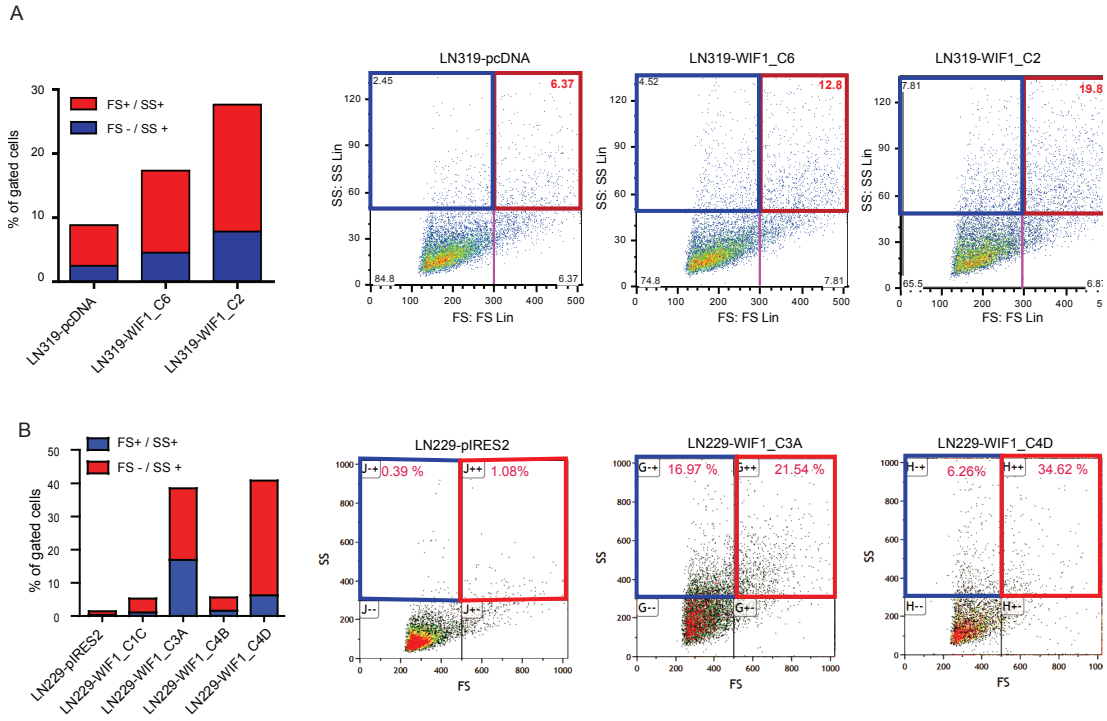

Figure 19. Cell morphology of the different LN319 (A) and LN229 (B) clones was analyzed by fluorescence-activated cell sorting (FACS). Senescence-like cells were defined as highly granulated cells, high side scatter (SS) (blue rectangle), and big cells, high forward scatter (FS) (red rectangle). Figure taken from Lambiv et al. [62]

Senescence-like cells were defined as: highly granulated cells = high SS and big cells = high FS. We detected an increased percentage of senescence-like cells in *WIF1*-transfected clones with a positive relationship to WIF1 secretion of the respective clones (Figure 19). Similar differences were observed upon double staining of the cells with SA-β-galactosidase and DAPI, which visualizes nuclear morphology. In the LN319- and LN229-derived *WIF1*-overexpressing clones, we scored an increased population of both multinucleated and SA-β-galactosidase positive cells (Figure 20).

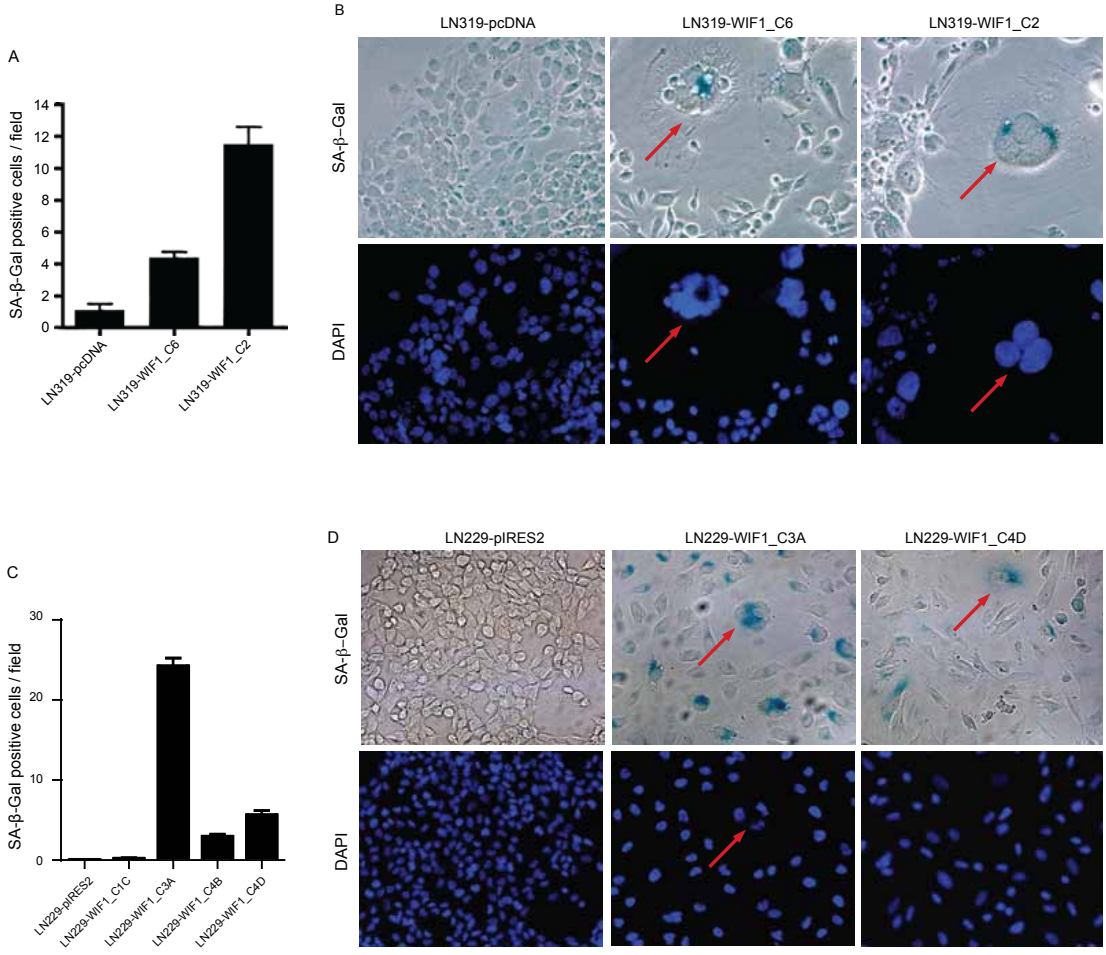

Figure 20. Quantification of LN319 (A) and LN229 (C) cells positive for SA-β-galactosidase activity scored in 10 different randomly chosen fields. (B, D) Representative images of clones stained for SA-β-galactosidase and DAPI are shown (200×). Large, SA-β-galactosidase positive (blue) and multinucleated cells are highlighted with red arrows. Figure taken from Lambiv et al. [62]

To preciselz study *WIF1* effects we decided to change our experimental approach: from the stable *WIF1*-expressing cell lines we established an inducible system. This choice was taken to be able to study the early events following *WIF1* induction and to avoid the possibility that the cells could circumvent the inhibition of the WNT pathway in response to chronic *WIF1* exposure.

Characterisation of the *WIF1*-Inducible Glioblastoma Cells

1. Development of a *WIF1*-Inducible Cell Line

We developed a *WIF1* inducible cell line in the LN229 using pTRE-Tight-BI vector (Clontec). Like all TET-ON systems, the reverse tetracycline transactivator (rtTA) protein is capable of binding the operator only if bound by a tetracycline (doxocyclin), thus the introduction of doxycycline to the system initiates the transcription of the genetic product. The advantage of this specific vector is that the inducible promoter is bidirectional: while inducing the gene of interest (*WIF1*) a red fluorescent protein (*dsRED*) is also expressed, providing a fluorescent tag useful to select the highly inducible clones (Figure 21).

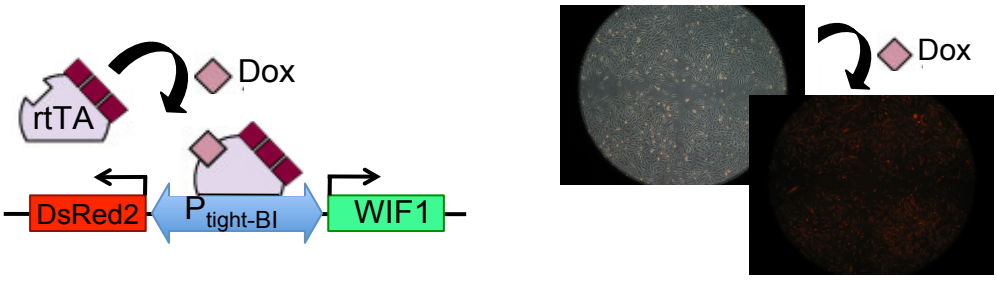

Figure 21. *WIF1*-inducible system. In the left panel shows the structure of the bidirectional promoter included in the pTRE-Tight-BI vector. In the right, representative pictures of dsRED expression are shown after 36 hours of doxocyclin induction.

To generate the inducible cell line we transfected the LN229 with three different vectors: the rtTA encoding plasmid (pUHG17-1), the Puromicyn gene to confer resistance to the Puromycin selection marker (pBABE-puro), and either the empty pTRE-Tight-BI vector or the *WIF1* encoding one. The cell line transfected with the empty pTRE-Tight-BI is named LN229_*dsRED* and it will serve as a control to exclude that either doxocyclin or the *dsRED* expression contribute to the final phenotype. The *WIF1* inducible cell line will be referred as LN229_in*WIF1*. Cells that stably integrated all three plasmids were selected. The clones that showed expression of dsRED without exposure to doxocyclin were discarded. The best clone for each cell line was then chosen accordingly to two features: 1) rapid induction of *dsRED* or *WIF1/dsRED* induction 2) highest and prolonged expression of the induced genes upon doxocyclin treatment. Figure 22 shows the induction kinetics for the two clones that were finally selected. It should be noted that the cell line LN229_*dsRED* shows a higher induction of *dsRED* compared to the LN229_ind*WIF1*. This difference can be attributed to concomitant expression of *WIF1* in the second cell line.

We also tested the secretion of WIF1 via ELISA and we followed the secretion over 8 days (Figure 23). While the peak for WIF1 transcription is around 24 hours, for the secretion of the protein an additional 24 hours are needed.

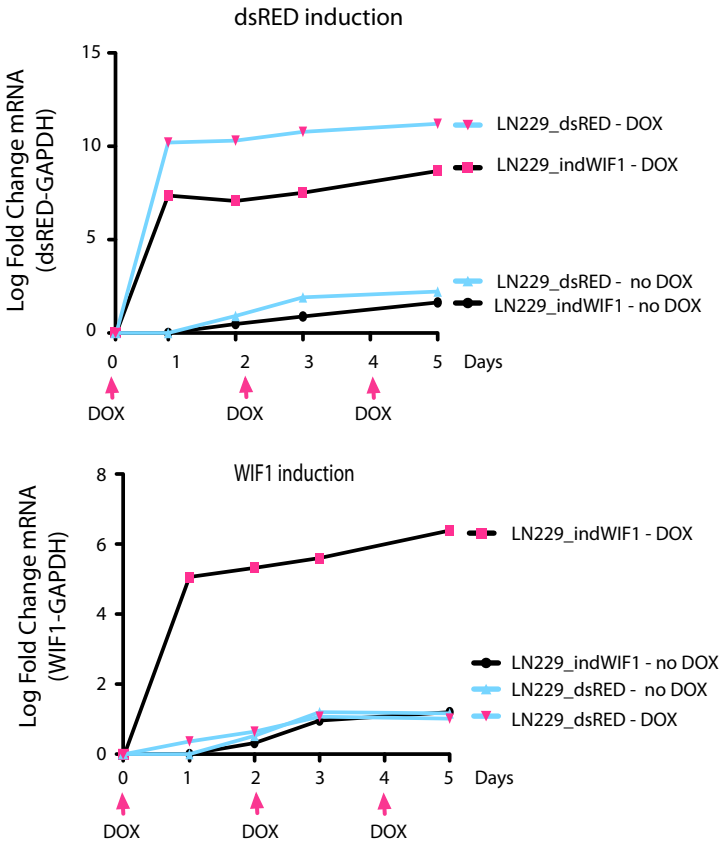

Figure 22 – The kinetics of induction of both *dsRED* (upper panel) and *WIF1* (lower panel) are measured in LN229_*dsRED* and LN229_ind*WIF1* by Real Time PCR. Doxocyclin was added at T zero (1µg/ml) and to maintain the induction it was re-added to the medium every 48 hours (0.5µg/ml)

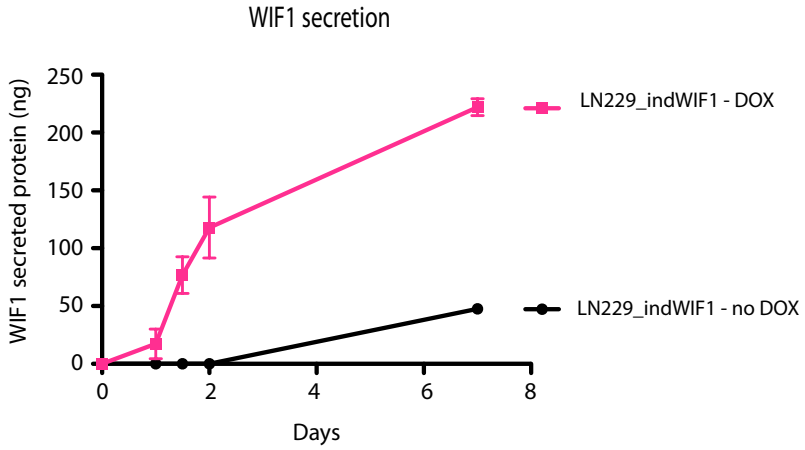

Figure 23 – WIF1 secretion upon Doxocyclin treatment measure by a specific ELISA. The medium was called every 12-24 hours for the early time points and then after 7 days from induction. Doxocyclin was added at T zero (1µg/ml) and to maintain the induction it was re-added to the medium every 48 hours (0.5µg/ml). The results of the ELISA were normalised for the cell number.

2. WIF1 Induction Impairs Cell Growth Both *in vitro* and *in vivo*

The first experiments focused on confirming the phenotype described in the *WIF1*-stable cell line. The growth potential was tested in both adherent-dependent and independent conditions. The LN229_dsRED were used as control for doxocyclin treatment and *dsRED* induction.

We confirmed the growth inhibiting potential of *WIF1*: the doxocyclin treatment reduced the growth in the LN229_ind*WIF1* while no differences were detected in the LN229_*dsRED* (Figure 24)

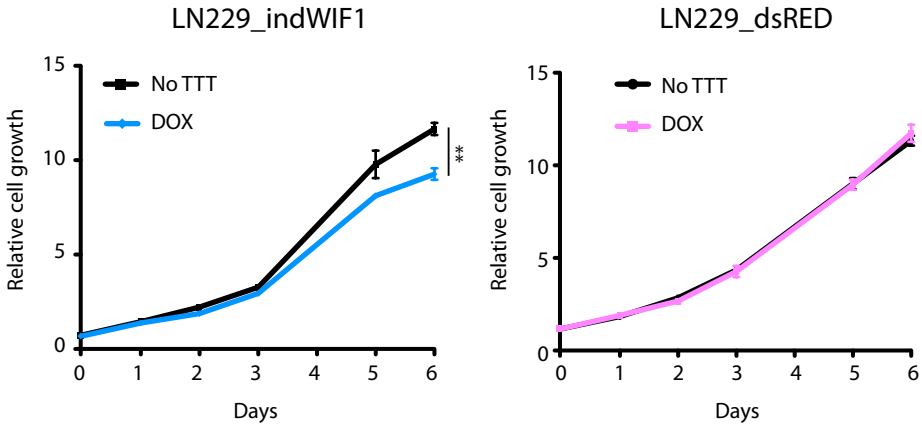

Figure 24. WIF1 induction reduces adherent-cell growth potential. The growth of both the LN229_ind *WIF1* (left panel) and the *LN229_dsRED* (right panel) was followed during 6 days. Doxocyclin was added at T zero (24 hours after seeding) at a concentration of 1µg/ml. To maintain the induction doxocyclin was re-added to the medium every 48 hours (0.5µg/ml).

Similar results were obtained in the soft-agar growth was assay. Only the LN229_ind*WIF1* showed a reduced ability to grow without adhesion when cultured with doxocyclin-conditioned medium. The effect on colony number is however not as pronounced as in the *WIF1*-stable expressing cell line (Figure 25).

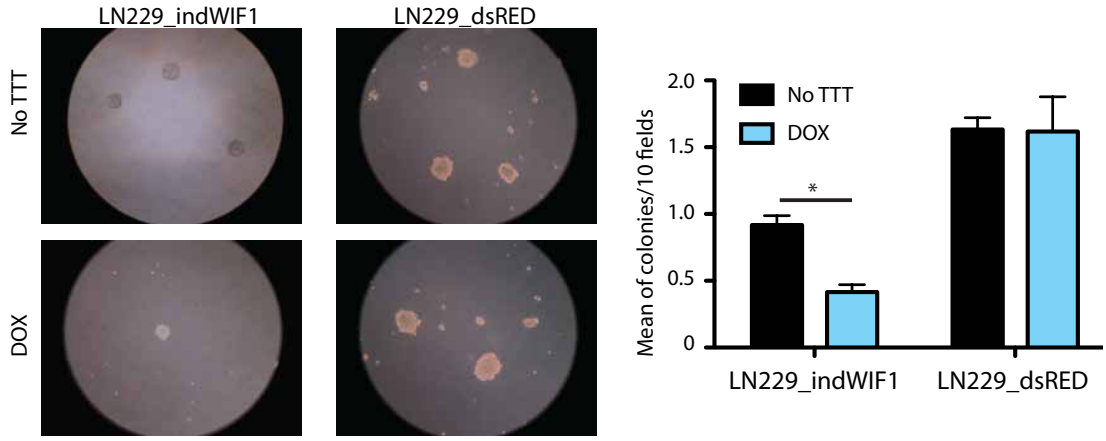

Figure 25. *WIF1* induction impairs non-adherent growth capability. The right panel shows a quantification of the colonies formed after three weeks of culture of both the LN229_ind and the control line *LN229_dsRED*. In the left part representative picture of the experiment are shown.

Similar results were obtained in vivo: we both subcutaneously (flank) and orthotopically (brain) injected the LN229_ind*WIF1* cells. For the flank injection the mice were divided into three groups (6 mice in each group) as following:

1) Control: mice fed with normal food during the whole experiment. 2) Late doxocyclin induced: mice were fed with normal food until the xenograft reached 300 mm^3, subsequently they were fed with doxocyclin supplemented food. 3) Doxocyclin induced: feed with doxocyclin supplemented food during the whole experiment. The flank xenografts were measured every 2-3 days and the mice were euthanized when the tumor volume reached 500 mm^3. The *WIF1* induced mice showed a reduced growth but due to very high variablility within the tumor size the results is not statistically significant. Same results were obtained in the late-induced group as shown in Figure 26A. Concerning the second model of in vivo tumorigenicity, the mice that were orthotopically injected were divided into two groups (6 mice in each group): 1) Control: feed with normal food 2) Doxocyclin induced: feed with doxocyclin supplemented food. The mice were

sacrificed when they started to show any neurological symptoms or significant weight loss. Here, we observed a statistically significant increase in survival of the *WIF1*-induced group although, in the end, all mice developed tumors (Figure 26B). This result could be explained by loss of *WIF1* induction in the xenografts. Indeed, the analysis of *WIF1* expression in the resected xenografts showed no residual *WIF1* expression (Figure 26C).

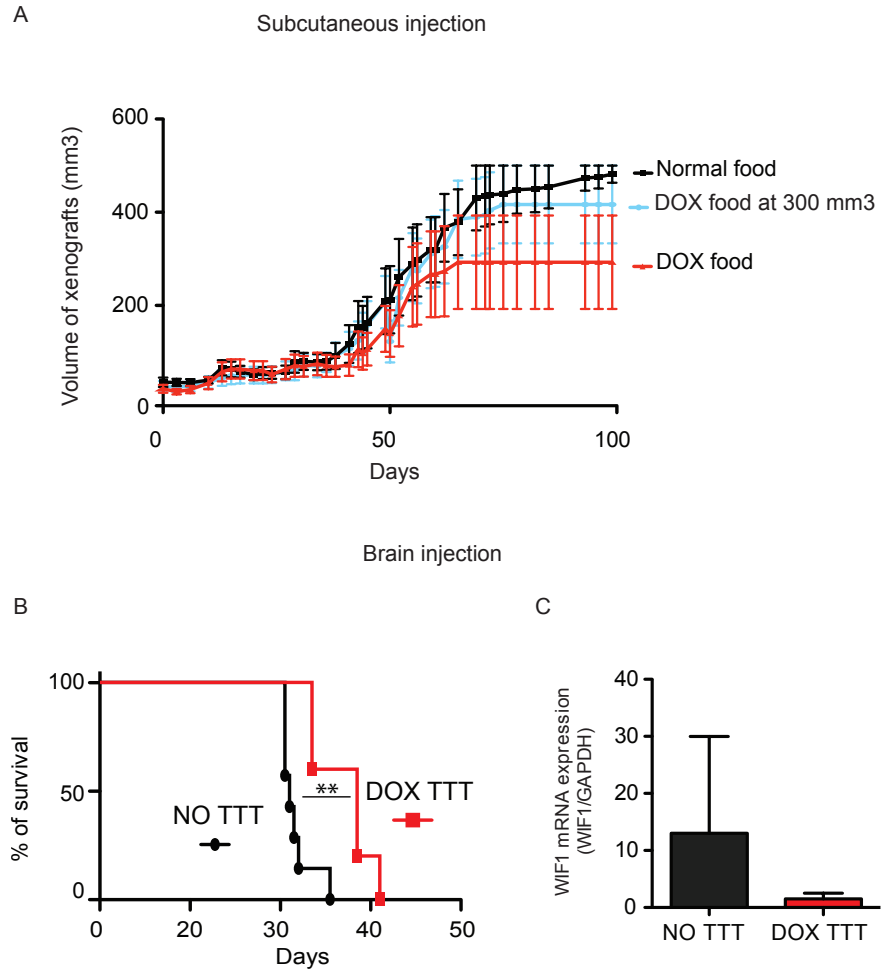

Figure 26. Analysis of the *in vivo* tumorigenicity of *WIF1*-induced glioma cell lines.
A) Subcutaneous injection of LN229_ind*WIF1* (6 mice each group). *WIF1* expression was induced feeding the mice with doxocyclin-supplemented food. The supplemented food was changed every 2-3 days to avoid loss of doxocyclin activity. The late-induced group was feed with doxocyclin-supplemented food after the xenograft reached a volume of 300 mm^3. The experiment was stopped when each tumor reached the volume of 500 mm^3.
B) Brain injection of LN229_ind*WIF1* (6 mice each group). *WIF1* expression was induced as explained in A), the mice were euthanized at first sign of neurological symptoms and /or weight loss.
C) Analysis of *WIF1* expression in the resected xenografts by Real Time PCR.

3. WIF1 Induction Reduces Migration Capability

While counting colonies for the soft agar assay, we noticed that in the LN229_ind*WIF1* treated with doxocyclin we could not detect any cells growing on the bottom of the plate. In the three other conditions a few cells managed to reach the bottom of the agar and to then expand in adhesion on the plate surface. Since this difference could be a consequence of migration modification we decided to investigate the motility of our cells by using both the trans-well assay (Figure 27A) and scratch assay (Figure 27B). *WIF1* expression reduced the ability to migrate in both assays.

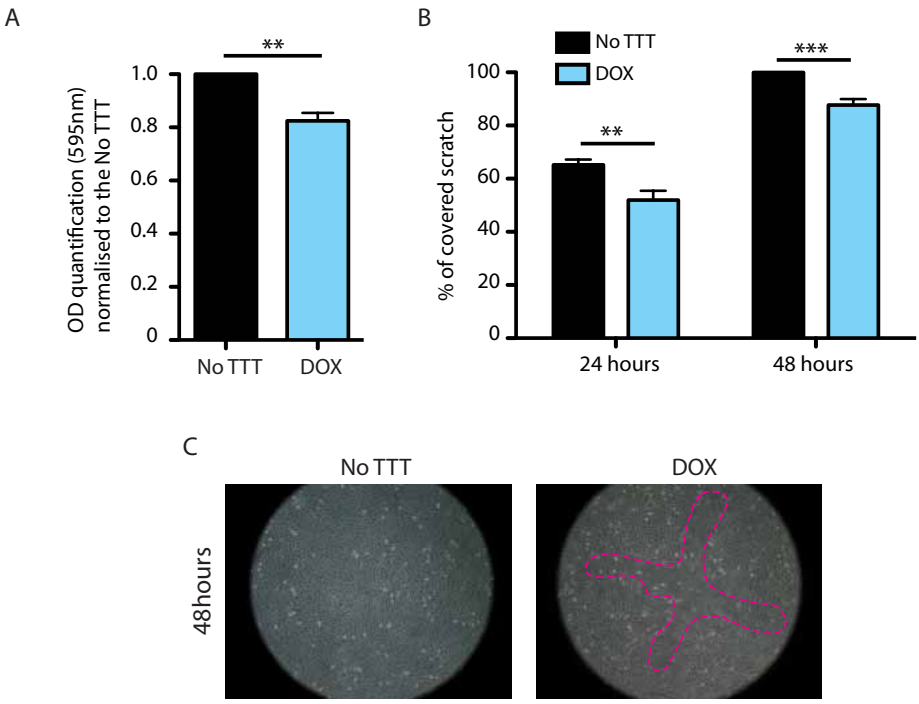

Figure 27. *WIF1* induction reduces migration in LN229_in*WIF1*. The motility was tested both using the trans-well assay (A) and scratch assay (B). For the trans-well assay, after the two days of induction with doxocyclin (1 µg/mL), the cells were trypsinized and seeded in the upper membrane of the trans-well. The experiment was stopped after 16 hours when the cells that had migrated into the lower side of the membrane were quantified by crystal violet staining. In the wound-healing assay, the scratch was performed two days after induction with doxocyclin (1 µg/mL). The experiment was stopped at two different time points: 24 and 48 hours. A and B shows the quantification of the two assays. Representative pictures of the scratch assay, after 48 hours, are shown in C (100x of magnification).

4. WIF1 inducible clones show a larger percentage of senescent cells

To measure the percentage of senescent cells in the context of the inducible system, we grew cells until confluency and maintained induction for a total of 10 days. We investigated two parameters: 1) percentage of flattened and enlarged cells 2) percentage of flattened and enlarged cells that are SA-β-Galactosidase positive. In both cases WIF1 induction increased the percentage of senescent cells (Figure 28).

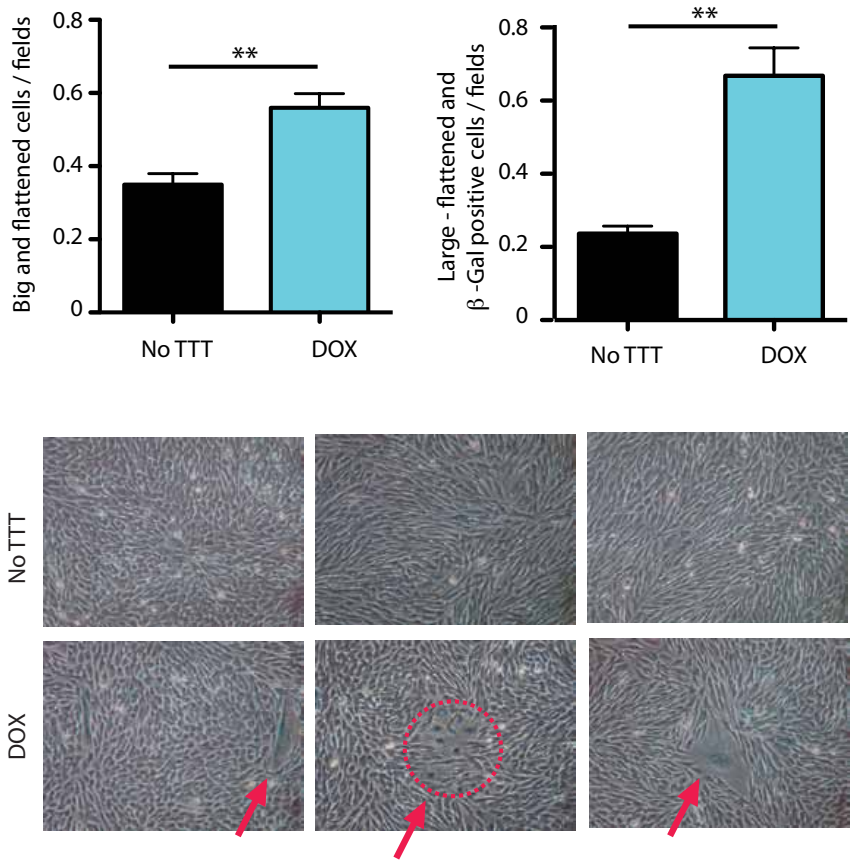

Figure 28. Quantification of the senescence phenotype in LN229_ind*WIF1* cells. A shows the count of big and flattened cells while B shows the quantification of SA-β-galactosidase positive cells (scored in 10 different randomly chosen fields. For "fields" is intended the whole area visible at the microscope at 100x magnification. (C) Representative images of LN229_ind*WIF1* (non-treated and DOX induced) stained for SA-β-galactosidase are shown (200×). Large, SA-β-galactosidase positive (blue) are highlighted with red arrows.

Luciferase-Based Analysis of Canonical WNT and WNT5α/JNK/AP-1 Non-Canonical WNT Signaling Pathways.

After having established the *WIF1* inducible system and having reproduced the phenotype described in the stable cell line we started the analysis of the different WNT signaling pathways. The choice for the reporter system was not trivial. For the canonical WNT pathway activity the TOP/FOP system gives a clear read-out but there is no gold standard for the analysis of non-canonical signaling pathway. In the context of glioblastoma the main non-canonical WNT signaling described is the WNT5a-dependent activation of the JNK pathway [58, 76]. Activation of the WNT/JNK pathway can be measured by using an AP-1 luciferase-based reporter system [77-79].

WIF1 expression clearly inhibits the WNT canonical pathway (Figure 29_A) but it did not induce any alterations in AP-1 transactivation (Figure 29_B). Together with the LN229_ind*WIF1*, the LN229*_dsRED* were tested to exclude pathway fluctuations due to both doxocyclin exposure and *dsRED* expression: as expected, there were no significant changes in the control cell line.

Given the complexity of this signaling pathway, these results do not exclude the involvement of the non-canonical pathway in general, but they rule-out the association of the JNK/AP1 signaling. To better define which branch of the non-canonical WNT pathway to investigate we took a different approach. We analysed the phosphorylation profiles of the main protein kinases (the complete list of kinases is shown in Figure 30) involved in different signaling pathways using the Human Phospho-Kinase Antibody Array (R&D system).

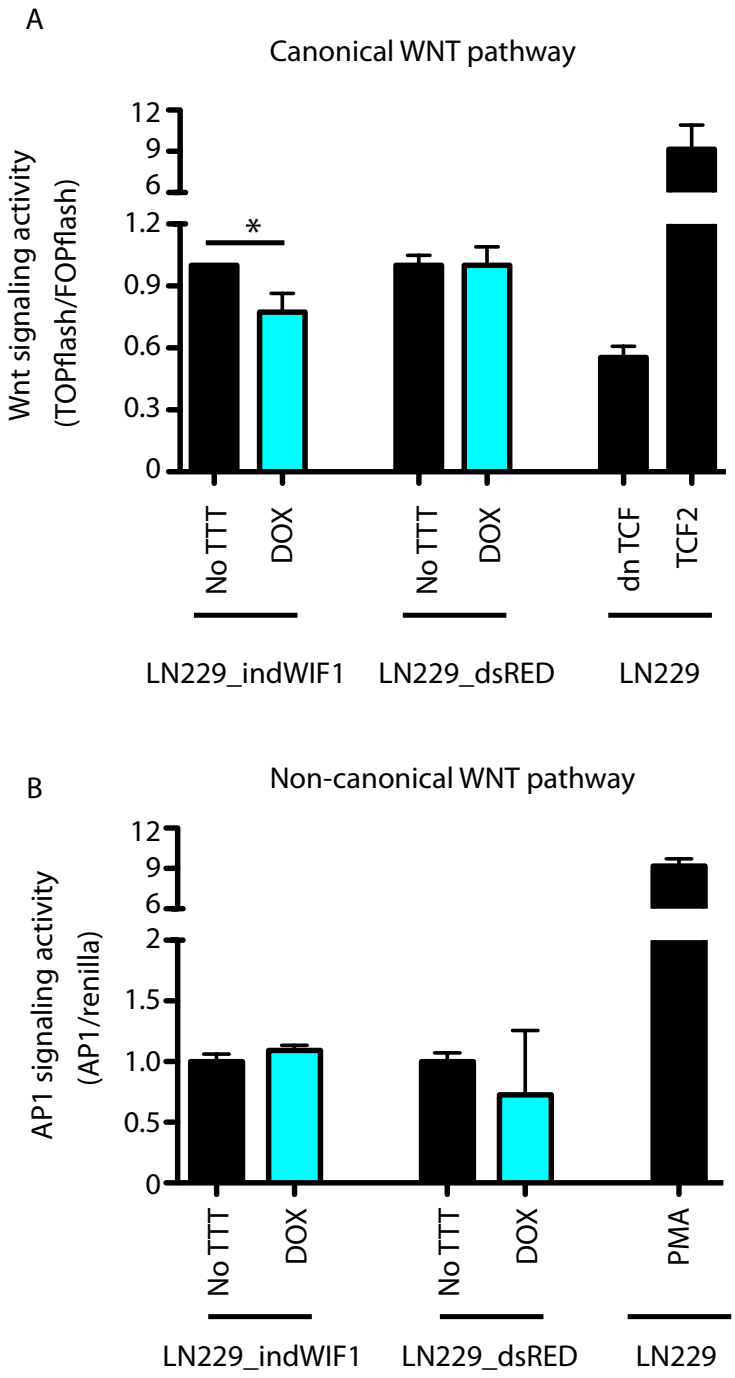

Figure 29. Luciferase based-pathway analysis: A) TOP flash/FOP flash reporter system was used to test the transactivation of β-catenin: the dominant negative form of *TCF* and a wildtype *TCF2* were co-transfected with the reporter as negative and positive control, respectively. B) AP1 reporter system was used to test the WNT5α_JNK non canonical WNT pathway: as positive control phorbol-12-myristate-13-acetate (PMA) was added to the culture media for 6h (200nM).

Phosphorylation of ERK and p38 are the main changes in WIF1 induced cells

We analyzed the phosphorylation profile of 46 kinases in the LN229_ind*WIF1* with and without *WIF1* induction. The two protein samples (control and doxocyclin induced) were hybridized on two identical antibody-spotted membranes and after the development the pixel density of each spot was analysed with imageJ. The results shown are the ratio between doxocyclin induced cells / untreated control. As expected from the AP1-pathway analysis, we did not detect any phosphorylation alterations either in JNK protein or in c-Jun [80]. Surprisingly, we detected a drastic reduction in phospho-p38 (ratio doxocyclin/control of 0.48), phospho-ERK (ratio doxocyclin/control of 0.75) and minor changes in phospho-CREB, phosho-MSK1/2 and phospho-p70, all of which are downstream of the ERK and p38 pathways (Figure 27).

To investigate the molecular mechanisms responsible for the inhibition of p38 phosphorylation, we tested the activation of the mitogen-activated protein kinase (MAPK) kinase 3 (MKK3). This kinase has been identified as a key activator of p38 in glioma and its activation correlates with p38 activity *in vivo* [81]. To validate the results of the phospho-array and to test the implication of MKK3, we transiently transfected the LN229 with either *WIF1* or the empty vector and collected the samples to analyse both the mRNA and protein levels.

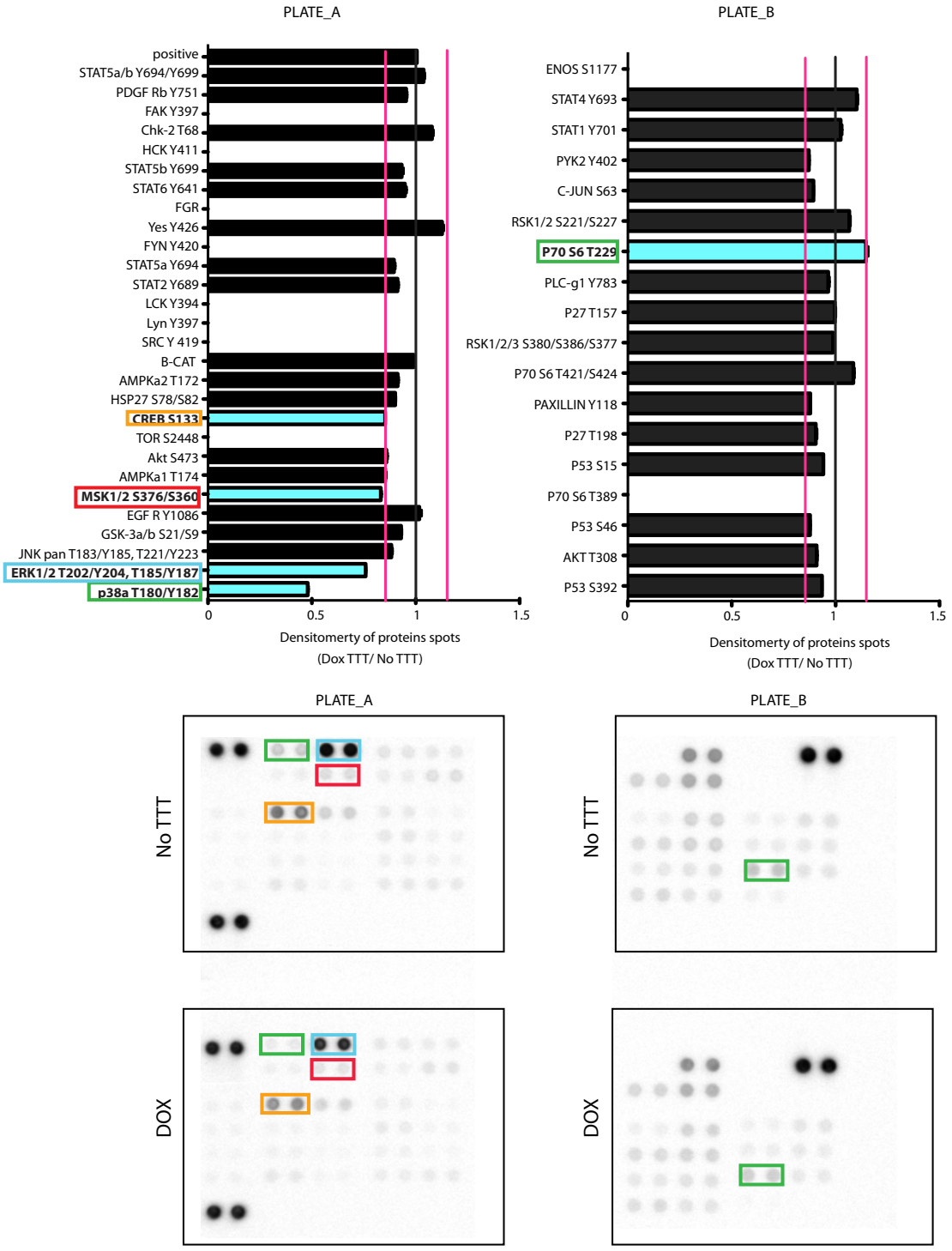

Figure 30. Phospho protein alteration in *WIF1* induced cells. Human Phospho-Kinase Array Kit (R&D Systems) was used to simultaneously detect phosphorylation sites in a panel of protein kinases involved in key signaling pathway in LN229_ind*WIF1* +/- doxocyclin. A) The quantification of each tested protein (mean of duplicate spots) is shown as ratio of DOX TTT/ control. Changes of -+ 15% (pink lines) were considered as significant. Empty columns in the bar chart mean that the tested protein was below the detection limit. B) Images of the protein arrays are shown. The proteins that showed modified levels upon *WIF1* expression are highlighted with colour boxes.

We confirmed the *WIF1*-dependent reduction of p-ERK and p-P38 but we did not detect any modification in MKK3/6 phosphorylation. JNK phosphorylation was also not changed, as expected from the previous phospho-array results (Figure 31)

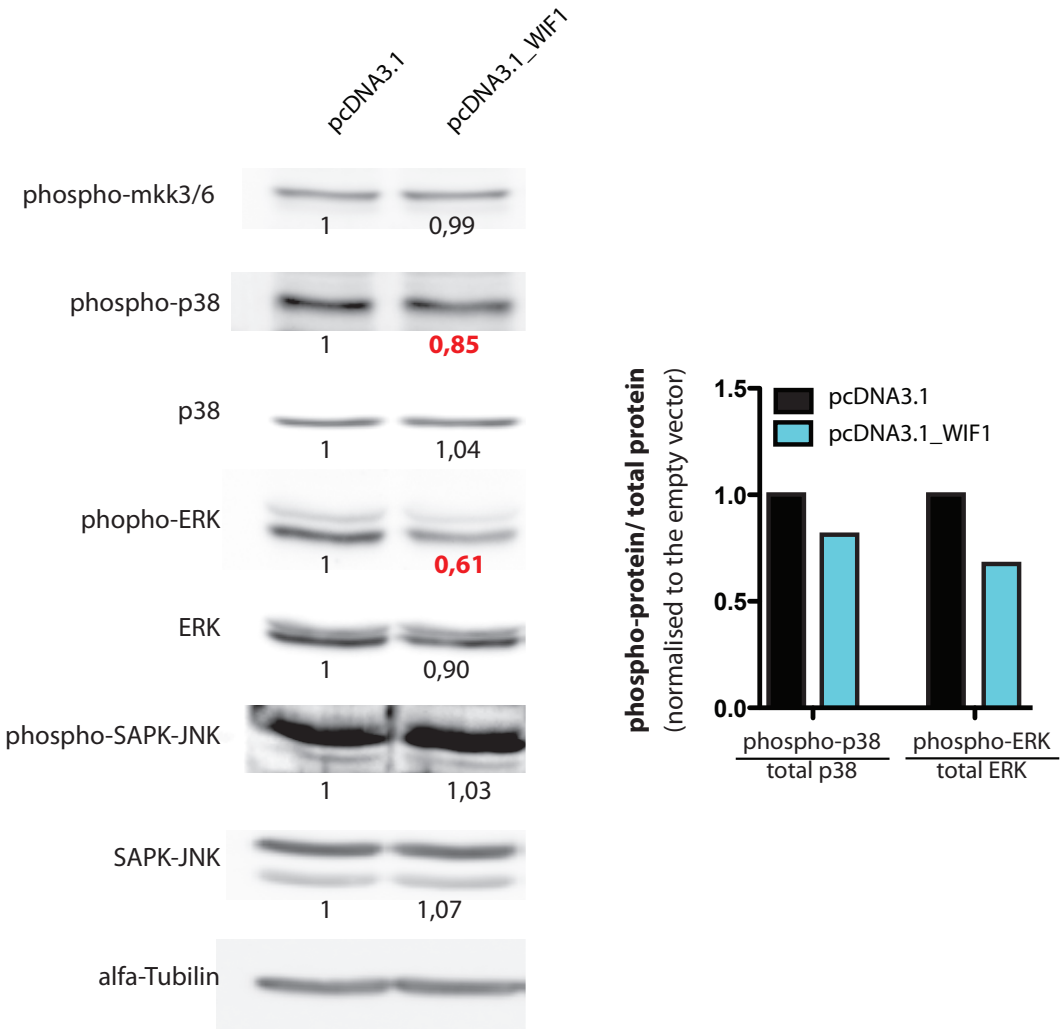

Figure 31. Western blot to confirm phospho-array results. The LN229 were transacted with either pvDNA3.1 or pcDNA3.1_*WIF1* and the proteins were collected 3 days after transfection. The number showed below each blot represent the quantification of the protein normalised to α-tubulin. On the right is shown the quantification of the p-protein normalised to the respective total protein.

The MKK3/6 was not affected, thus the p38 and ERK phosphorylation were not regulated *via* this pathway.

WNT5α has been also implicated in the Ca2+/WNT pathway [25] and there are few papers suggesting that the level of intracellular Ca^{2+} regulates MAPK signaling [82]. We tested the effect of *WNT5a* downregulation on the phosphorylation of p38, ERK and MKK3/6.

Firstly, we optimised the conditions to downregulate *WNT5α*. We tested 3 different *WNT5α* specific siRNAs, either alone or in combination with the others. The downregulation efficiency was tested by Real Time PCR three days after transfection and compared to the scramble siRNA. Si*WNT5α*_C was clearly the most efficient sequence and was kept for the subsequent experiments (Figure 32).

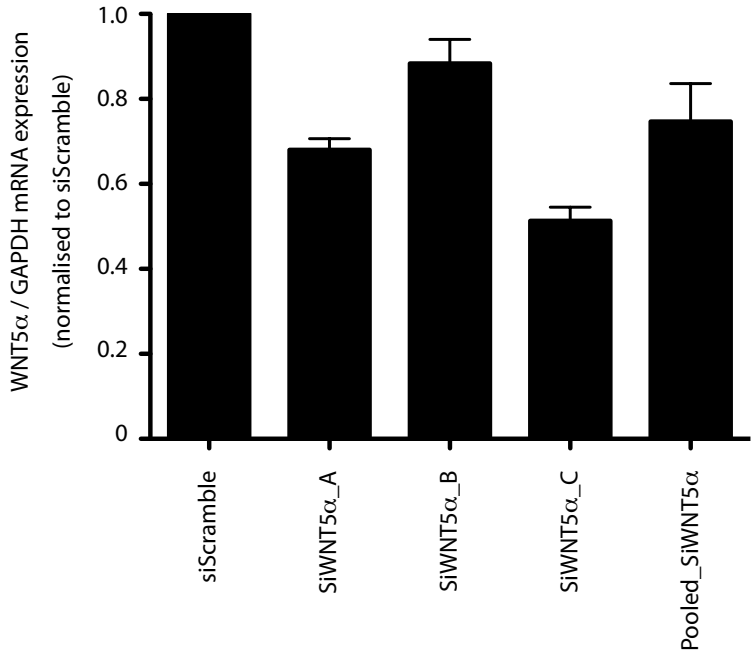

Figure 32. Si*WNT5α* efficacy testing. The three sequences were tested alone or in combination (Pooled_siRNA) at 25 nM final concentration. *WNT5α* mRNA was measured by Real Time PCR three days after transfection. *GAPDH* mRNA expression is used as housekeeping gene.

To test the effect on p38 and ERK, we downregulated *WNT5α* using the si*WNT5α*_C and a scramble control. All the samples were collected three days

after transfection. As shown in Figure 33, *WNT5a* downregulation efficiently inhibits phosphorylation of both p38 and ERK without affecting MKK3/6 status.

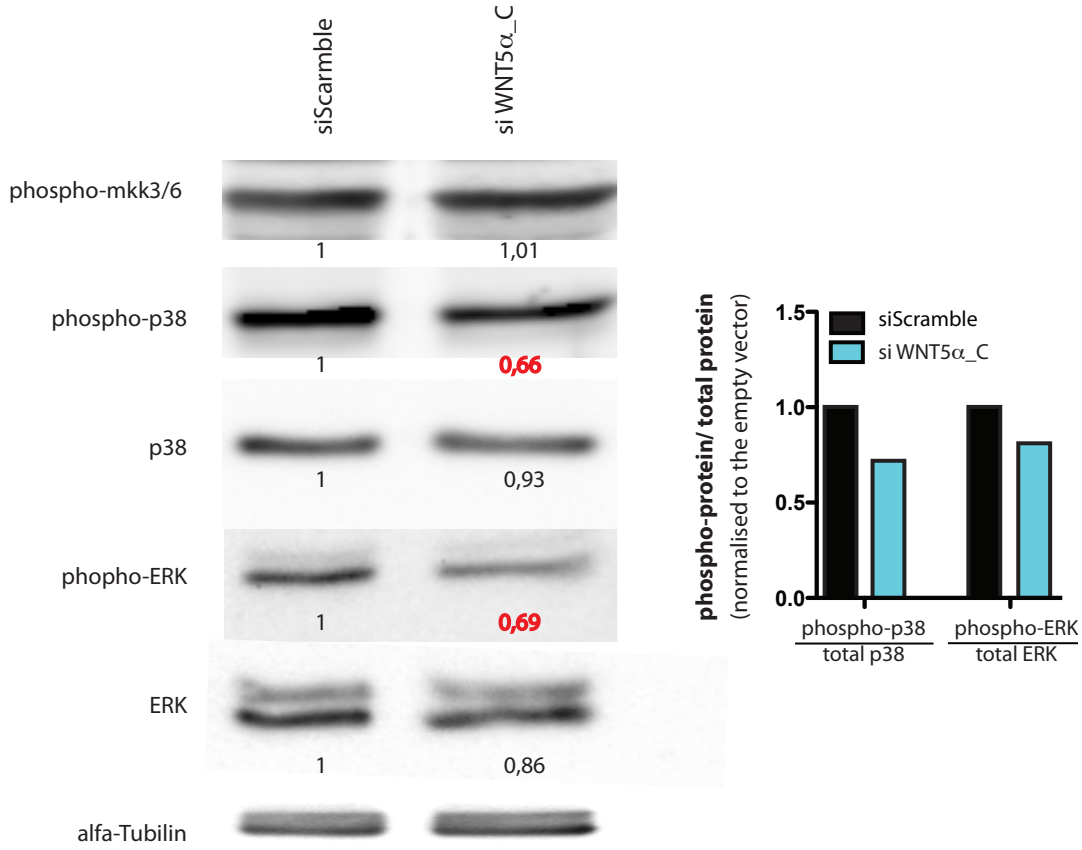

Figure 33. Downregulation of *WNT5α* inhibits phophorylation of both p38 and ERK. The LN229 were transfected with either siScrambled or si*WNT5α*_C and the proteins were collected 3 days after transfection. The numbers below each blot represent the quantification of the protein normalised to α-tubulin. The quantifications of the phospho-protein normalised to corresponding total protein are shown in the right panel.

These results show that *WIF1* upregulation and *WNT5α* downregulation have a similar effect on the phosphorylation level of both p38 and ERK, suggesting the involvement of a *WNT5α*-dependent non-canonical WNT pathway in the phenotype induced by *WIF1*.

This hypothesis is also supported by expression of WNT ligands analysis in glioblastoma. *WNT5α* is the only WNT ligand that shows overexpression in glioblastoma tumors when compared to non-tumoral brain samples (Figure 34).

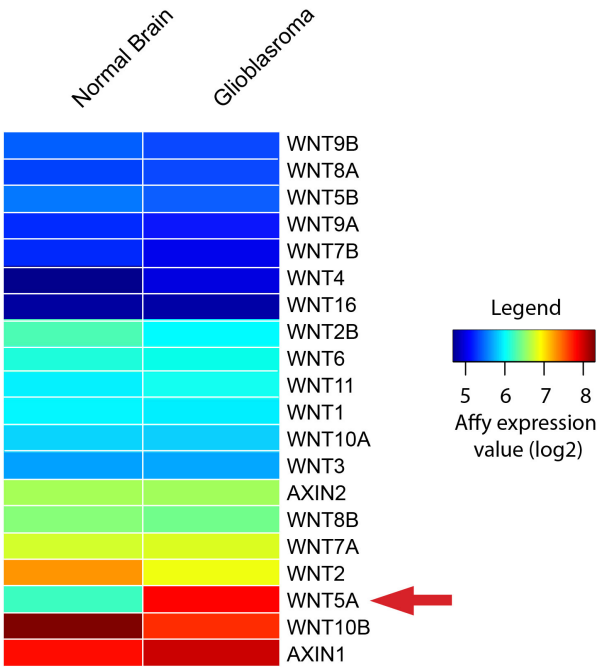

Figure 34. WNT-related genes heatmap. The expression of several WNT-related genes was analysed in the data set of Murat et al. The mean of the WNT-related genes in non-tumoral brain and glioblastoma are showed in the two column of the heatmap. The red arrow shows the location of *WNT5α.*

As mentioned above, the calcium pathway might explain some of our results, including changes of p38 and ERK phosphorylation and the inhibitory effect of migration. We are now performing experiments aimed at determining both the Ca^{2+} levels and the CAMKII activation: two important read-outs to define the activation of the WNT5α-calcium pathway.

Analysis of the Gene Expression Profile of WIF1 Induced Cells

In addition to the phospho-protein approach, we decided to investigate the *WIF1*-related phenotype by looking at differential gene expression profile. From the analysis of the kinetics of *WIF1* induction we knew that the time window to detect *WIF1* related effects was between 12h (peak of *WIF1* mRNA transcription) and 48h (stable secretion of WIF1). We collected the LN229_ind*WIF1* samples at three different time points after doxocyclin induction: 12 hours, 24 hours and 48 hours. The analysis of the expression profiles was performed at each time points, by comparison of the doxocyclin-induced cells to the respective paired control. Figure 35 shows the three heatmaps of the most variable transcripts calculated as logarithmic fold change compared to the non-treated samples. We selected the probes with a log fold change of > |0.7|. Despite the fact that there were relatively few modified genes, we could detect some very interesting potential targets. We used the following approach to select the final candidate genes:

- Probes showing a log fold change > |0.7| were selected.
- From the selected transcripts a few genes were chosen (according to literature) and variations were confirmed by Real Time PCR in both LN229_ind*WIF1* and LN229_ds*RED*. The second cell line was used to exclude the genes that were not *WIF1*-specific).
- Confirmation of the results was performed in additional glioma cell lines (a adherent cell line LN319 and a sphere-line LN2669_GS)

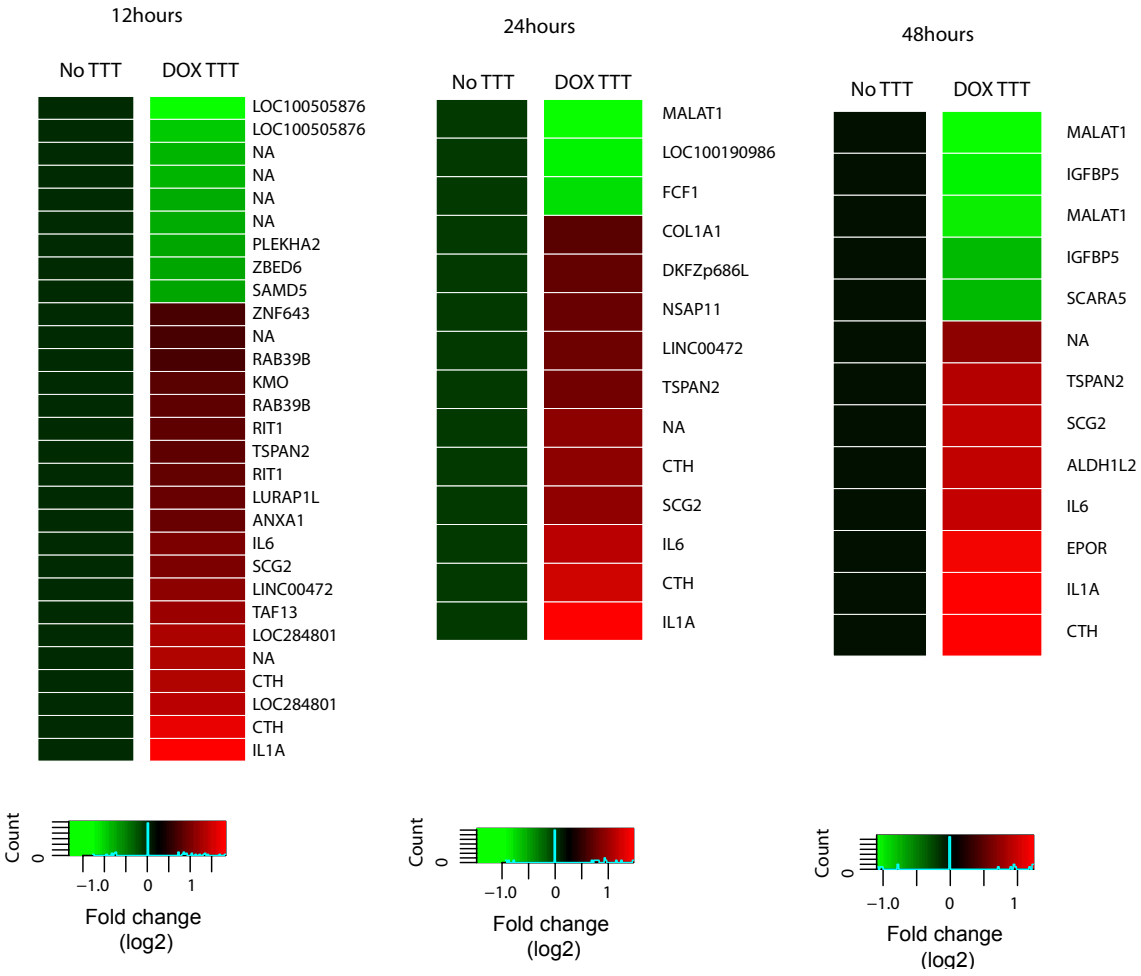

Figure 35. *WIF1*-induced most variable probes. The three heatmaps show the most variable probes (log-fold change) at each time points (12, 24 and 48 hours) when the *WIF1*-induced cells are compared with the not induced control. The analysis was performed on probe level thus explaining why only several genes are shown more than once.

After this selection we retained 7 genes for further analysis, 6 downregulated and 1 upregulated. Within the downregulated genes we were interested in the following: *MALAT1* (a non-coding RNA involved in migration), *IGFBP5* (a IGF-binding proteins whose expression has been correlated with glioma grade), *ALDH1L*, *CTH*, *SGC2*, and *IL6*. The only upregulated gene was *LURAP1L*, which encodes an adaptor protein whose function is completely unknown.

We measured, via Real Time PCR, the expression levels of the selected genes after 2 days of *WIF1* induction. We confirmed the *WIF1*-dependent alteration of three transcripts: *MALAT1, IGFBP5* and *LURAP1L* (Figure 36). The upregulation of *IL6* was detected also in the LN229_*dsRED*, suggesting that the doxocyclin treatment and/or the *dsRED* expression were likely responsible for the increased expression. Concerning the other genes tested we could not confirm the results obtained with the gene array.

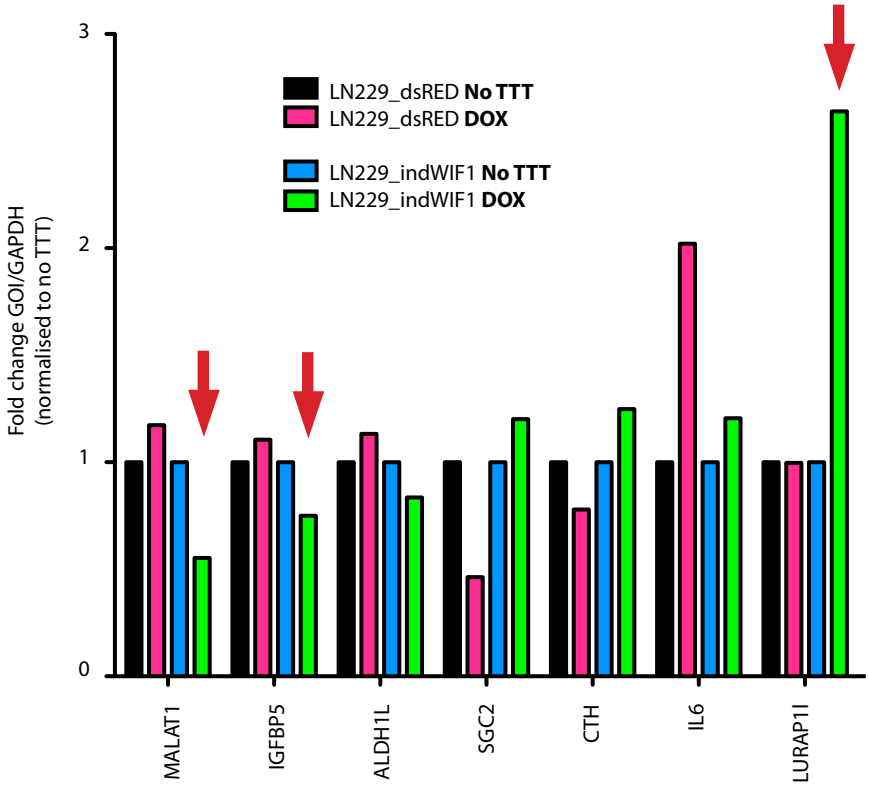

Figure 36. Real time analysis of the genes found altered in the gene expression profile. The red arrows mark the transcript that we confirmed as *WIF1*-dependent.

MALAT1 and *LURAP1L* were further confirmed in a different experimental setting: *WIF1* stable transfected cell lines. They showed *WIF1*-dependent expression alteration in both a second adherent cell line (LN319) and in a glioma sphere line (LN2669_GS). The expression of *WIF1* induced downregulation of

MALAT1 and upregulation of *LURAP1l* (Figure 37). By contrast, *IGFBP5* did not show any correlation with *WIF1* expression.

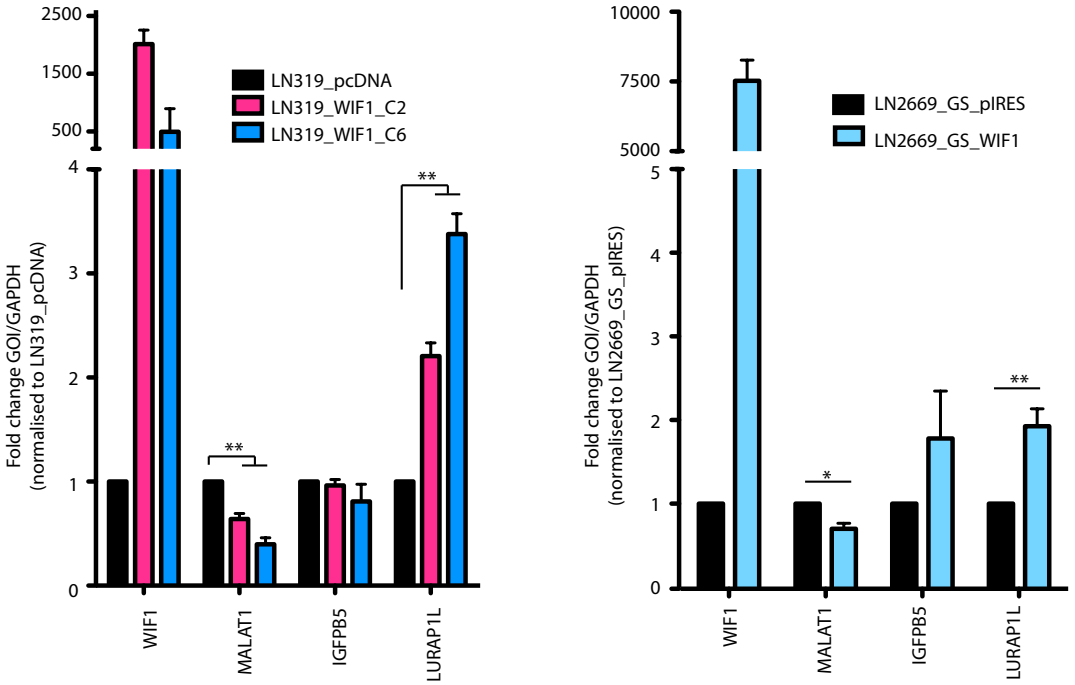

Figure 37. *WIF1* induces expression alteration of *MALAT1* and *LURAP1L* both in adherent cell line and glioma sphere line. Real-Time-PCR analysis was performed on both LN319 and LN2669_GS clones that stably express *WIF1*. *GAPDH* is used as housekeeping gene and the results showed are normalised to the respective empty vector controls.

MALAT1 is Overexpressed in Glioblastoma Samples

We then focused our effort on the characterisation of the two *WIF1*-regulated transcripts selected from the array and we started with *MALAT1*.

MALAT1, is a nuclear long non-coding RNA of more than 8 Kb. *MALAT1* has not been investigated yet in glioblastoma, so we started looking at the expression level of this gene in the data set of Murat et. al [59]. We found a statistically significant overexpression of *MALAT1* in glioblastoma when compared to non-

tumoral brain samples (Figure 38), suggesting that *MALAT1* could play a role in glioblastoma.

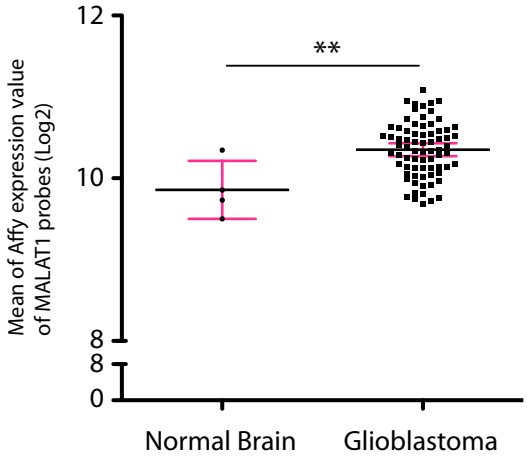

Figure 38. Data taken from the data set of Murat et al. All the probes specific for *MALAT1* are averaged and the samples are split into normal brain and Glioblastoma.

MALAT1 Expression Levels Correlate with Glioblastoma Extent

To test whether the level of MALAT1 expression correlates with total tumor volume or extent of necrosis in glioblastoma, we collaborated with Dr. Pascal Zinn, who has already analyzed the volumes of 78 glioblastoma lesions, using magnetic resonance images (MRIs) [83] that are available in The Cancer Imaging Archive (TCIA) (http://cancerimagingarchive.net/). Since the gene expression profiles of the same patients are also available on the TCGA, it was then possible to correlate the imaging features with the gene expression profiles [84]. The analysis of the post-contrast T1 weighted imaging (T1WI) of the MR-images was used for quantification of tumor volume and necrosis [85]. The

correlation of total tumor volume with *MALAT1* expression yielded an interesting result: the tumor extent was positively correlated with the expression of the non-coding RNA, thus reinforcing the hypothesis that *MALAT1* plays a role in glioblastoma tumorigenicity (Figure 39). No correlation was found between extent of necrosis and *MALAT1* expression levels.

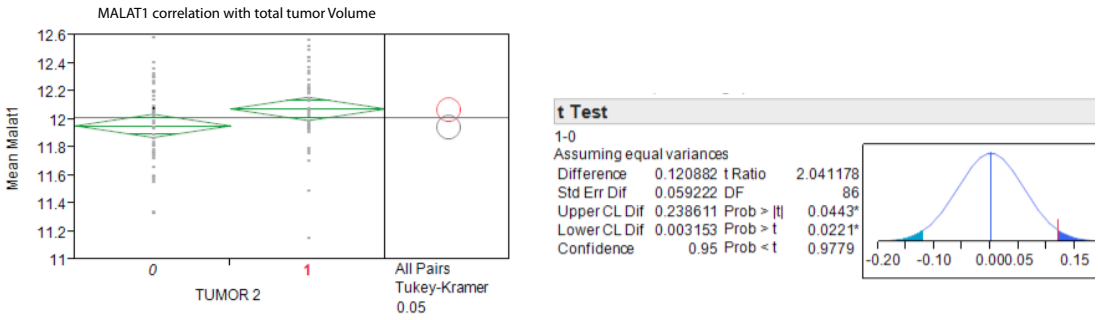

Figure 39. Correlation between the mean value of *MALAT1* specific probes (AGILENT) and tumor volume (dichotomised in two using the median value). On the right the statistical tests parameters are shown.

MALAT1 Downregulation Reduces Migration Capability *in vitro*

To test the role of *MALAT1* in the regulation of migration capability we transfected LN229 with a specific siRNA. The downregulation efficacy was assessed by Real Time PCR, measuring the final expression of *MALAT1* at two different time points: 48 and 72 hours. Additionally, we checked the expression of two known-*MALAT1* target genes, *CTHRC1* and *SLC26a2* [86], to ensure that the downregulation of *MALAT1* was indeed functional. Collagen triple helix repeat containing-1 (CTHRC1) is a secreted protein involved in vascular remodeling, and morphogenesis and it plays a role in the progression and metastasis of several cancer.

Both selected genes are involved in regulating the migration capability.

The strongest downregulation of *MALAT1* was achieved 48 hours after transfection while the target genes were affected at both time points (Figure 40). *SLC26A2* expression was restored 3 days after transfection, however, the specificity of the effect is visible at the first time point (2 days).

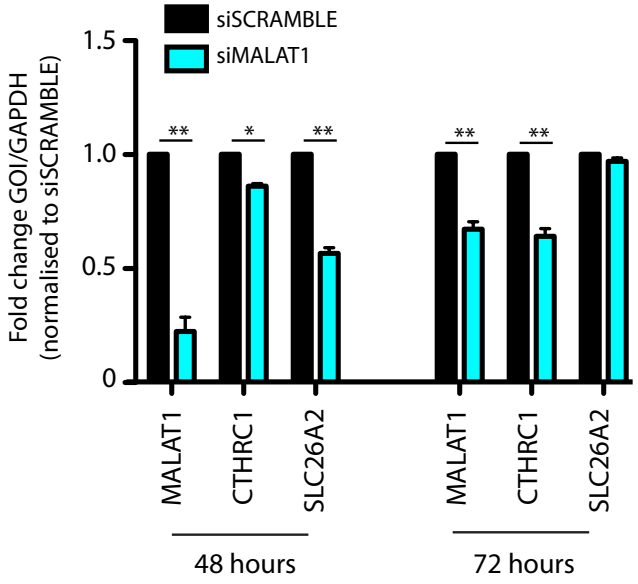

Figure 40. The downregulation of *MALAT1* affects expression of two target genes. The mRNA levels were measured by Real Time PCR, 48 and 72 hours after transfection. *GAPDH* mRNA was measured as housekeeping control.

To check the migration capability of the LN229 transfected with *siMALAT1* we used two different approaches: scratch assay and transwell assay. The scratch assay, or wound-healing assay, was performed starting 48 hours after transfection. *MALAT1* downregulation was sufficient to significantly reduce the area of the scratch covered (Figure 41A and C).

The growth was not altered by *MALAT1* downregulation, thus the results obtained with the scratch assay were indeed related to a deficit in migration rather than a difference in growth rate (Figure 41_B)

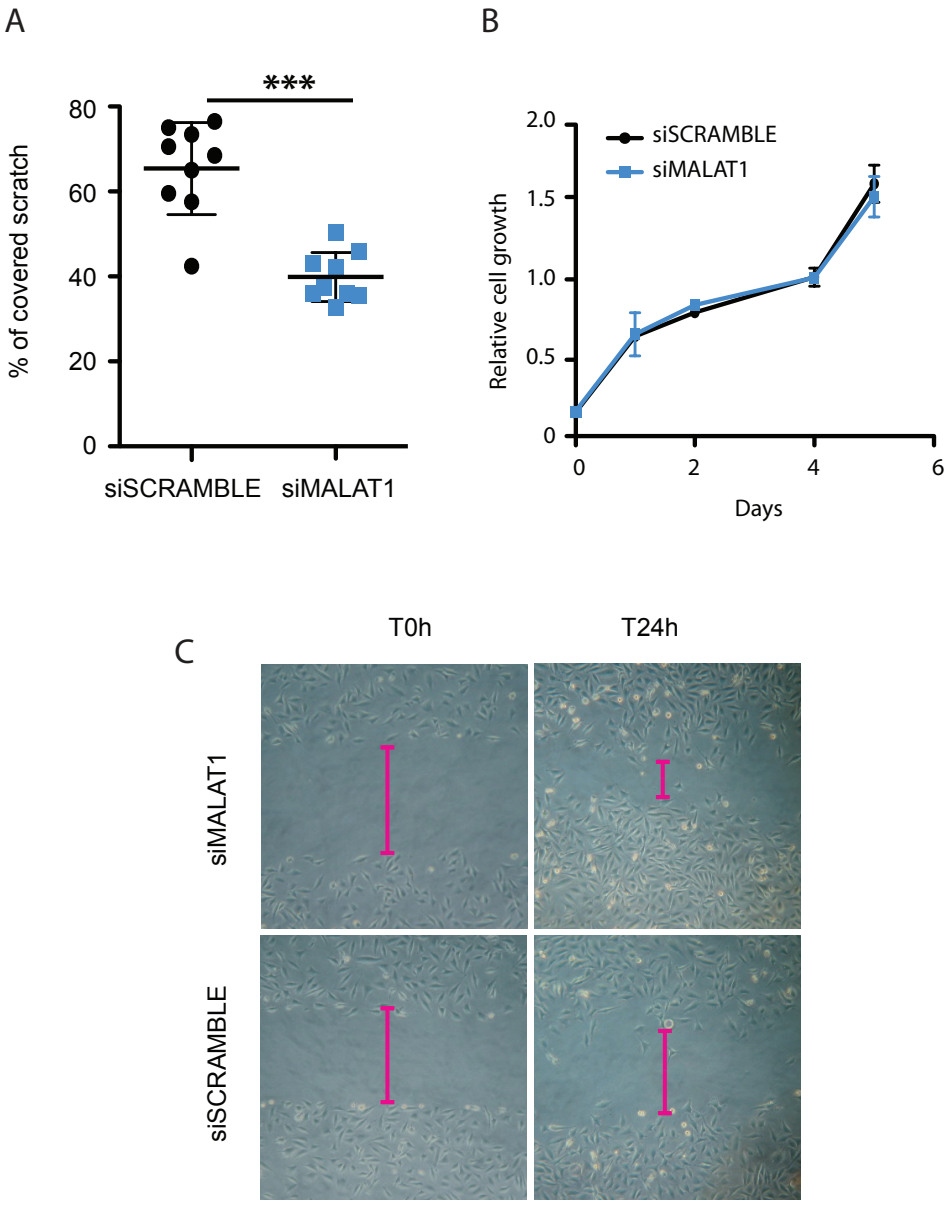

Figure 41. *MALAT1* downregulation reduces migration *in vitro.* The scratch assay quantification is shown in the upper section A) while representative picture of the assay are shown in C. The growth of the transfected cells is shown in B).

To confirm the reduction in migration we also used the trans-well assay. After transfection the cells were left to recover for 48 hours and then seeded on the upper-chamber of the trans-wells. 16-18 hours after, the cells that migrated to the lower side were quantified and, as expected, we could confirm a migration reduction in the LN229 transfected with *siMALAT1* (Figure 42).

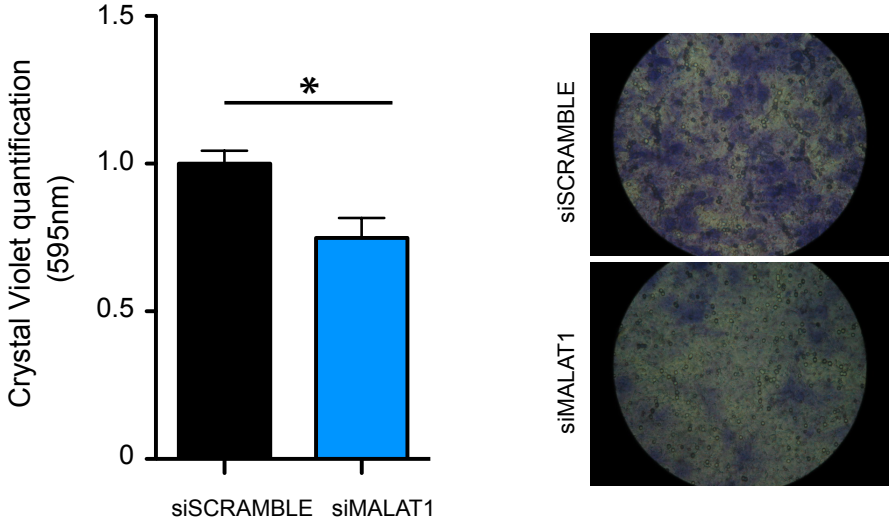

Figure 42. *MALAT1* downregulation reduces migration *in vitro.* The quantification of the trans-well assay is shown in the left panel while representative pictures of the trans-well lower membrane are shown on the right. The cells were transfected either with the *MALAT1*-specific siRNA or with the scrambled control. Two days after transfection the cells were collected and seeded in to the upper chamber of the trans-wells. The experiment was stopped and quantified after 16 hours.

MALAT1 Downregulation is *WNT5α*-Dependent

We have previously shown that the inhibition of p38 and ERK phosphorylation is *WNT5α* dependent. We then sought to test the regulation of *MALAT1* expression in the context of the non-canonical WNT pathway. We downregulated *WNT5α* using the specific *siWNT5α*_C and we measured the expression of *MALAT1* after 48 and 72 hours.

Interestingly, we detected an extremely strong downregulation of *MALAT1*, 72 hours after the *siWNT5α*_C transfection. We also measured *AXIN2* to control the status of the canonical pathway and we could not detect any changes (Figure 43).

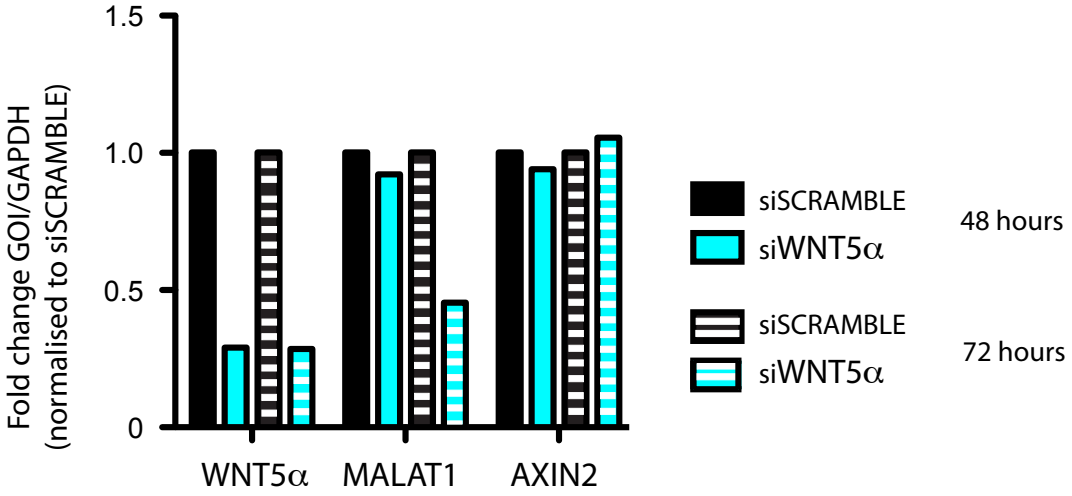

Figure 43. The downregulation of *WNT5α* affects *MALAT1* expression. The mRNA level were measured by Real Time PCR, 48 and 72 hours after transfection.

The observation that *MALAT1* downregulation was comparable in both *WNT5α* downregulated cells and in WIF1 induced samples suggest again that the phenotype we described might be *WNT5α*-dependent. We are now specifically downregulating only the WNT canonical pathway to test whether *MALAT1* expression is affected.

Migration *in vivo*: How *WIF1* and *MALAT1* Affect Cell Invasion

The inhibition of migration capability is a very intriguing result, but has to be confirmed in an *in vivo* setting. To assess invasion of glioblastoma cells *in vivo*,

it is necessary to use a glioma sphere line. Adherent cell lines do not grow invasively in mouse brain, while sphere lines can easily form neoplasms that resemble the original tumor. We already generated a *WIF1* stable sphere line in the LN2669_GS and we are now working on engineering a sphere line that has reduced expression of *MALAT1* by stable transfection of a *MALAT1*-specific short hairpin. These two lines will be injected orthotopically into imunocompromised mice and the resulting xenografts will be analysed for migration differences. We will score the number of cells that could reach the contralateral hemisphere. The sphere line LN2669-GS-*WIF1* and the respective empty vector control have already been injected. We confirmed again the anti-tumorigenic effect of *WIF1*: as shown in figure 44, the survival of mice injected with the LN2669-GS-*WIF1*cells is significantly longer. We are now waiting for the end of the experiment to perform the migration analysis.

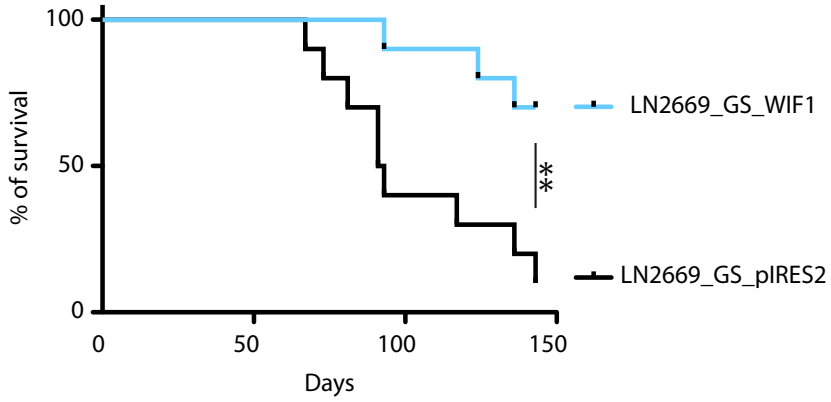

Figure 44. WIF1 prolonged survival of mice bearing intracranial LN2669_GS tumors. 10 mice were used in each group (LN2669-GS-pIRES2 and LN2669-GS-WIF1). After the injection the mice were constantly monitored and they were euthanized at the appearance of neurological symptoms or/and weight loss.

As mentioned above, the LN2669_GS_pIRES2 grow extremely invasively in mouse brain. We performed preliminary immunohistochemistry to test the infiltrative capability of these cells in our experimental setting. By a classical

hematoxylin and eosin (H&E) staining it is not possible to see any tumor-related alteration in the mouse brains, despite the fact that the injected cells have infiltrated nearly the whole organ, as shown in Figure 45. In order to visualize the infiltration of the tumor cells, a human-specific nuclear staining (IHC for human-specific nucleolin) was used, to distinguish between the xenograft and the host.

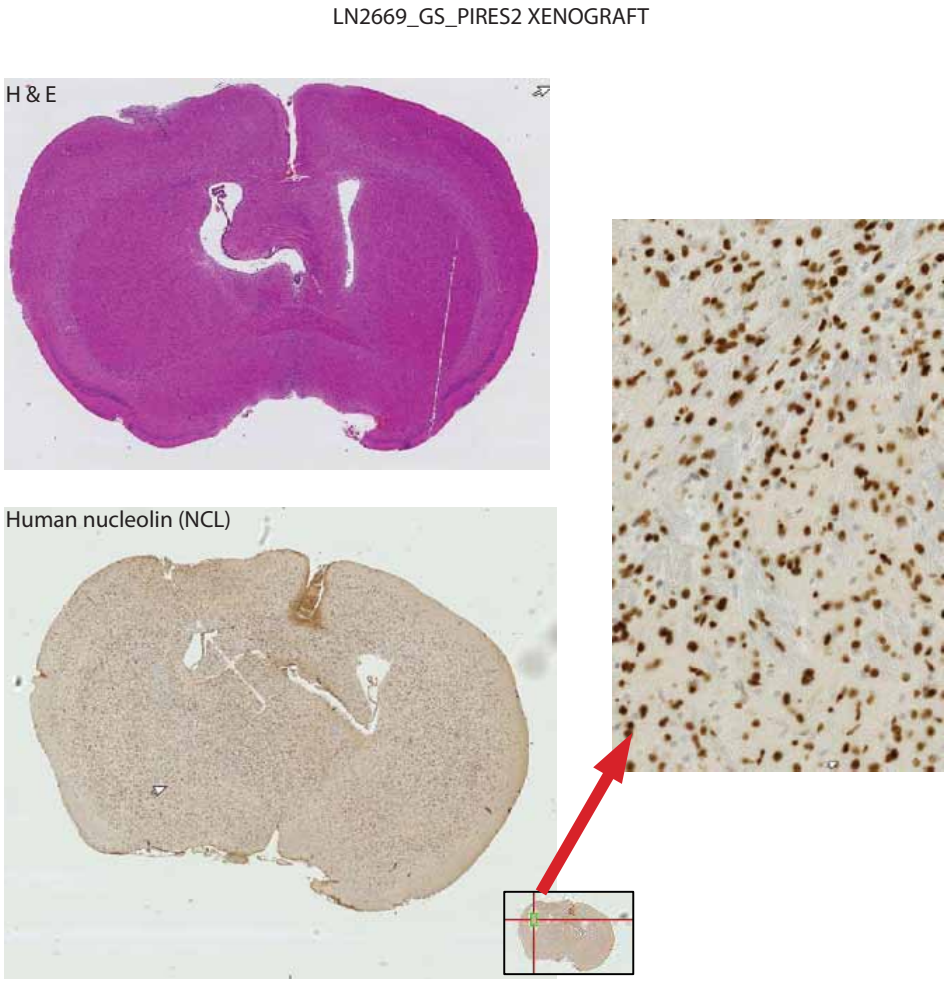

Figure 45. Analysis of LN2669_GS-pIRES2 xenogfrafts by immunohistochemistry. Representative nude mouse brain cross section showing brain tumor are shown. Top: hematoxylin and eosin staining while at the bottom the human-specific nucleolin antibody is used. On the right is shown a higher magnification of the human-specific nucleolin staining.

LURAP1L: a Potential Tumor Suppressor Gene Downstream of WIF1 Signaling Pathway

In addition to *MALAT1*, we identified a *WIF1*-specific alteration of a second transcript named Leucine Rich Adaptor Protein 1-Like (*LURAP1L*). *LURAP1L* was consistently upregulated upon WIF1 induction (log fold change= 0.9). *LURAP1L* encodes for an adaptor protein with a completely unknown function. We cloned the gene starting from a cDNA sample derived from LN229 and we compared the sequence with the transcript deposited at the NCBI.

Interestingly, we found two sequence alterations compared to the LURAP1L transcript deposited at the NCBI (Reference Sequence: XM_005251443.1). The two alterations were: 1) an insertion of 9 nucleotides (3 X GGC) within a stretch of GGC repeats and a point mutation AGC -> GGC. We decided to sequence *LURAP1L* mRNA in a non-tumoral brain sample and also in a second cell line LN319. Figure 46 shows the alignment of *LURAP1L* sequences derived form: the NCBI, the normal brain sample, the LN229, the LN319, and from the sequence we cloned in pIRES2.

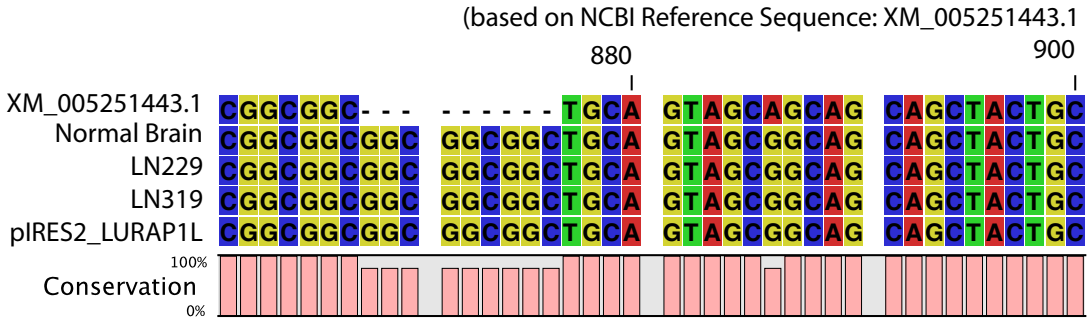

Figure 46. Alignment results for *LURAP1l* transcript sequences

We found the same alterations in all sequenced transcripts, including a non-tumoral brain sample, and all originating from different individuals. Hence, we decided to continue our experiments with our cloned sequence.

Next, we also confirmed the *WIF1* dependent up-regulation of LURAP1L on the protein level (Figure 47A). Differently from the WIF1-induced regulation of *MALAT1*, *LURAP1L* is not modulated by downregulation of *WNT5α*, suggesting that *LURAP1L* might be a canonical WNT pathway target gene (Figure 47B).

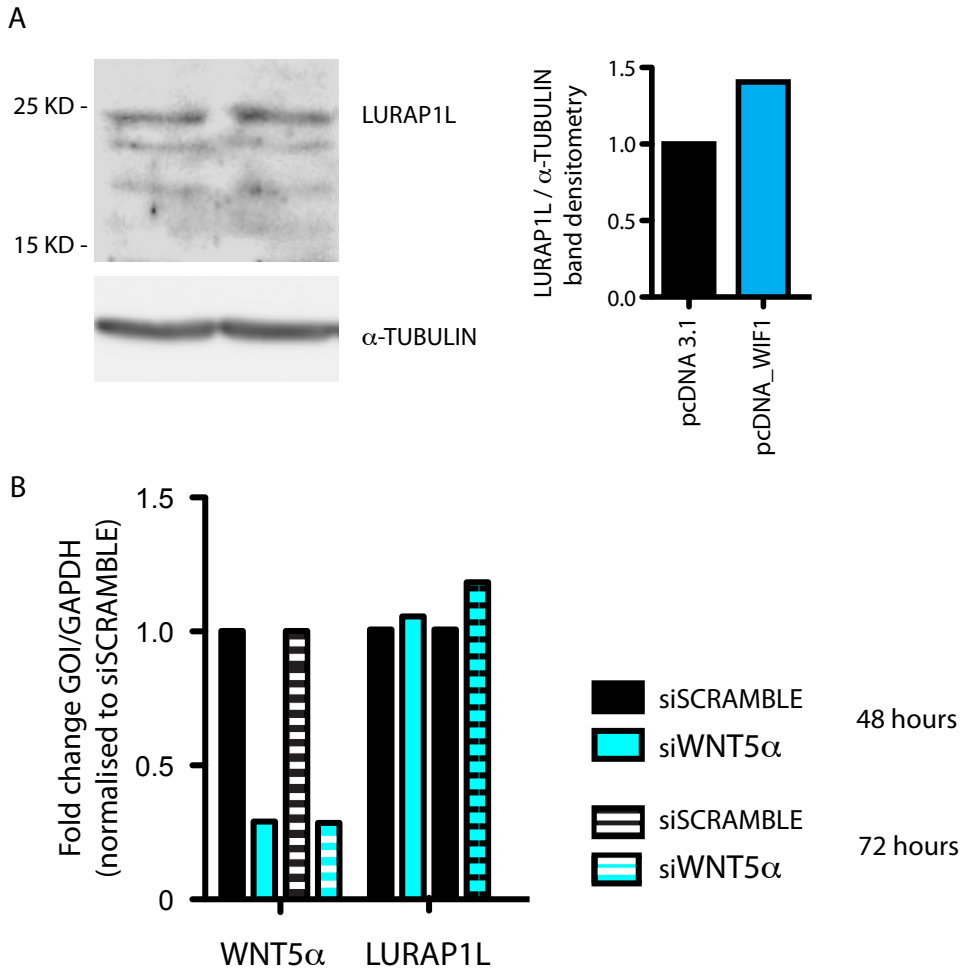

Figure 47. WIF1 upregulates LURAP1L protein level. A) Western blot analysis to detect LURAP1L protein in LN229 transfected with WIF1, three days after transfection. B) Real time analysis measuring the mRNA level of *LURAP1L* after *WNT5α* downregulation (siWNTalfa_C).

LURAP1l Overexpression Reduces Growth Capability

We transfected the pIRES2_*LURAP1L* plasmid and the respective empty vector (pIRES2_EGFP) in two different cell lines: LN229and LN2669_GS. For each cell line, we selected stable clones and we are currently performing experiments to determine the tumorigenic potential of the *LURAP1L* overexpressing cells. Preliminary results show that the overexpression of *LURAP1L* induces a tumor-suppressive phenotype in both cell lines we have tested so far.

We have selected three clones for the LN229_*LURAP1L* and we performed two tests to study the tumorigenic potential: the colony formation assay and adherent growth analysis. We detected a significant reduction of adherent growth rate in LN229_*LURAP1L* clones and the specificity of the observed results is supported by the *LURAP1L*-expression dose dependent-effect. The lowest growth rate has been observed in the clone (C1) that expresses *LURAP1L* to the highest level (Figure 48 A). Similar results have been observed for the colony formation assay. *LURAP1L* clones form colonies less efficiently when seeded at very low density (Figure 48 B). For what concern the analysis of the sphere line LN2669-GS overexpressing *LURAP1L* we decided to test directly the tumorigenic potential *in vivo*. As detailed above glioma derived sphere lines behave more like the original tumor and therefore their use as an *in vivo* model is more appropriate. We stereotactically injected the LN2669_GS_*LURAP1L* together with the respective control and we followed the survival of the mice. *LURAP1L* worked as a tumor suppressor also *in vivo*, it prolonged survival of the injected mice (Figure 49).

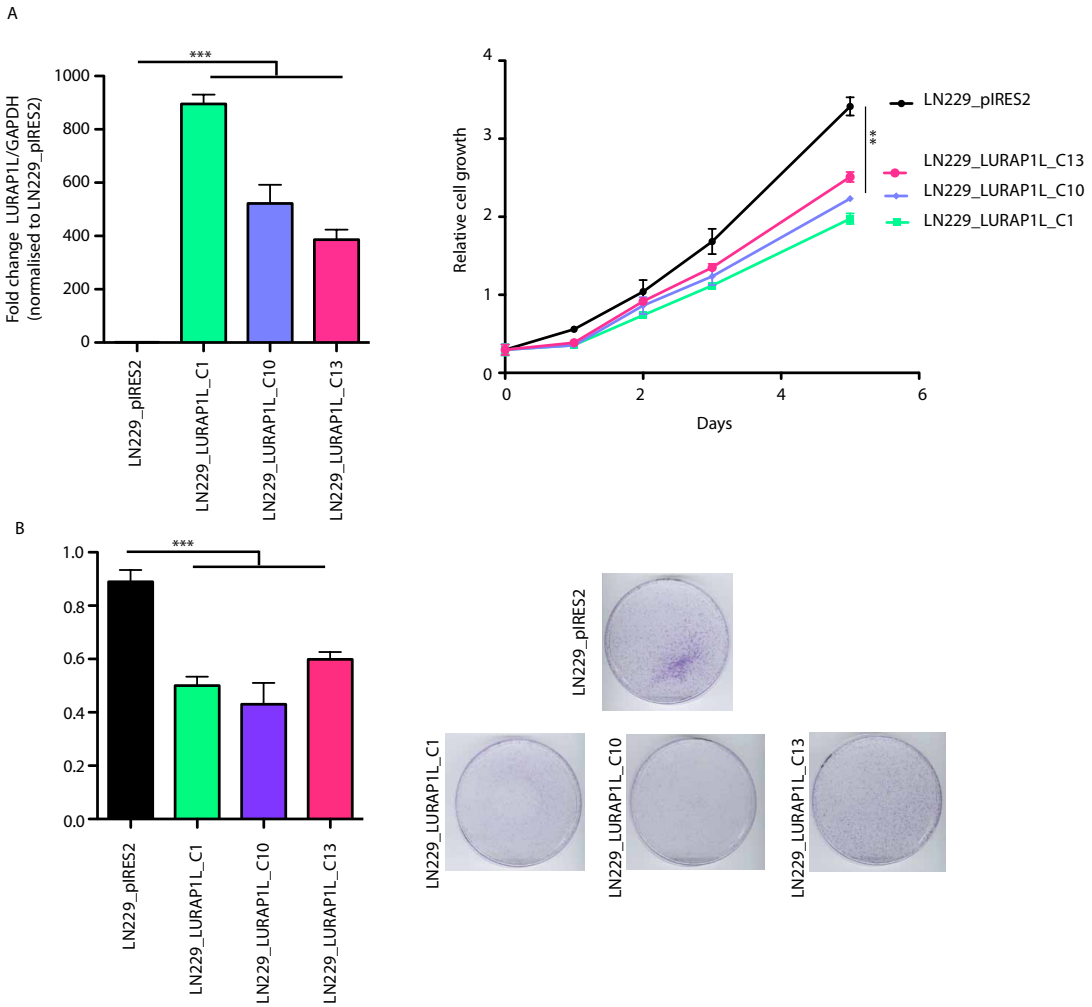

Figure 48. *LURAP1L* overexpression reduces growth *in vitro*. A) The *LURAP1L* expression for each clones has been measured by Real Time PCR and the relative growth is shown on the right. B) The colony formation assay quantification is shown on the left while representative picture of the assay are on the right.

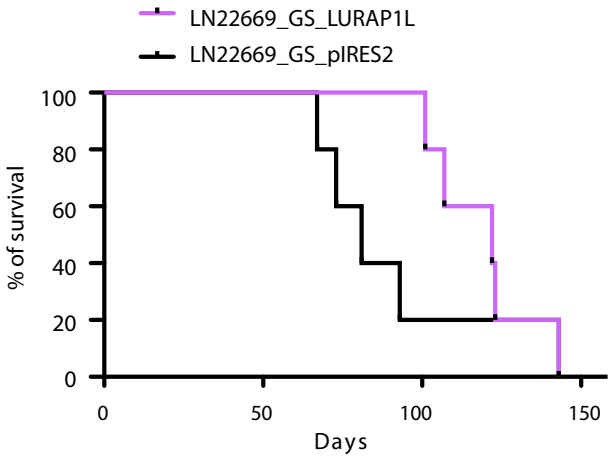

Figure 49. Nude mice were orthotopically injected with either LN2669_GS_pires2EGFP (5mice) or either LN2669_GS_*LURAP1L* (5mice). The injected mice were constantly checked and were euthanized when they started showing any neurological symptoms and /or weight loss.

We have now finished collecting all the samples and we will proceed with the molecular and immunohistochemical characterisation. Moreover, we are currently repeating the experiment to have enough samples to perform statistical analysis.

Conclusions and Future Perspectives

Little is known about the role of the WNT pathway in the malignant behavior of human glioblastoma. In a recent publication [62], we provided evidence that the WNT antagonist *WIF1* is targeted for silencing in glioblastoma, hence represents a good candidate tumor suppressor. In most glioblastomas, *WIF1* silencing is mediated by genomic deletion, promoter hypermethylation, or both. A recent study supports a role for a deregulated WNT pathway in malignant glioma, showing that additional WNT pathway inhibitors are epigenetically inactivated, including the family of secreted frizzled-related proteins, DICKKOPF, and NAKED [41].

Here we demonstrated that forced *WIF1* expression significantly attenuates cell proliferation *in vitro*, particularly striking for anchorage-independent growth, it associates with complete abrogation of tumorigenicity. In ephitelial and mesenchymal tumors, a tumor suppressive role for *WIF1* has been proposed. In gastrointestinal cancer cell lines, restoration of *WIF1* expression was shown to reduce growth in vitro [52], and in cell lines from human renal cell carcinoma, prostate cancer, and osteosarcoma *WIF1* overexpression has been reported to inhibit tumor growth in vivo [45, 48, 87]

Here we propose a mechanism by which *WIF1* overexpression may exert a growth-inhibiting effect. The *WIF1*-dependent emergence of enlarged, flattened cells associated with increased detection of SA-β-galactosidase positive, multinucleated cells suggests that WIF1 overexpression induces a senescence-like phenotype in glioblastoma cells. WNT signaling is involved in diverse

processes, from early embryonic patterning [88] to regulation of stem cell self-renewal and differentiation [89, 90]. Consequently, WNT pathway dysregulation can dramatically alter differentiation and cell fate decisions [91]. According to the literature, the relationship between WNT and senescence induction is still controversial [92]. Several reports show that downregulation of the canonical WNT pathway induces triggering of senescence, however the final steps to establish the senescence-phenotype are *p53* and *pRB* dependent [41, 93]. In our experimental setting, the *WIF1*-dependent induction of senescence had to be independent of both *p53* and *pRB*, as the two cell lines used carry mutations in both pathways [72]. Concerning the non-canonical WNT pathway, the relationship with senescence is even more complicated: *WNT5α* has been shown to either induce or block the onset of senescence depending on the tumor type [94]. In line with our results, Pulvirenti *et al*, have recently shown that in glioblastoma the knockdown of WNT5α induces a senescence-like phenotype [95], thus giving us the rationale to further investigate the WIF1-dependent non-canonical WNT pathway alterations. Several publications, including one in glioblastoma, showed a link between WNT5α-JNK-AP1 [58, 76]. They speculate about a direct mechanism of JNK activation by *WNT5α* signaling. This step would then trigger the phosphorylation of c-JUN that, once activated, homodimerizes and/or heterodimerizes with c-FOS generating the activator protein-1 (AP-1) transcription complex [96]. We tested the involvement of the JNK/AP1 pathway in the transduction of WIF1-downstream signaling, but we clearly had to reject this hypothesis. We detect no modifications in any of the proteins mentioned above. *WIF1* expression affected neither JNK nor c-JUN phosphorylation and it didn't alter the transactivation of AP1.

Conversely, *WIF1* expression drastically inhibited the phosphorylation of p38 and ERK. We found that these results were extremely interesting because both kinases have been implicated in the regulation of migration in cancer. P38 can be activated by environmental stress or various growth factors and it is involved in the regulation of a plethora of responses such as apoptosis, cell proliferation and invasion [97]. The response induced by p38 activation is cell-type and stimulus-specific [98]. Increased levels of phosphorylated p38 have been correlated with malignancy in many types of cancers and, interestingly, in glioma there is evidence that it correlates with the invasive potential [81, 99]. ERK also has many different functions including being a key regulator of cell proliferation [100, 101]. In glioblastoma it has been connected with augmented invasion: PKC is able to activate ERK at focal adhesions to mediate cell adhesion and motility [102].

We showed that the phosphorylation alterations in p38 and ERK, were also induced by *WNT5α* downregulation. These results suggest that the *WIF1*-induced phenotype might, partially, be generated by the inhibition of the non-canonical WNT pathways that are downstream *WNT5α*. We are now investigating which additional branches of the non-canonical WNT pathway could be involved. We are focusing our attention on the WNT/Ca^{2+} pathway. Some of our results could be explained by calcium level alterations: indeed, both the alteration of MAPK phosphorylation level and differences in migration capability have been described in the context of calcium regulation [82, 102].

The analysis of the gene expression profile of *WIF1* induced cells lead us to the identification of a non-coding RNA, *MALAT1*. *MALAT1* had the highest fold change of all downregulated transcripts. Physiologically, *MALAT1* localizes to

nuclear speckles [103] where it regulates alternative splicing by modulating the distribution and levels of splicing factors [104]. Thus, *MALAT1* is thought to have a variety of functions, primarily through post-transcriptional regulation of expression of many different genes [105]. Our interest in this gene was supported by a few recent publications were *MALAT1* expression was associated with cancer on many different levels, including migration and invasive properties [86, 106]. *MALAT1* is overexpressed in many different types of cancer including lung, breast, pancreas, colon, prostate, and liver cancers, implying a key role in cancer progression [107].

In glioblastoma, *MALAT1* has not yet been investigated. We clearly showed that *MALAT1* is upregulated in glioblastoma and that its expression positively correlates with the total volume of glioblastoma. Moreover, studying the regulation of expression of *MALAT1* via the WNT pathway we found that the WNT5α inhibition was sufficient to drastically reduce *MALAT1* expression. As discussed above, several of the WIF1-related effects run via inhibition of the non-canonical pathway.

The functional characterisation of MALAT1 yelded very interesting results, as in other types of cancer, the non-coding RNA expression is important to maintain the migration capability of the tumor cells. Glioblastoma is an extremely invasive type of cancer, where infiltration of surrounding tissue is one of the biggest problems for therapy because it is virtually impossible to perform a complete resection of the tumor. A better understanding of the mechanisms behind the high motility of glioblastoma could bring new ideas to develop novel therapeutic strategies. *MALAT1 per se*, would probably not be a good candidate because of its high basal level of expression in normal brain. However, *MALAT1* functions

through regulation of numerous different genes. As such, finding the most important effectors of *MALAT1*-related invasiveness would be the next logical step in our research.

In addition to *MALAT1*, we identified a second target gene whose expression levels were modulated by *WIF1*: *LURAP1L*. *LURAP1L* encodes an adaptor protein whose function is still unknown. In line with the tumor-suppressive function of *WIF1*, *LURAP1L* overexpression reduces the growth potential of glioblastoma cells both *in vitro* and *in vivo*. Additional experiments are needed to understand the molecular partners of *LURAP1L*, and to identify the pathways in which it is involved. What we can point out at the moment is that *LURAP1L* upregulation is induced by *WIF1* but is not *WNT5α*-dependent. These results clearly show that the final tumor suppressive phenotype induced by *WIF1* is a combination of both canonical and non-canonical WNT pathway inhibition. This should be taken into account when WNT inhibitors are developed for therapy, as both WNT pathways should be targeted. In other types of cancer, this issue is probably not as important, since in contrast to glioblastoma, *WNT5α* has been shown to work as a tumorsuppressor [94, 108-110]. However, in glioblastoma *WNT5α*-related pathways are important for the tumor aggressiveness, thus they should be considered as possible therapy targets [57, 95].

Material and Methods

Glioblastoma Tissues

Glioblastoma tissues were collected for translational research with informed consent of the patients. The protocols were approved by the local ethics committees.

Prediction of Genomic Copy Number Amplifications in Glioblastoma by a Hidden Markov Model

The glioblastoma micro-array gene expression data were obtained on Affymetrix HG-133 Plus2.0 GeneChips (Gene Expression Omnibus database at http://www.ncbi.nlm.nih.gov/geo/, accession number GSE7696) were used for amplification prediction. Probe sets were filtered to exclude those with low variance, suggestive of no or constant expression of the gene. For each gene with multiple probe sets, only the one with the highest variance was retained. Input to a hidden Markov model (HMM) as observed sequences were genewise-mean-centered, the log-scale robust multi-array average normalized expression data ordered by their positions on a chromosome (http://genome.ucsc.edu/; 2004 freeze) and discretized into 8 levels of expression intensity. The HMM had 2 hidden states: The “normal” state modeled the typical distribution, while the “activated” state modelled a distribution typical for highly amplified regions, which is shifted toward higher values. It generated for each sample and

chromosome a matrix of posterior state probabilities at each of the measured loci.

DNA Isolation, Methylation-Specific PCR

Genomic DNA was isolated from paraffin-embedded or fresh frozen tissue and subjected to bisulfite treatment using the EZ DNA Methylation Kit (Zymo Research) followed by nested methylation-specific PCR (MSP), as described previously [14]. During the bisulfite treatment, unmethylated cytosine, but not its methylated counterpart, is converted into uracil. MSP for WIF1 was performed via a nested approach using published primer sequences [49]. Peripheral blood lymphocytes and the colon cancer cell line SW48 were employed as the WIF1 methylation negative and positive controls, respectively

Glioblastoma Cell Lines

The adherent glioblastoma cell lines LN229, LN319, LN2669 were established in our lab, and U87MG was obtained from the American Type Culture Collection (ATCC). All glioma cell lines have been characterized for a defined set of molecular aberrations in our lab, as published previously [111] and were controlled by DNA fingerprinting as described [72]. The non–small cell lung carcinoma cell line A549 and the colon carcinoma cell line SW48 were obtained from ATCC. All adherent cell lines were cultured in Dulbecco's modified Eagle's medium (Invitrogen), supplemented with 5% fetal calf serum (Hyclone) and 100 units/mL penicillin, 100 units/mL streptomycin (Invitrogen). The glioblastoma cell line LN2669_GS was freshly isolated from glioblastoma tissue; the tumor

specimen was dissociated in presence of papain and DNase I as described previously [112]. Cells were cultured under stem-cell conditions to form spheres using Dulbecco's modified Eagle medium/F12 medium containing B27 supplement and 20 ng/mL of both epidermal growth factor (EGF) and fibroblast growth factor 2 (FGF2).

For global demethylation of DNA, glioblastoma cell lines were treated with 5 μM 5-aza-2′-deoxycytidine (Sigma-Aldrich Chemie) for 96 h, with 24-h medium renewal. For the analysis of AP1 signaling the cells were treated for 6-8h with 200nM phorbol-12-myristate-13-acetate (PMA).

LN229_indWIF1 and LN229_dsRED were treated with doxocyclin to induce either WIF1+dsRED or dsRED. The doxocyclin was resuspended in water (1mg/1mL) and was used at a final concentration of 1μg/mL.

Plasmids and Small Interference RNAs

The Wnt/β-catenin activity luciferase reporter vectors TOP_FLASH and FOP_FLASH comprise T-cell factor (TCF)/β-catenin responsive elements that express synthetic firefly luciferase from a PGL4.10 backbone with a minimal TATA box with 8 concatenated TCF binding sites and 8 mutated binding sites, respectively (a generous gift of Prof. Tatiana Petrova). The pRL CMV Renilla luciferase (Promega AG) plasmid was used to normalize for transfection efficiency. The *WIF1* expression vector and its empty control pcDNA3.1 vector were generous gifts from Professor Qian Tao, Cancer Center, Chinese University of Hong Kong [113]. To generate the stably transfected clones in the LN229 cell line *WIF1* was subcloned into the vector pIRES2-EGFP

(Clontec). *WIF1* knockdown was achieved using small interference RNAs (siRNAs; ON-TARGET plus SMART pool, Dharmacon RNA Technologies) targeting 3 domains of the WIF1 RNA, and the control experiments were performed with the corresponding ON-TARGET plus non-targeting pool.

Three different WNT5α specific siRNAs were obtained from Origene (ID 7474) together with a scrambled negative control. Each siRNA was tested alone or in a combination with the other to chose the best combination. The siWNT5a_C was found to be the most efficient and it was used for the next experiments (20nM final concentration).

MALAT1 specific siRNA was purchased from Ambion (Catalog Number 4455877) together with the scramble negative control (Catalog Number 4390843). Both siRNAs were used at a final concentration of 15nM.

LURAP1L was cloned starting from a cDNA sample derived from a LN229 cells. The DNA fragment obtained by PCR was cloned in pIRES2-EGFP. All cDNAs that were cloned in plasmids were sequenced before use.

Cell transfection and generation of stable cell lines

In the first part of the project the plasmids transfections were performed using Lipofectamine 2000 transfection reagent (Invitrogen), and siRNAs were transfected with INTERFERin (Polyplus-Transfection SA) reagent as suggested by the manufacturers. Later on we moved to a more efficient transfection system: the NEON electroporator (invitrogen). The different cell lines were electroporated using the 100 µl tips: the ratio of DNA/cells was usually 20µg of DNA/4*10^6 cells while the final concentration of transfected siRNA was 10-

15μM. For adherent cell lines the parameters were: 1400 Volts, 20 Width, 1 pulse. For sphere cell lines instead the voltage was increased to 1700.

For stable transfections, cells were transfected with the expression vector and followed by selection with G418. Resistant clones were selected and maintained in 400-800 μg/mL of G418.

Luciferase-based assays to measure signaling pathways activity

Canonical WNT pathway was detected using TOPflash/FOPflash reporter plasmid system, AP1 signaling using the pGL3-5xTRE-TATA. The preliminary experiments were done using the DUAL Luciferase system (promega) as suggested by the manufacture. For the second part of the experiment we followed the protocol suggested by Sambrook et al [114]. For the normalization of the transfection efficiency we co-transfected a GFP-encoding plasmid (pEGFP-N1). The luminescence and the fluorescence were both analyzed using a Synergy H1 Hybrid Multi-Mode Microplate Reader.

Crystal Violet Assay

For growth curves, 2-3 × 10^4 cells were seeded in 12-well plates. At every time point, culture medium was removed, cells were washed with 1 mL of 1X phosphate buffered saline (PBS), and 500 μL of crystal violet solution was added per well. After 10 min, crystal violet solution was removed and plates were washed with 1× PBS. Plates were left to dry, and 500 μL of 1% sodium dodecyl sulfate (SDS) in distilled water was added per well. Absorbance was then measured at 595 nm using a plate reader.

Colony formation Assay

5000 Cells were seeded in 10 cm plates and were left grown for 2 weeks, changing medium every three days.

The plates were then stained with crystal violet to take pictures of the all plate. To quantify the growth the crystal violet was dissolved as explained before and the OD were measure at 595nm.

Colony formation Assay in Soft Agar

Growth in soft agar was determined in 6-well plates containing 2 mL of 1% agar in complete medium as the bottom layer, and 1 mL of 0.4% agar in complete medium as the top layer. 2×10^3 cells were seeded in triplicate. Cultures were maintained under standard conditions, and after 3 weeks the number of colonies was determined with an inverted phase-contrast microscope, where a group of 50 cells was scored as colony.

Cell migration and invasion assays

The transwell (Corning) used were 6.5 mm diameter with 8.0 μm pores. Cells ($1*10^4$ cells) were suspended in 100 μL of DMEM containing 0.5% FCS and applied to the upper chamber. 600 μL of 5% FCS medium was applied to the lower chamber. After 16-18 hours, the cells on the upper side of the filters were wiped off and the cells that migrated to the lower side of the upper chamber were stained with crystal violet. To perform the scratch assay, the cells were

plated onto 35-mm-diameter dishes and the monolayer cells were manually scratched with a plastic tip; then, after being washed with PBS, the wounded monolayers of the cells were allowed to heal for 18–24 h in DMEM containing 5% FCS. Pictures were taken at the very same place at each time point. The area of the scratch not yet covered by cells was quantified using imageJ software, and the data were shown as % of covered scratch (T zero = 0%).

Nude Mouse Tumorigenicity Assay

Cells (7×10^6) were resuspended in Dulbecco's modified Eagle's medium and subcutaneously injected into the flanks of 6- to 9-week-old female Swiss nu/nu mice. Five mice per group were injected, and tumor size was measured weekly with a caliper. Tumor volume (mm3) was calculated as (length × width^2)/2. The protocol was authorized by the local veterinary authorities (VD1181.3-6).

For the orthotropic injection six-week-old female Swiss nu/nu old mice were used. $1*10^5$ glioma cells were resuspended in 5µl and stereotactically injected (coordinates: 0,5 mm anterior, 2mm lateral, 3mm depth from the dura). Mice were killed either when body weight loss or neurological symptoms (lethargy, ataxia, and seizures) were observed. For survival analyses, 6 to 12 mice were used per group. To test the tumorigenicity of the LN229_indWIF1 the injected mice were divided in two groups: 1) feed with normal food, 2) feed with doxocyclin supplemented food (625 µg/kg, changed every 2-3 days to avoid loss of doxocyclin activity) [115].

Flow Cytometry Measurement of Cell Morphology

Cells were grown until confluence detached using a solution of 2 mM ethylenediaminetetraacetic acid in PBS and resuspended in PBS. Cell size was evaluated by forward scatter (FS) and side scatter (SS) analysis using a Beckman Coulter FC500 5-color analyzer. More than 1×10^4 events were counted for all samples. Thresholds for FS and SS were arbitrarily defined.

Protein analysis

Protein were extracted starting from dry pellet frozen a - 80 °C. The pellets were dissolved in RIPA (radioimmunoprecipitaiton assay) buffer containing 50 mM Tris–HCl (pH 8.0), 150 mM NaCl, 1 mM EDTA, 0.4% deoxy-cholate, 1% NP-40 containing protease inhibitors including 0.5 mM phenylmethylsulfonylfluoride (PMSF), the protease inhibitor cocktail (Roche) and the PhosSTOP (Phosphatase Inhibitor Cocktail, Roche). The lysate was centrifuged at 14,000 g for 10 min at 4°C and the supernatant was collected as whole cell lysate. Protein concentration was measured using Bradford assay (Bio-Rad Laboratories). The protein samples were subjected to reducing SDS-PAGE using standard methods, using 40 µg for total-protein and 90µg for phospho-protein analysis. Western blots were probed with the following antibodies: phospho-MKK3/6 (cell signaling, #9231, 1:1000), phospho-p38 (cell signaling, #9211, 1:1000), p38 (cell signaling, #9212, 1:1000), Phospho-p44/42 MAPK -Erk1/2 (cell signaling, #9106, 1:1000), p44/42 MAPK -Erk1/2 (cell signaling, #9102, 1:1000), Phospho-SAPK/JNK (cell signaling, #4671, 1:1000), SAPK/JNK (cell signaling, #9258, 1:1000), α-tubulin (Sigma, T-6074, 1:3000).

The Human Phospho-Kinase Antibody Array (R&D system, catalog number: ARY003) was used to analyze the phosphorylation level of the main protein kinases at once and was performed following the manufacturer's instructions. The cells were seeded ($3*10^5$ /small flask) and left adhere for 24 hours, then the cells were treated with doxocyclin. For the assay 300 µg of proteins were used.

Enzyme-Linked Immunosorbent Assay

The cell supernatant, collected after 2 days of culture, was quantified for secreted WIF1 with a sandwich enzyme-linked immunosorbent assay (R&D System) following the manufacturer's instructions. Data were normalized to the cell number. For control experiments of small interfering WIF1 efficiency, the medium was collected after 3 days of culture, and data were normalized to protein content.

Histochemistry

Cells were seeded onto glass coverslips coated with poly-l-lysine and cultured until confluence. Cells were stained for the activity of SA-β-galactosidase using the β-Galactosidase Staining Kit (Biovision), following the manufacturer's instructions, and counterstained with 4′,6-diamidino-2-phenylindole (DAPI). SA-β-galactosidase activity and nuclear morphology were visualized by bright field and fluorescence microscopy (Leica Leitz DMRB). Cells were scored in 10 randomly taken fields.

RNA Isolation and Reverse Transcription PCR

Total RNA was extracted using the RNeasy total RNA extraction kit (Qiagen), and cDNA was synthesized using PrimeScript RT-PCR Kit (TAKARA). PCR was performed with gene-specific primers for WIF1 [49], POLR2A expression was assayed to control for mRNA integrity using published primers [116].

Real-time quantitative PCR was performed with Fast SybR Green Master Mix (Applied Biosystem) using the Rotor Gene 6000 Real-Time PCR system (Corbett Life Science). PCR reactions were run as triplicates. The temperature profile was as follows: 95°C (100 s) followed by 40 cycles at 95°C (3 s) to 60°C (20 s). The quality of the products was controlled by the melting curve. Transcript levels were normalized against human GAPDH [117].

Syber Green Primer list:

Gene	Forward primer (5'-3')	Reverse primer (5'-3')	Reference
WIF1	AAGGTTGGCATGGAAGACAC	TTAAGTGAAGGCGTGTGCTG	[118]
AXIN2	GAGACCCAGCAGCACCTTTC	CAATGGCAAACAGAATGTACAGATT	[119]
WNT5α	TAAGCCCAGGAGTTGCTTTG	GCAGAGAGGCTGTGCTCCTA	[120]
LURAP1L	TTCCGTGGGAAGTTATCTGG	ACGCTTGTGTAGTGCCTGTG	[118]
CTH	CACTGTCCACCACGTTCAAG	TACTTAGCCCCATCCAGTGC	[118]
MALAT1	CTTCCCTAGGGGATTTCAGG	GATGCAAATGCCTCTGAGTG	[118]
CTHRC1	TGGACACCCAACTACAAGCA	GCATTTTAGCCGAAGTGAGC	[118]
SLC26A2	GTTTCAAATGGGAGCAC	GCCCATCGCTACCTGATAAA	[118]
IGFBP5	GGTTTGCCTCAACGAAAAGA	AGTAGGTCTCCTCGGCCATC	[118]
IL6	CACACAGACAGCCACTCACC	TTTTCTGCCAGTGCCTCTTT	[121]
ALDH1L2	CCAGAGCCTCTTTGGACAAG	ACAGGGGTCCCATCTTTCTC	[118]

WIF1-induced LN229 gene expression profile

The LN229_indWIF1 were seeded in small flasks ($3*10^5$ cells/flask) and let adhere for 24 hours and then half of the flasks were then induced with doxocyclin. Three time point, after induction (T0) were collected: T1=12hours, T2=24hours and T3=48hours. The RNA was extracted using quiagen KIT, as described above, and the sample were sent to Geneva at the NCCR "Frontiers in Genetics", Genomics Platform. The samples were hybridized to Affymetrix HG-133Plus2.0 GeneChips (Affymetrix, Santa Clara, CA) and the analyses were carried out in R (http://www.R-project.org/), with Bioconductor packages [122]. Raw CEL files were processed using the robust multichip average (RMA) algorithm available in the affy package [123]. Probes were filtered using the coefficient of variation.

Statistical analysis

The Student t test was used to compare continuous variables between two groups. P values less than 0.05 were considered statistically significant. Results are marked with 1 asterisk (*) if $p< 0.05$ and 2 (**) if $p < 0.01$ and with 3(***) if $p<0.001$. All statistical tests were two-sided. Data are presented as mean values with standard deviation.

Glossary

ABBREVIATION	WORD
5-AZA	5-aza-cytidine
aCGH	Array Comparative Genomic Hybridization
ALDH	Aldehyde dehydrogenases
AP-1	Activator protein 1
APC	Adenomatosis polyposis coli
ARF	Alternate reading frame
ATF2	Activating transcription factor
ATRX	Alpha Thalassemia/Mental Retardation Syndrome X-Linked
BACs	Bacterial artificial chromosome
CaMK	Ca2+/calmodulin-dependent protein kinase
CDK	Cyclin-dependent kinase
CDKN	Cyclin-dependent kinase inhibitor
CIMP	CpG island methylator phenotype
CK1α	Casein kinase 1α
CNAs	Copy Number Aberrations
CREB	cAMP response element-binding protein
CTH	Cystathionase
DAPI	4',6-diamidino-2-phenylindole
DKK	Dickkopf
DNA	Deoxyribonucleic acid
dnTCF	Dominant negative form of TCF
DOX	Doxocyclin
dsRED	Discosoma red fluorescent protein
DVL	Dishevelled
EGFP	Enhanced green fluorescence protein
EGFR	Epidermal growth factor receptor
ELISA	Enzyme-linked immunosorbent assay
ERK	Extracellular signal-Regulated Kinase

FACS	Fluorescence-activated cell sorting
FAT	Protocadherin Fat
FS	Forward scatter
FZD	Frizzled
GAPDH	Glyceraldehyde 3-phosphate dehydrogenase
GBM	Glioblastoma
GICs	Glioma-initiating cells
GS	Glioma-sphere
GSK3	Glycogen synthase kinase 3
H&E	Hematoxylin and eosin
HMM	Hidden markov model
IDH	Isocitrate dehydrogenase
IGFBP	Insulin-like growth factor-binding protein
IL	Interleukin
JNK	c-Jun N-terminal kinases
LEF	Lymphoid enhancer-binding factor
LRP	Low-density lipoprotein receptor-related protein
LURAP1L	Leucine Rich Adaptor Protein 1-Like
MALAT1	Metastasis associated lung adenocarcinoma transcript 1
MAPK	Mitogen-activated protein kinase
MDM	Mouse double minute
MGMT	Methylguanine methyltransferase
MKK	Mitogen-activated Protein Kinase Kinase
mRNA	messenger RNA
MSP	Methylation-specific PCR
NCL	Nucleolin
NF1	Neurofibromin 1
NEAT2	Nuclear-enriched abundant transcript 2
PBLs	Peripheral blood lymphocytes
PBS	Phosphate buffered saline
PCP	Planar cell polarity

PCR	Polymerase chain reaction
PKA	Protein kinase A
PKC	Protein kinase C
PMA	Phorbol-12-myristate-13-acetate
PP2A	Protein phosphatase 2A
PTEN	Phosphatase and tensin homolog
RB	Retinoblastoma protein
RMA	Robust multichip average
RNA	Ribonucleic acid
ROCK	Rho-associated protein kinase
ROR	Receptor tyrosine kinase-like orphan receptors
RT	Radiotherapy
rtTA	Reverse tetracycline transactivator
SA-β-gal	Senescence associated β-galactosidase
SDS-PAGE	Sodium dodecyl sulfate polyacrylamide gel electrophoresis
sFRPs	Secreted Frizzled related proteins
SS	Side scatter
T1WI	T1 weighted imaging
TCF	T-cell factor
TCGA	The Cancer Genome Atlas
TCIA	The Cancer Imaging Archive
TERT	Telomerase reverse transcriptase
TLE1	Transducin-like enhancer of split 1
TMZ	Temozolomide
TP53	Tumor protein p53
WHO	World Health Organization
WIF1	WNT Inhibitory Factor 1

References

1. Louis DN, Ohgaki H, Wiestler OD, Cavenee WK, Burger PC, Jouvet A, Scheithauer BW, Kleihues P: **The 2007 WHO classification of tumours of the central nervous system**. *Acta Neuropathol* 2007, **114**(2):97-109.
2. Gladson CL, Prayson RA, Liu WM: **The pathobiology of glioma tumors**. *Annu Rev Pathol* 2010, **5**:33-50.
3. Schwartzbaum JA, Fisher JL, Aldape KD, Wrensch M: **Epidemiology and molecular pathology of glioma**. *Nat Clin Pract Neurol* 2006, **2**(9):494-503; quiz 491 p following 516.
4. Huse JT, Holland E, DeAngelis LM: **Glioblastoma: molecular analysis and clinical implications**. *Annu Rev Med* 2013, **64**:59-70.
5. Kleihues P, Ohgaki H: **Primary and secondary glioblastomas: from concept to clinical diagnosis**. *Neuro Oncol* 1999, **1**(1):44-51.
6. Riemenschneider MJ, Jeuken JW, Wesseling P, Reifenberger G: **Molecular diagnostics of gliomas: state of the art**. *Acta Neuropathol* 2010, **120**(5):567-584.
7. Parsons DW, Jones S, Zhang X, Lin JC, Leary RJ, Angenendt P, Mankoo P, Carter H, Siu IM, Gallia GL *et al*: **An integrated genomic analysis of human glioblastoma multiforme**. *Science* 2008, **321**(5897):1807-1812.
8. Liu XY, Gerges N, Korshunov A, Sabha N, Khuong-Quang DA, Fontebasso AM, Fleming A, Hadjadj D, Schwartzentruber J, Majewski J *et al*: **Frequent ATRX mutations and loss of expression in adult diffuse astrocytic tumors carrying IDH1/IDH2 and TP53 mutations**. *Acta Neuropathol* 2012, **124**(5):615-625.
9. Hegi ME, Stupp R: **Neuro-oncology: in search of molecular markers of glioma in elderly patients**. *Nat Rev Neurol* 2013, **9**(8):424-425.
10. Killela PJ, Reitman ZJ, Jiao Y, Bettegowda C, Agrawal N, Diaz LA, Jr., Friedman AH, Friedman H, Gallia GL, Giovanella BC *et al*: **TERT promoter mutations occur frequently in gliomas and a subset of tumors derived from cells with low rates of self-renewal**. *Proc Natl Acad Sci U S A* 2013, **110**(15):6021-6026.

11. Stupp R, Mason WP, van den Bent MJ, Weller M, Fisher B, Taphoorn MJ, Belanger K, Brandes AA, Marosi C, Bogdahn U *et al*: **Radiotherapy plus concomitant and adjuvant temozolomide for glioblastoma**. *N Engl J Med* 2005, **352**(10):987-996.
12. Stummer W, Reulen HJ, Meinel T, Pichlmeier U, Schumacher W, Tonn JC, Rohde V, Oppel F, Turowski B, Woiciechowsky C *et al*: **Extent of resection and survival in glioblastoma multiforme: identification of and adjustment for bias**. *Neurosurgery* 2008, **62**(3):564-576; discussion 564-576.
13. Newlands ES, Stevens MF, Wedge SR, Wheelhouse RT, Brock C: **Temozolomide: a review of its discovery, chemical properties, pre-clinical development and clinical trials**. *Cancer Treat Rev* 1997, **23**(1):35-61.
14. Hegi ME, Diserens AC, Gorlia T, Hamou MF, de Tribolet N, Weller M, Kros JM, Hainfellner JA, Mason W, Mariani L *et al*: **MGMT gene silencing and benefit from temozolomide in glioblastoma**. *N Engl J Med* 2005, **352**(10):997-1003.
15. Malmstrom A, Gronberg BH, Marosi C, Stupp R, Frappaz D, Schultz H, Abacioglu U, Tavelin B, Lhermitte B, Hegi ME *et al*: **Temozolomide versus standard 6-week radiotherapy versus hypofractionated radiotherapy in patients older than 60 years with glioblastoma: the Nordic randomised, phase 3 trial**. *Lancet Oncol* 2012, **13**(9):916-926.
16. Wang Y, Jiang T: **Understanding high grade glioma: molecular mechanism, therapy and comprehensive management**. *Cancer Lett* 2012, **331**(2):139-146.
17. Logan CY, Nusse R: **The Wnt signaling pathway in development and disease**. *Annu Rev Cell Dev Biol* 2004, **20**:781-810.
18. Croce JC, Wu SY, Byrum C, Xu R, Duloquin L, Wikramanayake AH, Gache C, McClay DR: **A genome-wide survey of the evolutionarily conserved Wnt pathways in the sea urchin Strongylocentrotus purpuratus**. *Dev Biol* 2006, **300**(1):121-131.
19. MacDonald BT, Tamai K, He X: **Wnt/beta-catenin signaling: components, mechanisms, and diseases**. *Dev Cell* 2009, **17**(1):9-26.

20. Willert K, Nusse R: **Wnt proteins**. *Cold Spring Harb Perspect Biol* 2012, **4**(9):a007864.
21. Kimelman D, Xu W: **beta-catenin destruction complex: insights and questions from a structural perspective**. *Oncogene* 2006, **25**(57):7482-7491.
22. Daniels DL, Weis WI: **Beta-catenin directly displaces Groucho/TLE repressors from Tcf/Lef in Wnt-mediated transcription activation**. *Nat Struct Mol Biol* 2005, **12**(4):364-371.
23. Katoh M: **WNT/PCP signaling pathway and human cancer (review)**. *Oncol Rep* 2005, **14**(6):1583-1588.
24. Semenov MV, Habas R, Macdonald BT, He X: **SnapShot: Noncanonical Wnt Signaling Pathways**. *Cell* 2007, **131**(7):1378.
25. De A: **Wnt/Ca2+ signaling pathway: a brief overview**. *Acta Biochim Biophys Sin (Shanghai)* 2011, **43**(10):745-756.
26. Bovolenta P, Esteve P, Ruiz JM, Cisneros E, Lopez-Rios J: **Beyond Wnt inhibition: new functions of secreted Frizzled-related proteins in development and disease**. *J Cell Sci* 2008, **121**(Pt 6):737-746.
27. Itasaki N, Jones CM, Mercurio S, Rowe A, Domingos PM, Smith JC, Krumlauf R: **Wise, a context-dependent activator and inhibitor of Wnt signalling**. *Development* 2003, **130**(18):4295-4305.
28. Semenov M, Tamai K, He X: **SOST is a ligand for LRP5/LRP6 and a Wnt signaling inhibitor**. *J Biol Chem* 2005, **280**(29):26770-26775.
29. Semenov MV, Tamai K, Brott BK, Kuhl M, Sokol S, He X: **Head inducer Dickkopf-1 is a ligand for Wnt coreceptor LRP6**. *Curr Biol* 2001, **11**(12):951-961.
30. Yamamoto A, Nagano T, Takehara S, Hibi M, Aizawa S: **Shisa promotes head formation through the inhibition of receptor protein maturation for the caudalizing factors, Wnt and FGF**. *Cell* 2005, **120**(2):223-235.
31. Parmalee NL, Kitajewski J: **Wnt signaling in angiogenesis**. *Curr Drug Targets* 2008, **9**(7):558-564.

32. Jin YR, Yoon JK: **The R-spondin family of proteins: emerging regulators of WNT signaling**. *Int J Biochem Cell Biol* 2012, **44**(12):2278-2287.
33. Reguart N, He B, Xu Z, You L, Lee AY, Mazieres J, Mikami I, Batra S, Rosell R, McCormick F *et al*: **Cloning and characterization of the promoter of human Wnt inhibitory factor-1**. *Biochem Biophys Res Commun* 2004, **323**(1):229-234.
34. Hsieh JC, Kodjabachian L, Rebbert ML, Rattner A, Smallwood PM, Samos CH, Nusse R, Dawid IB, Nathans J: **A new secreted protein that binds to Wnt proteins and inhibits their activities**. *Nature* 1999, **398**(6726):431-436.
35. Kawano Y, Kypta R: **Secreted antagonists of the Wnt signalling pathway**. *J Cell Sci* 2003, **116**(Pt 13):2627-2634.
36. Malinauskas T, Aricescu AR, Lu W, Siebold C, Jones EY: **Modular mechanism of Wnt signaling inhibition by Wnt inhibitory factor 1**. *Nat Struct Mol Biol* 2011, **18**(8):886-893.
37. Polakis P: **Wnt signaling in cancer**. *Cold Spring Harb Perspect Biol* 2012, **4**(5).
38. Nusse R, Varmus H: **Three decades of Wnts: a personal perspective on how a scientific field developed**. *EMBO J* 2012, **31**(12):2670-2684.
39. Burgess AW, Faux MC, Layton MJ, Ramsay RG: **Wnt signaling and colon tumorigenesis--a view from the periphery**. *Exp Cell Res* 2011, **317**(19):2748-2758.
40. Phesse TJ, Parry L, Reed KR, Ewan KB, Dale TC, Sansom OJ, Clarke AR: **Deficiency of Mbd2 attenuates Wnt signaling**. *Mol Cell Biol* 2008, **28**(19):6094-6103.
41. Gotze S, Wolter M, Reifenberger G, Muller O, Sievers S: **Frequent promoter hypermethylation of Wnt pathway inhibitor genes in malignant astrocytic gliomas**. *Int J Cancer* 2010, **126**(11):2584-2593.
42. Willert K, Jones KA: **Wnt signaling: is the party in the nucleus?** *Genes Dev* 2006, **20**(11):1394-1404.
43. Ramachandran I, Thavathiru E, Ramalingam S, Natarajan G, Mills WK, Benbrook DM, Zuna R, Lightfoot S, Reis A, Anant S *et al*: **Wnt inhibitory**

factor 1 induces apoptosis and inhibits cervical cancer growth, invasion and angiogenesis in vivo. *Oncogene* 2011.

44. Mazieres J, He B, You L, Xu Z, Lee AY, Mikami I, Reguart N, Rosell R, McCormick F, Jablons DM: **Wnt inhibitory factor-1 is silenced by promoter hypermethylation in human lung cancer**. *Cancer Res* 2004, **64**(14):4717-4720.
45. Rubin EM, Guo Y, Tu K, Xie J, Zi X, Hoang BH: **Wnt inhibitory factor 1 decreases tumorigenesis and metastasis in osteosarcoma**. *Mol Cancer Ther* 2010, **9**(3):731-741.
46. Deng Y, Yu B, Cheng Q, Jin J, You H, Ke R, Tang N, Shen Q, Shu H, Yao G *et al*: **Epigenetic silencing of WIF-1 in hepatocellular carcinomas**. *J Cancer Res Clin Oncol* 2010, **136**(8):1161-1167.
47. Kohno H, Amatya VJ, Takeshima Y, Kushitani K, Hattori N, Kohno N, Inai K: **Aberrant promoter methylation of WIF-1 and SFRP1, 2, 4 genes in mesothelioma**. *Oncol Rep* 2010, **24**(2):423-431.
48. Kawakami K, Hirata H, Yamamura S, Kikuno N, Saini S, Majid S, Tanaka Y, Kawamoto K, Enokida H, Nakagawa M *et al*: **Functional significance of Wnt inhibitory factor-1 gene in kidney cancer**. *Cancer Res* 2009, **69**(22):8603-8610.
49. Urakami S, Shiina H, Enokida H, Kawakami T, Tokizane T, Ogishima T, Tanaka Y, Li LC, Ribeiro-Filho LA, Terashima M *et al*: **Epigenetic inactivation of Wnt inhibitory factor-1 plays an important role in bladder cancer through aberrant canonical Wnt/beta-catenin signaling pathway**. *Clin Cancer Res* 2006, **12**(2):383-391.
50. Tang Y, Simoneau AR, Liao WX, Yi G, Hope C, Liu F, Li S, Xie J, Holcombe RF, Jurnak FA *et al*: **WIF1, a Wnt pathway inhibitor, regulates SKP2 and c-myc expression leading to G1 arrest and growth inhibition of human invasive urinary bladder cancer cells**. *Mol Cancer Ther* 2009, **8**(2):458-468.
51. Clement G, Guilleret I, He B, Yagui-Beltran A, Lin YC, You L, Xu Z, Shi Y, Okamoto J, Benhattar J *et al*: **Epigenetic alteration of the Wnt inhibitory factor-1 promoter occurs early in the carcinogenesis of Barrett's esophagus**. *Cancer Sci* 2008, **99**(1):46-53.

52. Taniguchi H, Yamamoto H, Hirata T, Miyamoto N, Oki M, Nosho K, Adachi Y, Endo T, Imai K, Shinomura Y: **Frequent epigenetic inactivation of Wnt inhibitory factor-1 in human gastrointestinal cancers**. *Oncogene* 2005, **24**(53):7946-7952.
53. Ai L, Tao Q, Zhong S, Fields CR, Kim WJ, Lee MW, Cui Y, Brown KD, Robertson KD: **Inactivation of Wnt inhibitory factor-1 (WIF1) expression by epigenetic silencing is a common event in breast cancer**. *Carcinogenesis* 2006, **27**(7):1341-1348.
54. Queimado L, Lopes CS, Reis AM: **WIF1, an inhibitor of the Wnt pathway, is rearranged in salivary gland tumors**. *Genes Chromosomes Cancer* 2007, **46**(3):215-225.
55. Gong A, Huang S: **FoxM1 and Wnt/beta-catenin signaling in glioma stem cells**. *Cancer Res* 2012, **72**(22):5658-5662.
56. Morris LG, Kaufman AM, Gong Y, Ramaswami D, Walsh LA, Turcan S, Eng S, Kannan K, Zou Y, Peng L *et al*: **Recurrent somatic mutation of FAT1 in multiple human cancers leads to aberrant Wnt activation**. *Nat Genet* 2013, **45**(3):253-261.
57. Yu JM, Jun ES, Jung JS, Suh SY, Han JY, Kim JY, Kim KW: **Role of Wnt5a in the proliferation of human glioblastoma cells**. *Cancer Lett* 2007, **257**(2):172-181.
58. Kamino M, Kishida M, Kibe T, Ikoma K, Iijima M, Hirano H, Tokudome M, Chen L, Koriyama C, Yamada K *et al*: **Wnt-5a signaling is correlated with infiltrative activity in human glioma by inducing cellular migration and MMP-2**. *Cancer Sci* 2011, **102**(3):540-548.
59. Murat A, Migliavacca E, Gorlia T, Lambiv WL, Shay T, Hamou MF, de Tribolet N, Regli L, Wick W, Kouwenhoven MC *et al*: **Stem cell-related "self-renewal" signature and high epidermal growth factor receptor expression associated with resistance to concomitant chemoradiotherapy in glioblastoma**. *J Clin Oncol* 2008, **26**(18):3015-3024.
60. Reifenberger G, Ichimura K, Reifenberger J, Elkahloun AG, Meltzer PS, Collins VP: **Refined mapping of 12q13-q15 amplicons in human**

malignant gliomas suggests CDK4/SAS and MDM2 as independent amplification targets. *Cancer Res* 1996, **56**(22):5141-5145.

61. Tsafrir D, Tsafrir I, Ein-Dor L, Zuk O, Notterman DA, Domany E: **Sorting points into neighborhoods (SPIN): data analysis and visualization by ordering distance matrices**. *Bioinformatics* 2005, **21**(10):2301-2308.
62. Lambiv WL, Vassallo I, Delorenzi M, Shay T, Diserens AC, Misra A, Feuerstein B, Murat A, Migliavacca E, Hamou MF *et al*: **The Wnt inhibitory factor 1 (WIF1) is targeted in glioblastoma and has a tumor suppressing function potentially by induction of senescence**. *Neuro Oncol* 2011, **13**(7):736-747.
63. Zheng S, Fu J, Vegesna R, Mao Y, Heathcock LE, Torres-Garcia W, Ezhilarasan R, Wang S, McKenna A, Chin L *et al*: **A survey of intragenic breakpoints in glioblastoma identifies a distinct subset associated with poor survival**. *Genes Dev* 2013, **27**(13):1462-1472.
64. Gebhart E: **Double minutes, cytogenetic equivalents of gene amplification, in human neoplasia - a review**. *Clin Transl Oncol* 2005, **7**(11):477-485.
65. Yang Z, Wang Y, Fang J, Chen F, Liu J, Wu J: **Expression and aberrant promoter methylation of Wnt inhibitory factor-1 in human astrocytomas**. *J Exp Clin Cancer Res* 2010, **29**:26.
66. Sun L, Hui AM, Su Q, Vortmeyer A, Kotliarov Y, Pastorino S, Passaniti A, Menon J, Walling J, Bailey R *et al*: **Neuronal and glioma-derived stem cell factor induces angiogenesis within the brain**. *Cancer Cell* 2006, **9**(4):287-300.
67. Phillips HS, Kharbanda S, Chen R, Forrest WF, Soriano RH, Wu TD, Misra A, Nigro JM, Colman H, Soroceanu L *et al*: **Molecular subclasses of high-grade glioma predict prognosis, delineate a pattern of disease progression, and resemble stages in neurogenesis**. *Cancer Cell* 2006, **9**(3):157-173.
68. Rich JN, Hans C, Jones B, Iversen ES, McLendon RE, Rasheed BK, Dobra A, Dressman HK, Bigner DD, Nevins JR *et al*: **Gene expression profiling and genetic markers in glioblastoma survival**. *Cancer Res* 2005, **65**(10):4051-4058.

69. Freije WA, Castro-Vargas FE, Fang Z, Horvath S, Cloughesy T, Liau LM, Mischel PS, Nelson SF: **Gene expression profiling of gliomas strongly predicts survival**. *Cancer Res* 2004, **64**(18):6503-6510.
70. Horvath S, Zhang B, Carlson M, Lu KV, Zhu S, Felciano RM, Laurance MF, Zhao W, Qi S, Chen Z *et al*: **Analysis of oncogenic signaling networks in glioblastoma identifies ASPM as a molecular target**. *Proc Natl Acad Sci U S A* 2006, **103**(46):17402-17407.
71. Knudson AG, Jr.: **Mutation and cancer: statistical study of retinoblastoma**. *Proc Natl Acad Sci U S A* 1971, **68**(4):820-823.
72. Bady P, Diserens AC, Castella V, Kalt S, Heinimann K, Hamou MF, Delorenzi M, Hegi ME: **DNA fingerprinting of glioma cell lines and considerations on similarity measurements**. *Neuro Oncol* 2012, **14**(6):701-711.
73. Jho EH, Zhang T, Domon C, Joo CK, Freund JN, Costantini F: **Wnt/beta-catenin/Tcf signaling induces the transcription of Axin2, a negative regulator of the signaling pathway**. *Mol Cell Biol* 2002, **22**(4):1172-1183.
74. Matsumura T: **Multinucleation and polyploidization of aging human cells in culture**. *Adv Exp Med Biol* 1980, **129**:31-38.
75. Chang BD, Broude EV, Dokmanovic M, Zhu H, Ruth A, Xuan Y, Kandel ES, Lausch E, Christov K, Roninson IB: **A senescence-like phenotype distinguishes tumor cells that undergo terminal proliferation arrest after exposure to anticancer agents**. *Cancer Res* 1999, **59**(15):3761-3767.
76. Yamamoto H, Oue N, Sato A, Hasegawa Y, Matsubara A, Yasui W, Kikuchi A: **Wnt5a signaling is involved in the aggressiveness of prostate cancer and expression of metalloproteinase**. *Oncogene* 2010, **29**(14):2036-2046.
77. Enomoto M, Hayakawa S, Itsukushima S, Ren DY, Matsuo M, Tamada K, Oneyama C, Okada M, Takumi T, Nishita M *et al*: **Autonomous regulation of osteosarcoma cell invasiveness by Wnt5a/Ror2 signaling**. *Oncogene* 2009, **28**(36):3197-3208.

78. Nishita M, Yoo SK, Nomachi A, Kani S, Sougawa N, Ohta Y, Takada S, Kikuchi A, Minami Y: **Filopodia formation mediated by receptor tyrosine kinase Ror2 is required for Wnt5a-induced cell migration**. *J Cell Biol* 2006, **175**(4):555-562.

79. Oishi I, Suzuki H, Onishi N, Takada R, Kani S, Ohkawara B, Koshida I, Suzuki K, Yamada G, Schwabe GC *et al*: **The receptor tyrosine kinase Ror2 is involved in non-canonical Wnt5a/JNK signalling pathway**. *Genes Cells* 2003, **8**(7):645-654.

80. Guo L, Guo Y, Xiao S, Shi X: **Protein kinase p-JNK is correlated with the activation of AP-1 and its associated Jun family proteins in hepatocellular carcinoma**. *Life Sci* 2005, **77**(15):1869-1878.

81. Demuth T, Reavie LB, Rennert JL, Nakada M, Nakada S, Hoelzinger DB, Beaudry CE, Henrichs AN, Anderson EM, Berens ME: **MAP-ing glioma invasion: mitogen-activated protein kinase kinase 3 and p38 drive glioma invasion and progression and predict patient survival**. *Mol Cancer Ther* 2007, **6**(4):1212-1222.

82. Chuderland D, Seger R: **Calcium regulates ERK signaling by modulating its protein-protein interactions**. *Commun Integr Biol* 2008, **1**(1):4-5.

83. Zinn PO, Mahajan B, Sathyan P, Singh SK, Majumder S, Jolesz FA, Colen RR: **Radiogenomic mapping of edema/cellular invasion MRI-phenotypes in glioblastoma multiforme**. *PLoS One* 2011, **6**(10):e25451.

84. **Comprehensive genomic characterization defines human glioblastoma genes and core pathways**. *Nature* 2008, **455**(7216):1061-1068.

85. Wang MY, Cheng JL, Han YH, Li YL, Dai JP, Shi DP: **Measurement of tumor size in adult glioblastoma: classical cross-sectional criteria on 2D MRI or volumetric criteria on high resolution 3D MRI?** *Eur J Radiol* 2012, **81**(9):2370-2374.

86. Tano K, Mizuno R, Okada T, Rakwal R, Shibato J, Masuo Y, Ijiri K, Akimitsu N: **MALAT-1 enhances cell motility of lung adenocarcinoma cells by influencing the expression of motility-related genes**. *FEBS Lett* 2010, **584**(22):4575-4580.

87. Yee DS, Tang Y, Li X, Liu Z, Guo Y, Ghaffar S, McQueen P, Atreya D, Xie J, Simoneau AR *et al*: **The Wnt inhibitory factor 1 restoration in prostate cancer cells was associated with reduced tumor growth, decreased capacity of cell migration and invasion and a reversal of epithelial to mesenchymal transition**. *Mol Cancer* 2010, **9**:162.
88. Moon RT, Brown JD, Torres M: **WNTs modulate cell fate and behavior during vertebrate development**. *Trends Genet* 1997, **13**(4):157-162.
89. van de Wetering M, Sancho E, Verweij C, de Lau W, Oving I, Hurlstone A, van der Horn K, Batlle E, Coudreuse D, Haramis AP *et al*: **The beta-catenin/TCF-4 complex imposes a crypt progenitor phenotype on colorectal cancer cells**. *Cell* 2002, **111**(2):241-250.
90. Reya T, Clevers H: **Wnt signalling in stem cells and cancer**. *Nature* 2005, **434**(7035):843-850.
91. Boerboom D, White LD, Dalle S, Courty J, Richards JS: **Dominant-stable beta-catenin expression causes cell fate alterations and Wnt signaling antagonist expression in a murine granulosa cell tumor model**. *Cancer Res* 2006, **66**(4):1964-1973.
92. Adams PD, Enders GH: **Wnt-signaling and senescence: A tug of war in early neoplasia?** *Cancer Biol Ther* 2008, **7**(11):1706-1711.
93. Ye X, Zerlanko B, Kennedy A, Banumathy G, Zhang R, Adams PD: **Downregulation of Wnt signaling is a trigger for formation of facultative heterochromatin and onset of cell senescence in primary human cells**. *Mol Cell* 2007, **27**(2):183-196.
94. Bitler BG, Nicodemus JP, Li H, Cai Q, Wu H, Hua X, Li T, Birrer MJ, Godwin AK, Cairns P *et al*: **Wnt5a suppresses epithelial ovarian cancer by promoting cellular senescence**. *Cancer Res* 2011, **71**(19):6184-6194.
95. Pulvirenti T, Van Der Heijden M, Droms LA, Huse JT, Tabar V, Hall A: **Dishevelled 2 signaling promotes self-renewal and tumorigenicity in human gliomas**. *Cancer Res* 2011, **71**(23):7280-7290.
96. Weston CR, Davis RJ: **The JNK signal transduction pathway**. *Curr Opin Cell Biol* 2007, **19**(2):142-149.
97. Ono K, Han J: **The p38 signal transduction pathway: activation and function**. *Cell Signal* 2000, **12**(1):1-13.

98. Wagner EF, Nebreda AR: **Signal integration by JNK and p38 MAPK pathways in cancer development**. *Nat Rev Cancer* 2009, **9**(8):537-549.
99. Greenberg AK, Basu S, Hu J, Yie TA, Tchou-Wong KM, Rom WN, Lee TC: **Selective p38 activation in human non-small cell lung cancer**. *Am J Respir Cell Mol Biol* 2002, **26**(5):558-564.
100. Roux PP, Blenis J: **ERK and p38 MAPK-activated protein kinases: a family of protein kinases with diverse biological functions**. *Microbiol Mol Biol Rev* 2004, **68**(2):320-344.
101. Kohno M, Pouyssegur J: **Pharmacological inhibitors of the ERK signaling pathway: application as anticancer drugs**. *Prog Cell Cycle Res* 2003, **5**:219-224.
102. Besson A, Davy A, Robbins SM, Yong VW: **Differential activation of ERKs to focal adhesions by PKC epsilon is required for PMA-induced adhesion and migration of human glioma cells**. *Oncogene* 2001, **20**(50):7398-7407.
103. Hutchinson JN, Ensminger AW, Clemson CM, Lynch CR, Lawrence JB, Chess A: **A screen for nuclear transcripts identifies two linked noncoding RNAs associated with SC35 splicing domains**. *BMC Genomics* 2007, **8**:39.
104. Tripathi V, Ellis JD, Shen Z, Song DY, Pan Q, Watt AT, Freier SM, Bennett CF, Sharma A, Bubulya PA *et al*: **The nuclear-retained noncoding RNA MALAT1 regulates alternative splicing by modulating SR splicing factor phosphorylation**. *Mol Cell* 2010, **39**(6):925-938.
105. Lin R, Roychowdhury-Saha M, Black C, Watt AT, Marcusson EG, Freier SM, Edgington TS: **Control of RNA processing by a large non-coding RNA over-expressed in carcinomas**. *FEBS Lett* 2011, **585**(4):671-676.
106. Xu C, Yang M, Tian J, Wang X, Li Z: **MALAT-1: a long non-coding RNA and its important 3' end functional motif in colorectal cancer metastasis**. *Int J Oncol* 2011, **39**(1):169-175.
107. Tano K, Akimitsu N: **Long non-coding RNAs in cancer progression**. *Front Genet* 2012, **3**:219.
108. Liang H, Chen Q, Coles AH, Anderson SJ, Pihan G, Bradley A, Gerstein R, Jurecic R, Jones SN: **Wnt5a inhibits B cell proliferation and functions**

as a tumor suppressor in hematopoietic tissue. *Cancer Cell* 2003, **4**(5):349-360.

109. Ying J, Li H, Yu J, Ng KM, Poon FF, Wong SC, Chan AT, Sung JJ, Tao Q: **WNT5A exhibits tumor-suppressive activity through antagonizing the Wnt/beta-catenin signaling, and is frequently methylated in colorectal cancer**. *Clin Cancer Res* 2008, **14**(1):55-61.
110. Kremenevskaja N, von Wasielewski R, Rao AS, Schofl C, Andersson T, Brabant G: **Wnt-5a has tumor suppressor activity in thyroid carcinoma**. *Oncogene* 2005, **24**(13):2144-2154.
111. Ishii N, Maier D, Merlo A, Tada M, Sawamura Y, Diserens AC, Van Meir EG: **Frequent co-alterations of TP53, p16/CDKN2A, p14ARF, PTEN tumor suppressor genes in human glioma cell lines**. *Brain Pathol* 1999, **9**(3):469-479.
112. Clement V, Sanchez P, de Tribolet N, Radovanovic I, Ruiz i Altaba A: **HEDGEHOG-GLI1 signaling regulates human glioma growth, cancer stem cell self-renewal, and tumorigenicity**. *Curr Biol* 2007, **17**(2):165-172.
113. Chan SL, Cui Y, van Hasselt A, Li H, Srivastava G, Jin H, Ng KM, Wang Y, Lee KY, Tsao GS *et al*: **The tumor suppressor Wnt inhibitory factor 1 is frequently methylated in nasopharyngeal and esophageal carcinomas**. *Lab Invest* 2007, **87**(7):644-650.
114. Sambrook J, Russell DW: **Assay for luciferase in extracts of Mammalian cells**. *CSH Protoc* 2006, **2006**(1).
115. Cawthorne C, Swindell R, Stratford IJ, Dive C, Welman A: **Comparison of doxycycline delivery methods for Tet-inducible gene expression in a subcutaneous xenograft model**. *J Biomol Tech* 2007, **18**(2):120-123.
116. Murat A, Migliavacca E, Hussain SF, Heimberger AB, Desbaillets I, Hamou MF, Ruegg C, Stupp R, Delorenzi M, Hegi ME: **Modulation of angiogenic and inflammatory response in glioblastoma by hypoxia**. *PLoS One* 2009, **4**(6):e5947.
117. Andreeff M, Ruvolo V, Gadgil S, Zeng C, Coombes K, Chen W, Kornblau S, Baron AE, Drabkin HA: **HOX expression patterns identify a common signature for favorable AML**. *Leukemia* 2008, **22**(11):2041-2047.

118. Untergasser A, Cutcutache I, Koressaar T, Ye J, Faircloth BC, Remm M, Rozen SG: **Primer3--new capabilities and interfaces**. *Nucleic Acids Res* 2012, **40**(15):e115.

119. Lal M, Song X, Pluznick JL, Di Giovanni V, Merrick DM, Rosenblum ND, Chauvet V, Gottardi CJ, Pei Y, Caplan MJ: **Polycystin-1 C-terminal tail associates with beta-catenin and inhibits canonical Wnt signaling**. *Hum Mol Genet* 2008, **17**(20):3105-3117.

120. O'Connell MP, Fiori JL, Baugher KM, Indig FE, French AD, Camilli TC, Frank BP, Earley R, Hoek KS, Hasskamp JH *et al*: **Wnt5A activates the calpain-mediated cleavage of filamin A**. *J Invest Dermatol* 2009, **129**(7):1782-1789.

121. Li X, Zhou Q, Hanus J, Anderson C, Zhang H, Dellinger M, Brekken R, Wang S: **Inhibition of multiple pathogenic pathways by histone deacetylase inhibitor SAHA in a corneal alkali-burn injury model**. *Mol Pharm* 2013, **10**(1):307-318.

122. Gentleman RC, Carey VJ, Bates DM, Bolstad B, Dettling M, Dudoit S, Ellis B, Gautier L, Ge Y, Gentry J *et al*: **Bioconductor: open software development for computational biology and bioinformatics**. *Genome Biol* 2004, **5**(10):R80.

123. Gautier L, Cope L, Bolstad BM, Irizarry RA: **affy--analysis of Affymetrix GeneChip data at the probe level**. *Bioinformatics* 2004, **20**(3):307-315.